Expanding the mutational spectrum and investigating the pathophysiology of *GOSR2* mediated progressive myoclonus epilepsy

A thesis

for the degree Doctor of Philosophy

at

University College London

by

Roman Praschberger

January 2018

Declaration

I, Roman Praschberger confirm that the work presented in this thesis is my own. Where information has been derived from other sources, I confirm that this has been indicated in the thesis.

To *science* – a collective
human endeavor driven by
curiosity and the ultimate
wish to better the world.

Abstract

In this PhD thesis I summarize my research into the genetics and pathophysiology of progressive myoclonus epilepsy (PME) associated with mutations in *GOSR2*. This disorder is characterized by early disease onset with ataxia around 3 years of age, followed by development of cortical myoclonus, generalized epilepsy and a rapid deterioration of motor function. Upon beginning my PhD, only one homozygous *GOSR2* mutation – c.430G>T (p.G144W) – had been shown to cause PME. Furthermore, because *GOSR2* encodes a Golgi SNARE protein (termed Membrin) that mediates ER-to-Golgi trafficking in every cell of the human body, it was an unresolved mystery how this mutation gives rise to a largely selective neuronal disorder.

I first describe my discovery of the novel c.491-493delAGA (p.K164del) *GOSR2* mutation in a PME patient who also carried the previously described c.430G>T variant in the compound heterozygous state. Overall, the clinical phenotype of this patient was remarkably consistent with previous cases, although her disease course appeared milder. My finding thus expanded the phenotypes and genotypes linked to this disorder, thus providing an additional tool to investigate the underlying disease mechanisms.

In the subsequent chapters I summarize our attempts to unravel why the nervous system is selectively affected in *GOSR2*-PME. To this end I examined how pathogenic Membrin mutations impacted ER-to-Golgi trafficking in patient-derived fibroblasts, and developed novel *Drosophila* models of *GOSR2*-PME to study neuronal pathophysiology. Intriguingly, while ER-to-Golgi trafficking was remarkably preserved in G144W mutant Membrin fibroblasts, neuronal integrity was severely disturbed in *GOSR2*-PME model *Drosophila*, where dendrites were significantly shorter. Neurons have special secretory demands owing to their very large surface area, and hence appear selectively vulnerable to partial loss of function mutations in Membrin. Thus, the results presented in this thesis provide a possible explanation for the nervous system specificity of *GOSR2*-PME.

Table of Contents

List of Figures

List of Tables

Abbreviations

AMMC	Antennal Mechanosensory Motor Center
AMRF	Action Myoclonus Renal Failure Syndrome
ANOVA	Analysis of Variance
ATP	Adenosine Triphosphate
BFA	Brefeldin A
BLAST	Basic Local Alignment Search Tool
BoNT	Botolinum Neurotoxin
BRP	Bruchpilot
BSA	Bovine Serum Albumin
CD4	Cluster of Differentiation 4
CDS	Coding Sequence
CHO	Chinese Hamster Ovary
CMV	Cytomegalovirus
COG	Conserved Oligomeric Golgi
COPI/II	Coat Protein Complex I/II
CRISPR	Clustered Regularly Interspaced Short Palindromic Repeats
CSP	Cysteine String Protein
CyO	Curly of Oyster
da	daughterless
DMEM	Dulbecco's Modified Eagle Medium
DMSO	Dimethyl Sulfoxide
DNA	Desoxyribonucleic Acid
dNTP	Deoxynucleosidetriphosphate
DPBS	Dulbecco's Phosphate Buffered Saline
DRPLA	Dentatorubral-pallidoluysian Atrophy
DTT	Dithiothreitol
EB	Ellipsoid Body
EDTA	Ethylenediaminetetraacetic Acid
EEG	Electroencephalography
EGFP	Enhanced Green Fluorescent Protein
EM	Electron Microscopy
EMG	Electromyography
EMS	Ethylmethanesulfonate
EPSP	Excitatory Postsynaptic Potential
ER	Endoplasmic Reticulum
ERES	ER Exit Sites
ERGIC	ER-Golgi intermediate compartment
FBS	Fetal Bovine Serum
FM	mutant FKBP (FK506-binding protein)
FRAP	Fluorescence Recovery After Photobleaching
FRET	Förster Resonance Energy Transfer
FRT	Flippase Recognition Target
GalT	Galactosyltransferase
GDP	Guanosine diphosphate
GEF	Guanine-nucleotide Exchange Factor
GFP	Green Fluorescent Protein

GLURIII	Glutamate Receptor subunit III
GM130	Golgi Matrix protein 130
GOSR2	Golgi SNAP Receptor complex member 2
GPP130	Golgi Phosphoprotein 130
GTP	Guanosine triphosphate
HEK	Human Embryonic Kidney
HEPES	4-(2-Hydroxyethyl)-1-Piperazineethanesulfonic acid
hGH	human Growth Hormone
HL3	Hemolymph-Like solution 3
HRP	Horseradish Peroxidase
IgG	Immunoglobulin G
kDa	Kilodalton
Kr	Krüppel
LDL	Low Density Lipoprotein
LDS	Lithium Dodecyl Sulfate
LIMP2	Lysosomal Integral Membrane Protein 2
MEAK	Myoclonus Epilepsy and Ataxia due to potassium (K^+) channel mutation
MEM	Minimum Essential Media
MERRF	Myoclonic Epilepsy with Ragged Red Fibers
MFI	Mean Fluorescence Intensity
MOPS	3-(N-Morpholino)Propanesulfonic acid
MRI	Magnetic Resonance Imaging
NA	Numerical Aperture
NBD	7-Nitro-2-1,3-Benzoxadiazol-4-yl
NCBI	National Center for Biotechnology Information
NCL	Neuronal Ceroid Lipofuscinosis
NMJ	Neuromuscular Junction
NSF	N-ethylmaleimide-Sensitive Factor
nsyb	neuronal synaptobrevin
PBS	Phosphate Buffered Saline
PBT	Phosphate Buffer Triton X-100
PCC	Pearson's Correlation Coefficient
PCR	Polymerase Chain Reaction
PDI	Protein Disulfide Isomerase
PFA	Paraformaldehyde
PMA	Progressive Myoclonus Ataxia
PME	Progressive Myoclonus Epilepsy
ppk	pickpocket
PVDF	Polyvinylidene Difluoride
RFP	Red Fluorescent Protein
RNA	Ribonucleic Acid
ROI	Region of Interest
SCA	Spinocerebellar Ataxia
Sco	Scutoid
SD	Standard Deviation
SDS	Sodium Dodecyl Sulfate
SEM	Standard Error of the Mean
SIFT	Sorting Tolerant From Intolerant
SM	Sec1/Munc18-like

SNAP	Soluble NSF-Attachment Protein
SNAP-25	Synaptosomal-associated Protein 25
SNARE	SNAP Receptor
SNP	Single Nucleotide Polymorphism
ssDNA	single stranded DNA
Tb	Tubby
TBST	Tris-Buffered Saline Tween 20
tdGFP	tandem GFP
TeNT	Tetanus Neurotoxin
TGN	Trans-Golgi Network
TM2/3/6B	Third Multiple 2/3/6B
TMR	Tetramethylrhodamin
TRAPP	Transport Protein Particle
UAS	Upstream Activating Sequence
ULD	Unverricht-Lundborg Disease
UTR	Untranslated Region
v-/t-SNARE	vesicle-/target-SNARE
VAMP	Vesicle-Associated Membrane Protein
VSV	Vesicular Stomatitis Virus
VTC	Vesicular Tubular Clusters
w	white
WT	Wild-Type
y	yellow

Chapter 1. Introduction

Scientific endeavor aims to provide a better understanding of the 'inner workings' of the world. This knowledge allows predictions to be made and targeted interventions to be undertaken in an attempt to benefit mankind. Especially in disease research this notion is a common driving force. Here, the ultimate aim consists in developing better treatments to alleviate human suffering. To discover such treatments one can either take a brute-force approach and test for treatments that reduce phenotypes in disease models or rationally design compounds that interfere with a previously discovered disease *mechanism*. The power of the latter approach is illustrated by the potency of the anti-cancer drug imatinib, which is a specific tyrosine-kinase inhibitor that targets the Bcr-Abl oncogene. It thereby directly interferes with a previously discovered molecular cause of chronic myeloid leukemia (Druker et al., 2001; 1996).

Also in neurology research our highest-resolution understanding of disease *mechanisms* stem from investigating the malfunctions of individual molecules, which can serve as a fundament for drug design. An incredible number of such culprit molecules has been uncovered by extensive studies into the genetics of neurological disorders, yet often the precise causal chains that lead to the respective phenotypic changes are unclear. Thus, important lessons about disease pathways can be learned by in depth functional investigations of such genetic variants. These findings in turn might one day serve as a stepping stone to ultimately be able to design treatments for the same or related disorders.

In the present study we are aiming to provide one such *mechanism* – ideally the most proximal causal 'bottleneck' – which bridges the gaping gorge between genotype and phenotype. The disease at hand is one specific form of progressive myoclonus epilepsy (PME) caused by mutations in the Golgi SNAP receptor complex member 2 (*GOSR2*) gene. Even though this is an extremely rare disorder it captured my attention because of its striking phenotype, that cannot intuitively be linked with the mutated gene's

physiological function. The nervous system of *GOSR2*-PME patients is in an almost constant state of hyperexcitablity, as they suffer from generalized action-myoclonus. In addition, they are severely uncoordinated, yet no profound neurodegeneration is apparent. Interestingly, these changes are the result of the mutation in a Golgi SNARE protein, which at first glance appears as an unlikely candidate to cause a disorder restricted to the nervous system. Because the neuronal intricacies of Golgi trafficking has received comparably little attention, it seemed that studying the pathophysiology of *GOSR2*-PME was not only interesting from a disease but also from a general cell biological point of view. The notion that in-depth disease studies can teach important lessons in physiology is prominently exemplified by the discovery of receptor-mediated endocytosis in fibroblasts derived from patients with familial hypercholesterinemia, which harbor LDL-receptor mutations (Brown and Goldstein, 1986).

In this section I will introduce the group of progressive myoclonus epilepsies; focus more specifically on *GOSR2*-PME; summarize the physiological role of Membrin, which is encoded by the *GOSR2* gene; and discuss SNARE proteins, the secretory pathway and its intricacies within neurons.

1.1 The progressive myoclonus epilepsies

The progressive myoclonus epilepsies (PME) are a heterogeneous group of severe neurological disorders characterized by myoclonus and epileptic seizures with a progressive disease course often involving cerebellar ataxia, and the development of dementia in some but not all forms (Michelucci et al., 2012). Overall, they are rare entities and their abundance varies with geographical location (Marseille Consensus Group, 1990). These disorders often manifest for the first time in childhood and thereafter relentlessly progress, with no effective treatment available to reverse or halt the disease course. While generalized seizures may be reduced with currently available antiepileptic drugs, myoclonus is often only poorly controllable (Michelucci et al., 2016). These myoclonic jerks are characterized by sudden, involuntary, brief muscle contractions leading to small movements. Also ‘negative myoclonus’ occurs in PME, where muscle tone is transiently lost (Kojovic et

al., 2011). These movement disorder features of PME are of cortical origin, and therefore constitute 'cortical myoclonus'. The causative cortical hyperactivity can appear subtle in EEG recordings. Averaging the EEG signal prior to the muscle jerks as detected by electromyography (EMG) in a time-locked manner increases sensitivity (Avanzini et al., 2016). While myoclonus is a defining feature of PME, other forms of epilepsy such as generalized or focal seizures can be infrequent or absent, and instead ataxia more dominant. Such syndromes are therefore rather referred to as progressive myoclonus ataxias (PMA), which are phenotypically continuous with the PMEs (Marseille Consensus Group, 1990). For simplicity, I will use the concept PME collectively for this spectrum. Because PME is a very widely encompassing term – it broadly describes neurological syndromes of cortical myoclonus and epilepsy with progressive disease features such as deteriorating ataxia and often cognitive decline – this group of disorders exhibits large phenotypic variability and contains many different individual diseases. The known causes of PME are mutations in single genes, of which several have been discovered to date. A large fraction of PME cases still lacks molecular diagnoses despite thorough investigation, which makes the discovery of more genes linked to this syndrome likely (Franceschetti et al., 2014; Muona et al., 2015). Amongst the PMEs two main subcategories can phenotypically be distinguished. One group of PMEs deteriorates cognitively to a substantial degree during the course of the disease while the other group largely retains normal cognitive abilities or only develops mild impairment (Michelucci et al., 2012).

1.1.1 PMEs with dementia

One common group of disorders within the PMEs that cause cognitive impairment are the neuronal ceroid lipofuscinoses (NCLs), where currently 14 loci are known (CLN1-14; for an overview of PME syndromes see Table 1) (Nita et al., 2016). These disorders are the most frequent causes of childhood neurodegeneration (Nita et al., 2016). According to age of onset, infantile, late-infantile, juvenile and adult onset NCL are distinguished from each other. Several NCLs also affect the retina, leading to blindness. The defining feature of these disorders is the accumulation of auto-fluorescent

lipofuscin in neurons and non-neuronal cells. Characteristically, in electron microscopy, distinct aggregate profiles can frequently be seen (Minassian, 2014). Interestingly, many of the NCL genes encode lysosomal degradation enzymes, therefore linking these disorders to the lysosomal compartment (Nita et al., 2016). Another common PME with dementia is Lafora disease, caused by mutations of the genes encoding laforin and malin (Turnbull et al., 2016). In this disorder abnormal insoluble glycogen accumulates in neurons and also outside the brain (Girard et al., 2013). These deposits are termed Lafora bodies and can be diagnostic if detected in skin biopsies (Turnbull et al., 2016). Mutations in the mitochondrial genome can also give rise to PME with cognitive decline, such as in Myoclonic Epilepsy with Ragged Red Fibers (MERRF), which is most commonly causes by an A>G mutation at position 8344 in the mitochondrial lysine tRNA gene *MT-TK* (Lamperti and Zeviani, 2016). Sialidoses, which are caused by *NEU1* mutations, are amongst the more common forms of PME. Of the two subforms the milder sialidosis I has a more typical PME phenotype while type II exhibits additional disease features, such as dysmorphic facial features or hepatomegaly (Franceschetti and Canafoglia, 2016). Due to sialidase-1 (encoded by *NEU1*) deficiency, lysosomal sialic acid removal is impaired in this disorder and therefore leads to storage of incompletely degraded macromolecules (Franceschetti and Canafoglia, 2016). Also dentatorubral-pallidoluysian atrophy due to mutations in the *DRPLA* (*ATN1*) gene can give rise to PME with cognitive decline, with the additional clinical feature of choreoathetosis (Tsuji, 2012).

PME	Gene	Mechanism	Clinical notes	References
with dementia				
NCL	CLN1-14	enrichment of lysosomal genes; frequently lysosomal storage material	blindness; (late-) infantile, juvenile and adult onset forms	Nita et al., 2016
Lafora disease	*laforin*, *malin*	involvement in glycogen metabolism	cellular inclusions of insoluble glycogen called Lafora bodies	Turnbull et al., 2016

MERRF	*MT-TK*	mitochondrial defects	ragged red fibres in muscle biopsy; multi-system disorder	Lamperti and Zeviani, 2016
Sialidosis type I	*NEU1*	impaired lysosomal sialic acid removal	visual impairment, macular cherry red spot	Franceschetti and Canafoglia, 2016
DRPLA	*ATN1*	polyglutamine disease	dentatorubral-pallidoluysian atrophy can present as PME	Tsuji, 2012
Gaucher disease type III	*GBA*	defects in lysosomal β-glucocerebrosidase	neuronopathic Gaucher disease (type III) can present as PME	Park et al., 2003
without dementia				
ULD	*CSTB*	deficiency of the cysteine proteinase inhibitor cystatin B	'pure' form of PME, phenotypic severity variable	Lalioti et al., 1997a; 1997b; Pennacchio et al., 1996; Crespel et al., 2016
AMRF	*SCARB2*	mutations in the lysosomal sorting receptor LIMP-2	*SCARB2* mutations can also cause PME *without* renal failure	Balreira et al., 2008; Berkovic et al., 2008; Dibbens et al. 2009
***PRICKLE1*-PME**	*PRICKLE1*	gene linked to planar cell polarity pathway and neurite growth	impaired upgaze reported in a fraction of patients	Bassuk et al., 2008; Liu et al., 2013
North Sea PME	*GOSR2*	study aim of this thesis	areflexia, scoliosis, elevated creatine kinase levels	Corbett et al., 2011; Boissé Lomax et al., 2013
MEAK	*KCNC1*	R320H mutant $K_V3.1$ causes loss of function and acts as a dominant-negative	transient symptom improvement with fever	Muona et al., 2015; Oliver et al., 2017
SMA-PME	*ASAH1*	reduced acid ceramidase activity	spinal muscular atrophy associated with PME	Zhou et al., 2012;

Table 1. List of different PMEs
This heterogeneous group of disorders – commonly characterized by myoclonus, ataxia, epilepsy and a progressive disease course – was further subdivided according to whether mental deterioration is a prominent part of the syndrome.

1.1.2 PMEs without dementia

The paradigmatic PME with generally preserved cognition is Unverricht-Lundborg disease (ULD). It is regarded the 'purest' form of PME due to lack of additional neurological features and was the first disorder that was named PME (Genton et al., 2016). The pathogenic changes that give rise to ULD are homozygous mutations in the Cystatin-B encoding gene *CSTB* or repeat expansions close to its transcription start site (Lalioti et al., 1997a; 1997b; Pennacchio et al., 1996). Cystatin-B deficient mice exhibit myoclonic seizures and mild ataxia, with apoptosis of cerebellar granule cells (Pennacchio et al., 1998). In human ULD patients phenotypic severity varies widely from fully wheelchair bound states to mild disease courses with normal professional employment (Crespel et al., 2016). Besides *CSTB*, several other genes have been linked to PME with largely preserved cognition. Mutations in *SCARB2*, the gene encoding the lysosomal sorting receptor (LIMP-2) for β-glucocerebrosidase, have originally been discovered as the cause of action-myoclonus renal failure syndrome (AMRF) (Balreira et al., 2008; Berkovic et al., 2008). This PME form exhibits as distinguishing features proteinuria and renal failure. Later, homozygous mutations in this gene have been shown to also cause PME without renal failure (Dibbens et al., 2009). Peripheral neuropathy and auditory changes have infrequently been reported in this disease, thereby partially recapitulating features of Limp2 knock-out mice, which otherwise do not exhibit myoclonus or epilepsy (Berkovic et al., 2008; Dibbens et al., 2016). Despite rapid disease progression with premature death approximately one decade after disease onset, cognitive function remains remarkably preserved in *SCARB2*-PME (Dibbens et al., 2016). Also mutations in *PRICKLE1*, a gene involved in the planar cell polarity pathway, have been shown to cause PME without gross intellectual impairment (Bassuk et al., 2008). The first symptom typically is ataxia around 4 years of age and impaired upgaze and mild sensory neuropathy have been reported as additional features in some of these patients. Pronounced cognitive decline seems not to be part of *PRICKLE1*-PME (Bassuk et al., 2008). Recently, mutations in *KCNC1*, encoding the Kv3.1 potassium channel subunit, have been shown to cause PME with

largely preserved intellect (Muona et al., 2015). This syndrome is also referred to as myoclonus epilepsy and ataxia due to potassium (K^+) channel mutation (MEAK). In contrast to autosomal-recessive inheritance in the other PMEs without dementia, MEAK is caused by the same R320H dominant-negative loss of function mutation, which typically arises *de novo* and rarely is transmitted across generations (Oliver et al., 2017). It was suggested that $K_V3.1$ has an important role in fast-firing GABAergic interneurons and therefore it was speculated that hyperexcitability in MEAK could be explained by preferential impairment of inhibitory neurotransmission (Muona et al., 2015).

Several other genetic mutations can give rise to a PME phenotype, which are rare and/or unlike *GOSR2*-PME and therefore not elaborated upon here in further detail.

1.2 *GOSR2*-PME

Mutations in *GOSR2* were first described as a novel cause of PME by Corbett and colleagues (Corbett et al., 2011). They applied homozygosity mapping to an Australian PME patient with second-cousin consanguineous British parents and subsequently identified the same homozygous G144W (c.430G>T) *GOSR2* mutation in four further pedigrees. Subsequently Lomax et al. provided a more detailed clinical description of this disorder based on the previous six and an additional six patients (Boissé Lomax et al., 2013). Because the birthplaces of the patients' parents all clustered in proximity of the North Sea – they originated form the Netherlands, Germany, Denmark, Belgium, the UK and Norway – they termed this disorder 'North Sea PME'. Van Egmond et al. published an additional five *GOSR2*-PME patients (van Egmond et al., 2015; 2014). All of these 17 patients exhibited the same homozygous G144W *GOSR2* mutation, which likely originated approximately 3600 years ago in a single founder (Boissé Lomax et al., 2013; Corbett et al., 2011). The *GOSR2*-PME summary below is based on information derived

from these four reports (Corbett et al., 2011; Boissé Lomax et al., 2013; van Egmond et al., 2015; 2014).

The clinical characteristics of the *GOSR2*-PME patients are remarkably uniform. Typically, the first symptom is ataxia with onset between one and five years of age. Subsequently, within the first decade of life, cortical myoclonus develops. These muscle jerks are pronounced upon action, less frequent or absent if patients are at rest or relaxed, can be focal or multi-focal, and often are generalized. Furthermore, they are sensitive to photic, tactile and auditory stimuli and emotional stress (Boissé Lomax et al., 2013; van Egmond et al., 2014). Usually after the onset of myoclonus other forms of seizures develop. Generalized tonic-clonic seizures are present in most *GOSR2*-PME patients, also absence seizures are frequently observed and other seizure types such as febrile seizures, status myoclonicus, nocturnal myoclonus, clonic seizures, tonic seizures and drop attacks have been reported. Due to rapid disease progression patients are wheelchair-bound mostly by their second decade of life. This is usually not due to a lack of strength, but rather because of the highly disabling action-myoclonus and ataxia (Boissé Lomax et al., 2013). Because of the relentless motor deterioration, premature death in the third or fourth decade of life has frequently been reported. In contrast to this rapid worsening of movement disorder features in *GOSR2*-PME, cognitive functions remain mostly unchanged, except in some patients where mild deficits have been reported in the last years prior to their death (Boissé Lomax et al., 2013). The absence of deep-tendon reflexes – areflexia – has been reported in most patients with *GOSR2*-PME, which seems to be specific to this PME subtype. Furthermore, the development of scoliosis prior to adolescence is very common. The presence of early onset areflexia and scoliosis in a PME patient without dementia thus can be important clinical clues towards an underlying pathogenic *GOSR2* mutation. In addition to scoliosis, also other skeletal abnormalities have been described. Four *GOSR2*-PME patients have been reported to have pes cavus, a distinct foot shape with an unusually high arch. This deformity is also seen in peripheral neurological disorder such as Charcot-Marie-Tooth disease (Saporta et al., 2011). Three *GOSR2*-PME

patients have been reported with syndactyly, where fingers or toes are fused to each other (Boissé Lomax et al., 2013; van Egmond et al., 2014). Neurodegeneration appears not to be a prominent feature of *GOSR2*-PME as MRI scans were mostly reported to be normal. Neuropathological examination of the Australian case revealed only a minor loss of cerebellar Purkinje cells and no abnormal storage material, such as Lafora bodies (Corbett et al., 2011). One characteristic laboratory finding in *GOSR2*-PME patients is the elevation of serum creatine kinase levels, which has been reported in most patients. However, muscle biopsies were usually normal (Boissé Lomax et al., 2013; van Egmond et al., 2014). Nerve conduction studies revealed neuropathy in some patients. While Corbett et al. reported mostly normal electromyography (EMG), van Egmond et al. found in the majority of their patients clear signs of neuromuscular junction motor unit abnormalities (Corbett et al., 2011; van Egmond et al., 2014). EEG recordings typically exhibit generalized epileptic discharges in *GOSR2*-PME, which are often accentuated in the posterior regions of the brain and can be triggered with photic stimulation. Also focal and multi-focal discharges are frequently present. Furthermore, concomitant EEG-EMG recordings in several patients have revealed that cortical epileptic discharges precede the muscle jerks, which is neurophysiological evidence of cortical myoclonus (Corbett et al., 2011; van Egmond et al., 2015). This finding illustrates the epileptic nature of these myocloni. Because they are so frequent and pronounced and *GOSR2*-PME patients also have various other forms of epilepsy, it is clear that this is a disorder of profound nervous system hyperexcitability. Given the treatment difficulty inherent to many forms of PME, *GOSR2*-PME patients typically require a combination of several anti-epileptic drugs (Boissé Lomax et al., 2013). One recent study suggested that some *GOSR2*-PME patients might benefit from the modified Atkins diet. This is based on health-related quality of life improvements in one out of four tested patients, however with no effect on seizure frequency (van Egmond et al., 2017).

Taken together, mutations in *GOSR2* cause an almost exclusive neurological disorder characterized by early onset ataxia and severe hyperexcitability,

with a rapid deterioration of motor function. Despite our knowledge of the causative genetic mutations, we have no understanding as how this ataxia and hyperexcitability might arise from these genomic sequence alterations, as the known function of *GOSR2* is not intuitively linked to a selective neurological ataxia-epilepsy disorder.

1.3 Physiological role of the *GOSR2* encoded protein Membrin

The *GOSR2* gene does not encode an ion channel or neurotransmitter receptor, which would directly suggest a disease mechanism accounting for alterations in nervous system excitability and motor coordination. It encodes a Golgi SNARE protein, termed Membrin, which mediates membrane fusion at the Golgi apparatus and thereby facilitates anterograde cargo trafficking via the ER-Golgi route. Because this is a fundamental process required in every cell of the human body, it is surprising that *GOSR2* mutations result in an almost purely neurological disease; indeed, consistent with the ubiquitous necessity of the Golgi apparatus, many mutations affecting this organelle result in broad syndromes affecting multiple organ systems (De Matteis and Luini, 2011; Freeze and Ng, 2011).

Membrin is a 212 amino acid, cytoplasmically oriented single-pass transmembrane protein (Käll et al., 2004). Besides its critical soluble NSF attachement protein receptor (SNARE) motif (residues 129-182 (Kloepper et al., 2007)), Membrin is also predicted to form a coiled coil in its N-terminal portion (residues 61-107 (Lupas et al., 1991)), the function of which is thus far unclear. Along its SNARE motif, Membrin forms a quaternary SNARE complex with its partner SNAREs Sec22b, Syntaxin-5 and Bet1 and thereby contributes to fusion of opposing lipid bilayers (Xu et al., 2000; Parlati et al., 2000).

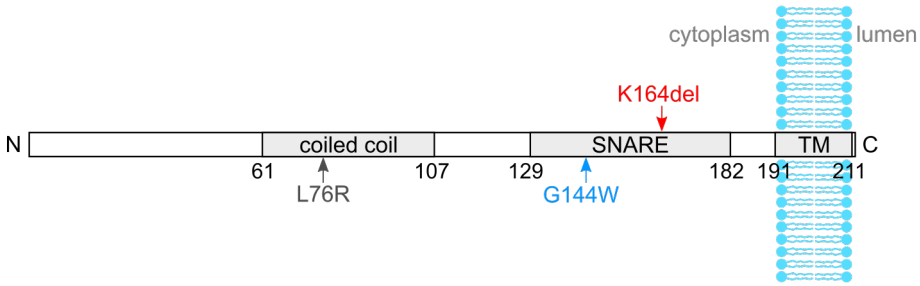

Figure 1. Membrin domain structure
Coiled coil, SNARE and trans membrane (TM) domains are shown. Arrows indicate the positions of the two pathogenic SNARE motif mutations studied in this thesis as well as a coiled coil mutation, that is associated with essential hypertension (see below).

The yeast orthologue of *GOSR2* (which encodes Membrin) was originally discovered as *BOS1*. Following up on Peter Novick's and Randy Schekman's seminal genetic screen of the secretory pathway (Novick et al., 1980; Schekman and Novick, 2004), Newman and Ferro-Novick modified the selection methods for EMS mutated yeast in order to specifically enrich for early secretory pathway defects (Newman and Ferro-Novick, 1987). They retrieved the temperature sensitive *bet1-1* mutant – which is 'blocked early in transport' – and subsequently cloned the corresponding *BET1* gene (Newman et al., 1990). In doing so, they also retrieved *BOS1*, which was a gene-dosage dependent 'bet one suppressor' that was nonetheless incapable of functionally replacing the *BET1* gene (Newman et al., 1990). In this study, they also established the genetic interaction with a third early secretory pathway gene – *SEC22* – by showing that overexpression of *BET1* or *BOS1* could suppress the *sec22-3* phenotype and crossing *bet1-1* and *sec22-3* caused synthetic lethality. *BET1*, *BOS1* and *SEC22* mutants all presented phenotypically in a similar pattern with bloated ER and an accumulation of vesicles, thereby suggesting a failure of fusion of ER-derived vesicles with the Golgi apparatus (Newman et al., 1990; Novick et al., 1980; Shim et al., 1991). Indeed, depletion of functional Bos1 by an anti-Bos1 antibody impaired ER-to-Golgi transport (Lian and Ferro-Novick, 1993). Disruption of *BOS1* was not tolerated, as mutated spores could not be cultured and only initiated one round of mitosis (Shim et al., 1991). This finding illustrates that *BOS1* is an essential gene in yeast. Because the

human and *Drosophila* genomes harbor single *BOS1* orthologues – *GOSR2* and *membrin* respectively – a central importance of this gene in the eukaryotic taxon can be inferred (Kloepper et al., 2007). Consistently, homozygosity for a *membrin* null allele has been shown to cause early developmental lethality in *Drosophila* (Ghabrial et al., 2011).

Mammalian Membrin was first described as a protein that co-immuno-precipitates with Syntaxin-5, Sec22b and Bet1 (and GOS28, rsly1) (Hay et al., 1997). This name was chosen because Membrin was a member of this complex and a role in membrane trafficking was hypothesized by the authors of this study. Another group named the same protein GS27 – Golgi SNARE protein of 27 kDa (Lowe et al., 1997). However, its calculated molecular weight is approximately 25 kDa and also Hay et al. suggested earlier this comparably lower molecular weight (Gasteiger et al., 2003; Hay et al., 1997). It is thought that ER-to-Golgi and intra-Golgi trafficking rely upon the action of two sets of SNARE proteins which share the t-SNARE heavy chain Syntaxin-5 (Malsam et al., 2008). The Membrin-Sec22b-Syntaxin5-Bet1 complex is believed to mediate early membrane fusion between ER and cis-Golgi and potentially also in intra-Golgi transport. In contrast, the complex GOS28-Ykt6-Syntaxin5-GS15 is thought to act at later stages, within Golgi cisternae located in the middle and the trans face. This idea is suggested by the fact that Membrin, Bet1 and Sec22b localize largely to the ER, ER-Golgi intermediate compartment (ERGIC) and the cis-Golgi, whereas the highest concentrations of the GS15 SNARE are found at the trans cisternae (Hay et al., 1998; Volchuk et al., 2004). Besides being critical for membrane fusion in the early secretory pathway, Membrin also appears to be an Arf1 receptor, which is an important regulator of ER-Golgi trafficking. Thereby it facilitates the localization of Arf1 to the Golgi apparatus (Honda et al., 2005). Also, a direct interaction of Membrin with the conserved oligomeric Golgi (COG) complex subunits COG6 and 8 has been described (Willett et al., 2013).

1.4 SNARE proteins

To understand at the molecular level how mutations in Membrin cause PME we need to further dissect the general mode of action of SNARE proteins, as

Membrin belongs to this group. The function of SNARE proteins is contained in their family name in two distinct ways: Firstly, like a mechanical trap/snare, these proteins, localized on opposing lipid bilayers, rapidly change confirmation once in contact with each other, generating a force that eventually mediates fusion of these membranes (Rothman, 2014; Südhof, 2014; Südhof and Rothman, 2009). Secondly, 'SNARE' being a nested acronym, the direct molecular interaction necessary to recycle the individual components of the SNARE complex after a completed round of fusion is summarized: These proteins are SNAp REceptors, as they bind the adaptor protein SNAP (soluble NSF attachment protein), which in turn binds NSF (N-ethylmaleimide sensitive factor), which hydrolyses ATP in order to dissolve the cis-SNARE complex (Söllner et al., 1993a; 1993b). Importantly, SNARE proteins are *sufficient* to overcome the repulsive forces of two adjacent lipid bilayers on their own and thus are the 'minimal machinery' for membrane fusion (Weber et al., 1998). This notion is underlined by experiments where only SNARE proteins and no accessory regulatory proteins are purified and introduced into artificial liposomes. Even in such a reductionist model SNARE proteins are capable of mediating membrane fusion (Weber et al., 1998). However, the remarkable speed of fusion that occurs during stimulated secretion of neurotransmitter has so far not been successfully replicated in cell-free systems (Jahn and Scheller, 2006).

1.4.1 SNARE mode of action

SNAREs are membrane-anchored proteins with the majority of their amino acid residues facing the cytoplasm, where the force-generating complex is formed. Usually the C-terminus contains a single transmembrane domain and only few residues are located inside the lumen of intracellular compartments or in the extracellular space in case of cell surface SNAREs. In contrast, SNAP-25-like SNARE proteins are attached to lipid membranes via a palmitoyl group (Veit et al., 1996). Also Syntaxin-17 is unusual as it has two C-terminal transmembrane domains (Kienle et al., 2009a). In close proximity of the membrane anchors, SNARE proteins harbor stereotypic stretches of 53 amino acids – the SNARE domain. When a single v-SNARE-containing vesicle approaches its target compartment, which harbors the

three complementary t-SNARE domains, the motifs form alpha-helices that tightly interact with each other, giving rise to a stable tetra helical bundle (Sutton et al., 1998). This trans-SNARE complex, or SNAREpin, exerts the driving force to overcome the repulsive forces of the two adjacent lipid bilayers (Südhof and Rothman, 2009). Ultimately, this process leads to membrane fusion and to the SNARE complex being deposited in the target membrane as a cis-SNARE complex.

The most detailed structural and biophysical understanding of SNARE-mediated membrane fusion stems from over two decades of research into the synaptic SNARE complex, which mediates neurotransmitter release and thus is of central interest to neuroscience: The neurotransmitter-loaded synaptic vesicle contains the v-SNARE VAMP2 (vesicle-associated membrane protein 2), also referred to as Synaptobrevin-2, which interacts with the target membrane t-SNAREs SNAP-25 (synaptosomal-associated membrane protein 25) and Syntaxin-1A (see Figure 5 of Sutton et al., 1998; Südhof, 2014). SNAP-25 contributes two SNARE domains to the t-SNARE complex, which is different to other intracellular fusion steps, where usually all three t-SNARE domains are contributed by distinct proteins. The intracellular t-SNAREs thereby are comprised of one Syntaxin-1A like ‘heavy chain’ and two ‘light chains’ (Fukuda et al., 2000). Because the folding energy of a single synaptic SNARE complex amounts to 68 (±4) k_BT (k_B – Boltzmann’s constant, T – temperature), which is approximately the same energy that repulses membranes, it is thought that even one SNARE complex is sufficient to mediate membrane fusion (Gao et al., 2012; Zhang, 2017).

1.4.2 SNARE structure

The cytoplasmic portions of VAMP2, Syntaxin-1A and SNAP-25 are largely unstructured until their initial engagement (Fasshauer et al., 1997a; 1997b; Margittai et al., 2001). They then form alpha-helices, which align in a tetra helical bundle. Because the crystal structure of this synaptic SNARE complex was reported by Sutton et al. in 1998 at 2.4 Å resolution (see Figure 2C and Figure 5 of Sutton et al., 1998), we now have a detailed understanding of the

precise molecular interactions (Sutton et al., 1998). The SNARE domains wrap around each other in a contorted manner and form a 120 Å long, stable four-helix bundle of cylindrical shape (Sutton et al., 1998). The cross-section is circular with varying radii across different positions of the complex. All SNARE motifs are aligned in a parallel manner so that the N- and C-termini of the VAMP2, Syntaxin-1A and both SNAP-25 SNARE domains are aligned with each other's respective counterpart (Sutton et al., 1998). The SNARE domains interact along leucine-zipper-like layers. These layers are positioned at every third or fourth residue and frequently are occupied by hydrophobic residues. They range from the identifying residue numbers -7 to +8 from the N- to C-terminus of the SNARE domains, where -7 to -1 are part of the N- and +1 to +8 part of the C-terminal SNARE domain portions (see Figure 2C of Sutton et al., 1998). The C-terminal halves of the Syntaxin-1A/B, VAMP1/2 and SNAP-25 SNARE domains are targets of clostridial neurotoxins (see Figure 5 of Sutton et al., 1998) (Schiavo et al., 1992; 2000). Eight botulinum toxin serotypes and tetanus toxin have distinct cutting sites. By cleaving the un- or partially assembled synaptic SNARE complex they inhibit neurotransmission and thus cause the very severe disorders botulism or tetanus respectively (Schiavo et al., 2000; Sutton et al., 1998; Zhang et al., 2017). Between layers -1 and +1 is the central 'ionic layer' (layer 0) with the positively charged side chain of an arginine residue (R) and three glutamine (Q) side chains. The presence of three central glutamines and one arginine is highly conserved across different SNARE complexes and across evolution. Therefore an additional classification of SNARE proteins, besides the topological distinction between v- and t-SNAREs, has been introduced, which distinguishes Q-SNAREs from R-SNAREs (Fasshauer et al., 1998). The Q-SNAREs have further been subdivided into three distinct classes – Q_a, Q_b and Q_c-SNARE domains, which are similar to the Syntaxin-1A, N-terminal SNAP-25 and C-terminal SNAP-25 SNARE domains respectively (Bock et al., 2001). Typically, fusogenic SNARE complexes consist of one R- and one Q_a-, one Q_b- and one Q_c-SNARE domain. The R-SNARE is also often the v-SNARE, as is the case for the synaptic SNARE complex. However, this is not true for all SNARE pairs.

The synaptic SNARE complex has been shown to ‘zipper up’ along the mostly hydrophobic layers from the N- to the C-terminus (Gao et al., 2012; Melia et al., 2002). High resolution biophysical studies utilizing optical tweezers have established distinct steps in the assembly of SNARE complexes: an initial slow N-terminal assembly followed by fast C-terminal zippering, which constitutes the energetically important driving force of membrane fusion (Gao et al., 2012; Zorman et al., 2014). The C-terminal complex formation is followed by assembly of the linker domain, which bridges the SNARE domains with the transmembrane domains and thus is of critical importance for transmitting the fusion force upon the lipid bilayers (Gao et al., 2012; Stein et al., 2009). Between N- and C-terminal zippering, around the ionic layer, a pause in complex formation has been noted, which is thought to allow for clamping of the synaptic SNARE complex by complexin (Gao et al., 2012; Giraudo et al., 2006; Huntwork and Littleton, 2007).

1.4.3 SNARE evolution

SNAREs are ubiquitously important force-generators across the whole eukaryotic taxon and act at many diverse intracellular fusion steps. Accordingly, eukaryotic genomes encode several different SNARE proteins destined for distinct compartments. While the yeast and *Drosophila* genomes contain 24 and 26 SNARE genes respectively, the human genome contains an enlarged set of 44 (Bock et al., 2001; Kienle et al., 2009a). The first expansion of SNARE proteins is thought to have taken place between uni- and multicellular evolution and have affected mostly endosomal SNAREs. The second expansion is thought to have occurred in vertebrate evolution and have affected primarily secretory SNARE proteins (Kloepper et al., 2008). Importantly, along the early secretory pathway, where Membrin acts (see below), the same set of SNAREs has largely been preserved throughout evolution (Kloepper et al., 2007). This supports the utility of simpler models, such as *Drosophila* and yeast, in order to investigate the pathophysiology of *GOSR2*-PME.

1.4.4 Overview of different SNAREs in a cell

SNARE proteins not only mediate membrane fusion at presynaptic termini and thereby enable neurotransmitter release, but also fuse membranes at several distinct intracellular transport steps. They act at the ER, the Golgi, the trans-Golgi network, endosomes, the cell surface, lysosomes in animals and the vacuole in yeast (Jahn and Scheller, 2006). 20 distinct subgroups of SNARE proteins have been determined using bioinformatics tools and these SNAREs can be allocated to five steps along the secretory pathway (Kloepper et al., 2007). Accordingly, the eukaryotic ancestor is thought to have contained 20 SNARE proteins (Kloepper et al., 2007). The similarity of the crystal structures of the early (Syntaxin-13 (Q_a), Vti1a (Q_b), Syntaxin-6 (Q_c) and VAMP4 (R)) and late (Syntaxin-7 (Q_a), Vti1b (Q_b), Syntaxin-8 (Q_c) and VAMP8 (R)) endosomal SNARE complexes with the synaptic SNARE complex suggests a high degree of structural and functional stereotypy across other SNARE complexes, even to a higher degree than sequence similarities would suggest (Antonin et al., 2002; Zwilling et al., 2007).

Despite a high degree of conservation of the SNARE domain across the SNARE family, specificity of distinct intracellular fusion steps is necessary to maintain ordered membrane and cargo flow. Thus the ‘SNARE hypothesis’ suggests that this specificity is encoded in the SNARE protein sequence (Rothman, 2014). This idea has been systematically tested in reconstituted liposomes, where only v-SNAREs together with their respective t-SNARE partners, and not the other t-SNAREs of the SNARE family, mediated fusion (McNew et al., 2000).

1.4.5 Early secretory pathway SNAREs

In respect to the Membrin-containing cis-Golgi SNARE complex we can infer its functional microanatomy from liposome fusion assays performed with the yeast orthologues Bos1 (Membrin), Sed5 (Syntaxin-5), Sec22 (Sec22b) and Bet1 (Parlati et al., 2000). Only one out of eight possible combinations was fusogenic, hence we can infer that in mammals the situation might be analogous. The Q_b-SNARE Membrin and the R-SNARE Sec22b would thus

be the t-SNARE light chains, the Q_a-SNARE Syntaxin-5 the t-SNARE heavy chain and the Q_c-SNARE Bet1 the v-SNARE. This is different to the situation at the presynaptic terminal, where an R-SNARE – VAMP2 – is also the v-SNARE. Based on the fact that Sec22b is an R-SNARE it was previously proposed that similarly to the synaptic SNARE complex, the v-SNARE at the cis-Golgi would be Sec22b (Xu et al., 2000). However, only binding studies of these SNARE proteins have been reported, and not liposome fusion assays. Interestingly, Sec22b is not only part of the cis-Golgi but also the ER localized SNARE complex, which mediates fusion of Golgi derived vesicles with this compartment and thus facilitates retrograde transport in the early secretory pathway. At the ER it acts as a v-SNARE in concert with Syntaxin-18, Sec20 and Use1 (Malsam and Söllner, 2011). Also within the Golgi apparatus one SNARE protein – Syntaxin-5 – is shared between two distinct complexes. Based on the observation that mammalian Syntaxin-5 and its yeast orthologue Sed5 formed complexes with seven SNARE proteins, Parlati et al. used liposome fusion assays to systematically search for the fusogenic complexes (Parlati et al., 2002). They found that, besides Bos1-Sed5-Sec22-Bet1, also Gos1-Sed5-Ykt6-Sft1 (mammalian orthologues: GOS28-Syntaxin5-Ykt6-GS15) formed a functional Golgi SNARE complex (Parlati et al., 2002). These complexes are thought to act sequentially along the Golgi apparatus from cis to trans (Volchuk et al., 2004). Interestingly, subunits of these cis- and trans-Golgi SNARE complexes partially inhibit the non-cognate SNARE complexes in a concentration-dependent manner and therefore act as ‘i-SNAREs’ (Varlamov et al., 2004). This mechanism is thought to further increase specificity of the precise site of membrane fusion across the Golgi stack (Varlamov et al., 2004).

1.4.6 The *GOSR2*-PME causing Membrin mutation

Given the critical importance of the SNARE domains in the formation of SNARE complexes, it is not surprising that mutations in this motif – particularly alterations which modify the interaction of layer residues – disrupt SNARE function. Many different SNARE mutations have been reported in different organisms such as yeast, mouse and human (Fasshauer et al., 1998; Jeans et al., 2007; Rao et al., 2001; Schubert et al., 2014; Shen et al.,

2014). Their effects upon SNARE complex formation and membrane fusion depend upon the precise position in respect to the layers of the SNARE complex and on the nature of the change. The phenotypic result in turn will depend upon which of the many different fusion events mediated by SNARE proteins are disrupted as a result of the SNARE mutations.

Prior to my PhD research, *GOSR2*-PME had only been associated with a single homozygous missense mutation – G144W (Corbett et al., 2011). This exchange of a glycine for a tryptophan occurs at layer -3 in the N-terminal half of Membrin's SNARE domain. Layer -3 is a position of comparably small cross-sectional SNARE complex radius in the synaptic SNARE complex and is occupied by one large and three small residues – phenylalanine (Syntaxin-1A), methionine (VAMP2), glycine and alanine (SNAP-25) (see Figure 2D of Sutton et al., 1998 and Figure 2 of Fasshauer et al., 1998) (Sutton et al., 1998). As a comparison, the central layer of the synaptic SNARE complex exhibits a larger radius (see Figure 2D and Figure 3 of Sutton et al., 1998). The amino acid composition at layer -3 is conserved in the orthologous yeast secretory complex Sso-Sec9-Snc1, where the exchange of the small glycine in the N-terminal SNARE motif of Sec9 at layer -3 for aspartic acid causes exocytosis defects (Brennwald et al., 1994; Novick et al., 1980). Layer -3 glycine to glutamate mutations in *Drosophila* SNAP-25 causes temperature-induced SNARE complex instability, reduction in evoked release and paralysis (Rao et al., 2001). Similarly, layer -3 at the cis-Golgi complex consists of one large and three small residues - phenylalanine (Syntaxin-5), serine (Bet1), glycine (Membrin) and methionine (Sec22b) (Figure 2). Given the presence of one bulky phenylalanine in this complex at layer -3, the exchange of a small hydrogen for a large indol side chain in the Membrin SNARE domain at this position suggests that the N-terminal assembly of this complex might be impaired due to steric constraints. Also, biophysical studies of the synaptic SNARE complex suggest that the layer -3 G144W Membrin mutation might be disruptive, as it highlights special vulnerability of this position in an alanine substitution screen. While single alanine replacements of all tested N-terminal layers resulted in no profound N-terminal SNARE domain assembly deficiency, only the methionine to alanine

substitution at layer -3 had marked detrimental effects in the synaptic complex (Ma et al., 2015). Layer +1 leucine to serine substitution in the Membrin yeast orthologue Bos1 has been reported to impair the respective SNARE complex and interfere with trafficking (Fasshauer et al., 1998). One mutation outside Membrin's SNARE domain and within its coiled coil domain – L76R – has been associated with essential hypertension, however the mechanism remains unclear (International Consortium for Blood Pressure Genome-Wide Association Studies, 2011; Meyer et al., 2009; Simino et al., 2014). Taken together, the position and nature of the disease-causing G144W *GOSR2*-PME mutation suggests disruption in cis-Golgi SNARE complex formation and in turn reduced membrane fusion rates.

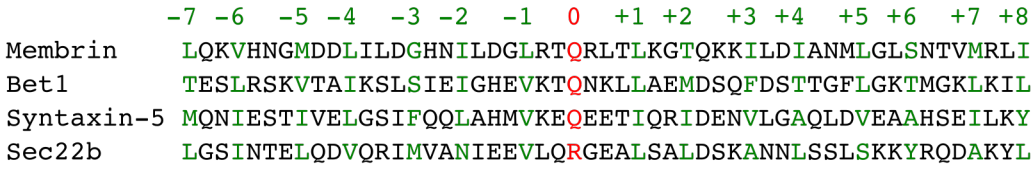

Figure 2. Alignment of cis-Golgi SNARE domain sequences
SNARE domains of Membrin (uniprot O14653-1), Bet1 (O15155-1), Syntaxin-5 (Q13190-1) and Sec22b (O75396-1) were determined as previously described and subsequently aligned (Kloepper et al., 2007). Interacting layers, ranging from -7 to -1 in the N-terminal and +1 to +8 in the C-terminal halves of the SNARE motifs are highlighted in green. Central layer glutamines and arginine are red. The PME-associated Membrin G144W mutation causes the exchange of a small glycine for a large tryptophan at layer -3, which physiologically harbors a bulky phenylalanine.

1.5 The Golgi apparatus

The Golgi apparatus was first described in 1898 by Camillo Golgi – from whom it now derives its name – as an 'internal reticular apparatus' surrounding the nucleus of Purkinje cells (Farquhar and Palade, 1998). Yet over the following 50 years it was widely argued to be an artifact of metallic impregnations used to visualize this structure and thus generally not accepted as a novel cell organelle (Bechtel, 2006). Only with the advent of thin-section electron microscopy could the light microscopic metallic depositions be correlated to a distinct membrane complex, which rapidly convinced the scientific community of the true existence of the Golgi apparatus (Farquhar and Palade, 1981; 1998).

The Golgi apparatus is a central distribution and modification hub within the secretory pathway, which is the protein, lipid and carbohydrate synthesis and transport route within eukaryotic cells (Palade, 1975). To increase compartmentalization of biochemical reactions and facilitate cellular secretion, eukarya have developed a sophisticated endomembrane system separating distinct organelles and vesicular shuttle carriers from the cytosol. Proteins that are destined for such intracellular sub-compartments, as well as secreted and membrane-associated proteins undergo a different fate than their cytosolic counterparts. While the latter proteins are synthesized on free cytosolic ribosomes, in the former case these synthetic machines attach to the surface of the endoplasmic reticulum (ER), which is a highly branched tubular network that is continuous with the nuclear membrane (Nixon-Abell et al., 2016). The ER-attached ribosomes confer its rough appearance when viewed under the electron microscope – therefore termed 'rough ER' – and allow proteins to be co-translationally translocated into the ER lumen (Palade, 1975; Walter et al., 1984). There, protein folding and correct formation of disulfide bonds facilitated by chaperones and oxidoreductases, and carbohydrate protein modifications are undertaken (Braakman et al., 2013; Bulleid et al. 2012). Eventually, proteins and ER-synthesized lipids are selected and shuttled to the Golgi apparatus and transition this compartment from its cis to trans face. Finally, at the trans-Golgi network (TGN), cargos are again selected into vesicular carriers and shuttled to distinct intracellular sites such as lysosomes, endosomes, secretory vesicles and the cell surface. The discovery of this directed process originating in the ER and its underlying microanatomy was pioneered in detailed electron-microscopic studies and pulse-chase experiments by George Palade (Palade, 1975). The opposite direction of cargo flow – from outside to inside – is also critical in eukaryotic cells. This process is termed endocytosis and can be selective or non-selective in respect to the endocytosed molecules (Goldstein et al., 1979; Silverstein et al., 1977). A common denominator across the different transport steps of the secretory pathway is the necessity of vesicles to bud off donor membranes to then be transported to, and fuse with, target membranes (Rothman, 1994). Specificity in cargo selection within forming vesicles, and fusion of these vesicles with target membranes, is critical in

maintaining cellular integrity (Rothman, 2014). The former is mediated by vesicle coating proteins and sorting receptors, while the latter is thought to be mediated by the specificity of the SNARE fusion machinery (Barlowe et al., 1994; Bonifacino and Glick, 2004; Mancias and Goldberg, 2008; McNew et al., 2000; Rothman and Wieland, 1996).

1.5.1 Golgi apparatus structure

The Golgi apparatus, also called ‘Golgi complex’ or simply ‘Golgi’, consists of several disc-like membrane sacs stacked in close proximity, which appear as stacked tubuli in electron microscopy (EM) sections (Klumperman, 2011). These individual membrane sheets are referred to as Golgi cisternae, of which there usually are 4-11 per Golgi apparatus in mammalian cells (Klumperman, 2011). Centrally, the cisternal diameter often amounts to only 10-20 nm, while the rims are usually wider (Klumperman, 2011). In mammalian cells, individual complexes can be laterally connected via a reticular network termed ‘non-compact zone’ and thereby form ribbon-like structures (Klumperman, 2011). In *Drosophila* tissues usually no ribbons are formed, but individual stacks rather group laterally as duplicates (Kondylis and Rabouille, 2009). Cis- and trans-faces of the Golgi apparatus are distinguished from each other based on distinct biochemical properties and molecular compositions (Alberts, 2015). The trans-most cisterna is followed by the trans-Golgi network (TGN). Prior to the cis-most cisterna – between ER and Golgi – vesicular tubular clusters (VTCs) can be found, which comprise the biochemically unique ER-Golgi intermediate compartment (ERGIC) (Schweizer et al., 1991). Surrounding the Golgi, vesicular carriers are abundantly present, with different molecular identities. At the EM-level the spiky clathrin coat can readily be distinguished from dense COPI coating. COPII coated vesicles are usually found at the ER-Golgi interface (Klumperman, 2011).

1.5.2 Carbohydrate processing

The Golgi apparatus is a central processing station for carbohydrate side-chains, which are common post-translation protein modifications initiated in

the ER (Stanley, 2011). In a highly sequential process, sugars are removed and added, which ultimately radically alters the glycosylation profile of glycoproteins. These step-wise biochemical alterations are facilitated by the compartmentalization of glycosyltransferases and glycosidases into distinct cisternae. Due to the stacked nature of the Golgi, the subsequent carbohydrate-processing enzymes are in close proximity while being spatially separated. Unlike in mammals and *Drosophila*, Golgi cisternae are dispersed in yeast, which suggests that a stacked conformation is not absolutely necessary to facilitate efficient sequential modifications and trafficking (Preuss et al., 1992). Several different protein glycosylation pathways operate in mammalian cells, and also lipids can by modified with carbohydrates (Freeze and Ng, 2011). Sugars can either be N- or O-linked onto asparagine or serine/threonine amino acid side chains (Stanley, 2011). To illustrate the sequential action of glycosylation enzymes and glycosidases in the ER and Golgi, I will to briefly summarize the key steps of the N-glycosylation pathway. Initially, an oligosaccharide consisting of three glucose (Glc), 9 mannose (Man) and two N-acetylglucosamine (GlcNAc) groups is attached via the latter sugar group to asparagine residues of nascent proteins in the ER lumen (Freeze and Ng, 2011). Within the ER, three Glc and subsequently one Man unit are enzymatically removed. Thereafter, as a first step in the Golgi, 'Golgi mannosidase I' cleaves three Man after which N-acetylglucosamine transferase I (GlcNAcT-I) adds one GlcNAc. This is followed by the action of 'Golgi Mannosidase II', which removes two Man (Alberts, 2015). Up to this point N-glycans are regarded as 'high mannose'. Thereafter, a further GlcNAc can be added and the glycan is now referred to as 'complex'. Further to this, additional sugars such as galactose, fucose, GlcNAc and sialic acid can be added (North et al., 2010; Stanley, 2011). The sequential nature of this glycosylation pathway can effectively be exploited in the study of Golgi trafficking. One widely used tool is Endo H (endoglycosidase H), which cleaves asparagine-linked 'high mannose' glycans only and therefore only carbohydrate side chains prior to modifications undertaken by Golgi mannosidase II. With this tool, the experimenter can assess whether a secretory cargo has been transported past the medial Golgi, where this enzyme is enriched (Velasco et al., 1993).

The lack of GlcNAcT-I in the 15B chinese hamster ovary (CHO) cell line has been utilized to develop a cell-free transport model of the vesicular stomatitis virus (VSV) glycoprotein from 15B cells infected with VSV into wild-type, uninfected CHO cells (Balch et al., 1984). This system has provided pioneering insights into vesicular cargo trafficking (Rothman, 2014).

1.5.3 ER-Golgi anterograde transport

ER-derived secretory pathway cargo molecules are first packaged into transport vesicles, then translocate to the cis-Golgi (and ERGIC, see below), where they fuse in a Membrin-dependent manner and thus deposit their contents into the cisternal lumen and membrane (Brandizzi and Barlowe, 2013). These are highly orchestrated processes with much of the underlying molecular machinery known today. Vesicle budding and accompanying cargo selection occurs at specialized ER exit sites (ERES) (Bannykh et al., 1996; Brandizzi and Barlowe, 2013). There, the Sec12 guanine nucleotide exchange factor (GEF) converts the inactive Sar1-GDP into the active Sar1-GTP, which then becomes membrane-associated (Brandizzi and Barlowe, 2013). Sar1-GTP recruits the Sec23/Sec24 pre-budding complex and an outer layer, which is comprised of a Sec13/31 octahedral cage that deforms the membrane to form an approximately 60 nm COPII vesicle (Barlowe et al., 1994; Bi et al., 2002; 2007; Fath et al., 2007). Sec24 isoforms are critical for selecting the cis-Golgi SNAREs into COPII vesicles (Mancias and Goldberg, 2008). While initially it was reported that Membrin residues I118 and M120 directly interact with Sec24C/D, a later study suggested that Membrin itself does not directly bind to Sec24 but is sorted indirectly via binding to Syntaxin-5 (Mancias and Goldberg, 2008; Adolf et al., 2016). After budding off the ERES cargo carriers are transported towards the cis-Golgi. This process involves the dynein-dynactin complex, which translocates the attached containers along microtubules towards their minus ends at the microtubule organizing centre, where the Golgi resides (Allan et al., 2002; Yadav and Linstedt, 2011). If microtubules are disrupted by nocodazole treatment, Golgi mini-stacks form at ERES in mammalian cells (Cole et al., 1996; Presley et al., 1997). However, this microtubule-dependent transport appears not to occur in plant cells (Brandizzi and Barlowe, 2013). Transport

vesicles are then captured by tethering proteins prior to SNARE-mediated membrane fusion, which occurs at close proximity between vesicle and target membrane. One important multi-domain elongated tethering protein is p115 (Uso1 in yeast), which is recruited by Rab1-GTP (Lorente-Rodríguez and Barlowe, 2011; Wang et al., 2015). Rab1-GTP and its yeast orthologue Ypt1 in turn are activated by the multi-component transport protein particle I (TRAPP I), which is also capable of binding Sec23 – a component of the COPII coat – and therefore represents a central component of the cis-Golgi cargo entry machinery (Cai et al., 2007a; 2007b; 2008). The final Membrin-Sec22b-Syntaxin5-Bet1 (yeast Bos1-Sec22-Sed5-Bet1) fusion reaction is thought to be regulated and facilitated by the Sec1/Munc18-1 (SM) protein Sly1, which binds a distinct region of the Syntaxin-5 N-terminus (Dascher and Balch, 1996; Lorente-Rodríguez and Barlowe, 2011; Yamaguchi et al., 2002).

1.5.4 The ER-Golgi intermediate compartment (ERGIC)

COPII-mediated anterograde cargo transport from the ER directly to the cis-Golgi is a simplified model, which holds true for yeast, but omits a critical intermediate step in mammalian cells. There, the ERGIC/VTC serves as the first sorting station after exit from ERES. This compartment is characterized by ERGIC-53, which is the procathepsin Z sorting receptor (Appenzeller-Herzog and Hauri, 2006; Schweizer et al., 1988). These ERGIC-53 positive membranes can be found both in vicinity to ERES and close to the Golgi apparatus (Ben-Tekaya et al., 2005). With a 15°C block, cargo can be trapped in this compartment and subsequently released at 32°C (Schweizer et al., 1990). Two models of ER-to-Golgi transport via the ERGIC have been proposed (Appenzeller-Herzog and Hauri, 2006). The transport complex model posits that ERES-derived COPII vesicles undergo homotypic fusion – alternatively, it has been suggested that larger membrane saccules can form at the ER, which do not appear to fuse in a SNARE-dependent manner (Mironov et al., 2003) – and these transport complexes then translocate towards the Golgi apparatus (Appenzeller-Herzog and Hauri, 2006). There two mechanisms have been proposed: Either the transport carriers fuse with

each other and mature into the cis-Golgi cisternae, or they fuse with the latter compartment directly (Appenzeller-Herzog and Hauri, 2006). The alternative model for ER-to-Golgi trafficking suggests that the ERGIC is a stable compartment and that it receives cargo via COPII vesicles. Secretory molecules would then exit the ERGIC and translocate towards the Golgi in anterograde carriers (Appenzeller-Herzog and Hauri, 2006). This latter stable compartment model is favored by live-imaging experiments, which have revealed long-lived stationary GFP-ERGIC-53 labelled structures (Ben-Tekaya et al., 2005). Given that Membrin, Sec22b, Syntaxin-5 and Bet1 localize to VTC/ERGIC it is likely that the Membrin-Sec22b-Syntaxin5-Bet1 complex not only mediates cargo entry into the cis-Golgi, but also membrane fusion at the ERGIC (Volchuk et al., 2004). Indeed, it has been shown that COPII homotypic fusion is dependent upon Syntaxin-5 and Sly1 (Rowe et al., 1998; Xu and Hay, 2004).

1.5.5 Golgi-ER retrograde transport

To enable a net balance of ER and Golgi size, and to maintain their molecular compositions, transport not only occurs from the ER to the Golgi but also from the Golgi to the ER. While anterograde cargo transport from the ER to the Golgi is mediated by COPII coated vesicles, the reverse transport axis is thought to rely upon a different vesicle population – COPI coated cargo carriers (Brandizzi and Barlowe, 2013). This coat consists of seven subunits. Similar to the clathrin coat, an inner and outer shell can be distinguished (Popoff et al., 2011). The cycle of COPI assembly and vesicle budding off the cis-Golgi is initiated by Arf1 (Brandizzi and Barlowe, 2013). Arf1's activity in turn relies upon its conversion from the GDP into the GTP bound state by guanine nucleotide exchange factors (GEF) such as GBF1 – which is inhibited by the drug brefeldin A (BFA) and golgicide A (Helms and Rothman, 1992; Lippincott-Schwartz et al., 1989; Lorente-Rodríguez and Barlowe, 2011; Sáenz et al., 2009). At the ER, cargo is thought to enter this compartment via the Sec20-Use1-Syntaxin18-Sec22b SNARE complex (Malsam and Söllner, 2011). That reverse transport of proteins and lipids from the Golgi to the ER is critical for maintaining organellar identity is illustrated by the KDEL retrieval pathway for ER lumen-residing proteins.

When escaped into the early secretory pathway they are recognized via a C-terminal lysine-aspartate-glutamate-leucine (KDEL) sequence by the KDEL receptor, which in turn associates with the COPI coat and thereby relocates these proteins into their target ER compartment (Majoul et al., 2001; Munro and Pelham, 1987).

1.5.6 Intra-Golgi transport

The mode of cargo transport from cis to trans across the Golgi stack is still unresolved and an area of ongoing controversy (Emr et al., 2009; Glick and Luini, 2011). Two main models have been proposed, which either regard the individual Golgi cisternae as fixed entities or as cargo carriers themselves. In the first model cargo is thought to be transported by COPI vesicles between successive cisternae, while resident proteins must be excluded in order to maintain the individual enzymatic signatures (Glick and Luini, 2011). Such a view is supported by findings that small cargos are still capable of moving across a modified Golgi apparatus, where individual cisternae are synthetically 'glued' to each other and therefore cannot themselves progress (Dancourt et al., 2016). Alternatively, the cisternal progression/maturation model posits that entire cisternae shuttle cargos within them and change their molecular make-up by recycling the resident enzymes via COPI vesicles (Glick and Luini, 2011). Such transitions have been visualized in yeast, where an un-stacked Golgi allows for live imaging of distinct cisternae with diffraction limited optics (Losev et al., 2006; Matsuura-Tokita et al., 2006). However, in the stacked mammalian Golgi apparatus cisternal maturation cannot be optically resolved by conventional means. Progress in live super-resolution microscopy may ultimately allow to directly assess whether cisternal progression facilitates anterograde cargo transport across the Golgi complex (Rothman, 2010). As of now the main argument for cisternal progression is the finding that large procollagen fibrils, which extend the size of typical COPI vesicles several-fold, are efficiently transported across the Golgi apparently without leaving the cisternal lumen (Bonfanti et al., 1998). In a more recent study it was suggested that the dilated cisternal rims are capable of progression – which therefore could account for the rapid transport of large molecules – while the more central parts remained in place

(Lavieu et al., 2013). It has also been suggested that inter-cisternal tubules might contribute to efficient intra-Golgi transport (Marsh et al., 2004; Trucco et al., 2004). While the precise mode of Golgi trafficking is still debated, it should be said that at a joint meeting of several leading Golgi researchers in 2009 extensive support was voiced for a cisternal progression model (Emr et al., 2009).

Once the anterograde secretory pathway cargo has reached the trans-Golgi network (TGN), it is distributed to various intracellular locations or guided towards the plasma membrane (Alberts, 2015). One well established post-Golgi trafficking pathway is the receptor-mediated selective delivery of lysosomal enzymes, which serves here as an example (reviewed in Ghosh et al., 2003 and Kornfeld, 1987). Within the Golgi a mannose-6-phosphate (M6P) group is added to acid hydrolases, which then is recognized in the TGN by one of two M6P receptors. The receptor-acid hydrolases complexes then pinch off the TGN in clathrin coated vesicles and are delivered to early endosomes (Ghosh et al., 2003). There, the enzymes dissociate from the M6P-receptors due to the lower pH, which allows for recycling of the receptors back to the TGN and acid hydrolase delivery to lysosomes.

1.6 Secretory pathway in neurons

Despite the Golgi apparatus having been originally discovered in the nervous system more than a hundred years ago, most of the seminal work in understanding this organelle has been carried out in non-neuronal cells (Farquhar and Palade, 1998). This is not surprising, as non-neuronal cells are experimentally more easily accessible. Yet the secretory pathway faces special challenges in neurons, as their great size, intricate shape and highly specialized functions pose unique demands. Nerve cells have up to 10 000 times larger surface areas than many non-neuronal cells, which requires high rates of secretory trafficking – especially during development – in order to provide sufficient lipid and protein supplies (Ehlers, 2013; Horton and Ehlers, 2004). In addition, neurons are often highly branched and elongated, with their most distal processes far away from the nucleus, which contains the

blueprints for proteins that are required at these remote locations. Thus, long-range transport must occur at the RNA and/or protein levels.

1.6.1 Secretory pathway in dendrites

In neuronal dendrites, the full machinery of the secretory pathway has been described (Hanus and Ehlers, 2008). They contain mostly smooth ER – also some attached ribosomes can be observed – ERGIC as well as Golgi mini stacks, termed ‘Golgi outposts’ (Hanus and Ehlers, 2016; Valenzuela and Perez, 2015). Diffusion of secretory cargo within the continuous dendritic ER lumen is restricted by local zones of increased ER complexity mainly around dendritic branch points, which are also the primary sites for Golgi outposts (Cui-Wang et al., 2012). These stacked mini Golgi complexes are not present in all neurons and overall are infrequent (Horton et al., 2005). Moreover, in dendritic spines a ‘satellite secretory pathway’ has been described (Gardiol et al., 1999; Pierce et al., 2001; 2000). The complete secretory machinery as well as the presence of mRNAs encoding secretory pathway dependent proteins in dendrites suggest local trafficking of such proteins as an additional path besides canonical trafficking via the somatic rough ER and Golgi apparatus (Cajigas et al., 2012). Also, long-range retrograde trafficking occurs, where cargo transitions through the somatic Golgi after local synthesis at dendritic ER-associated ribosomes (Horton and Ehlers, 2003). Post-ER trafficking has been shown to be spatially restricted in response to increased neuronal activity (Hanus et al., 2014). Interestingly, it has recently been suggested that many proteins might bypass the Golgi apparatus in neurons (Hanus et al., 2016). This idea is based on the finding that in neurons, unlike in non-neuronal cells, hundreds of cell surface proteins harbor ‘high mannose’ type carbohydrates side-chains (Hanus et al., 2016). Such a glycosylation pattern is otherwise found on proteins that have not transitioned the Golgi apparatus and thus were not turned into complex N-glycans (see above ‘Carbohydrate processing’) (Freeze and Ng, 2011; Stanley, 2011).

1.6.2 Secretory pathway in axons

In contrast to dendrites, classical Golgi stacks have not been found in axons or at the presynaptic termini, yet Golgi apparatus resident proteins have been detected by means of immuno-fluorescence microscopy in axons (González and Couve, 2014; González et al., 2016; Merianda and Twiss, 2013). While the smooth ER is present also in axons, attached ribosomes are either scarce or absent (Cornejo et al., 2017). Nevertheless, proteins critical for ER-associated protein synthesis, such as Sec61, ribophorin I & II, SRP54 and PDI have been immuno-localized in axons (González et al., 2016; Merianda and Twiss, 2013; Merianda et al., 2009). Also, the ER-exit protein Sar1, the COPII component Sec23 and the ERGIC marker ERGIC53 have been detected in axons (Aridor and Fish, 2009; González et al., 2016). These observations, and the finding that many mRNAs encoding secretory pathway dependent transmembrane proteins are present in axons, suggest that a local secretory pathway might contribute to the proteome of this compartment (Cornejo et al., 2017). Indeed, it has recently been shown that the β_2 voltage-gated sodium channel subunit can be trafficked locally from the ER to the plasma membrane in axons without access to the soma (González et al., 2016). We can speculate that such a route might involve Golgi-like membranes, which contain a similar enzymatic set-up as the somatic Golgi, but do not organize in a classical stacked order. Alternatively, Golgi processing might be by-passed, as indicated by the presence of immature carbohydrates on many neuronal cell surface proteins. Amongst them are also several voltage-gated sodium channel subunits (Hanus et al., 2016).

1.7 Aims and research questions

The aims of my PhD were to study the genetics of progressive myoclonus epilepsy, which led to the discovery of the novel K164del *GOSR2* mutation, and to shed light upon the obscure pathophysiology of *GOSR2*-PME.

Expanding the genotype of *GOSR2*-PME is not only relevant to the study of clinical genotype-to-phenotypes relationships, but is also important for disease mechanism research. The availability of additional alleles with

varying severity aids interpretation of experimental results and thereby facilitates investigating the pathophysiology of this disorder.

Solely by looking at the molecular change in the SNARE domain of Membrin due to the G144W and K164del mutations, one can hypothesize that membrane fusion mediated by the Membrin-Sec22b-Syntaxin5-Bet1 complex might be reduced. This in turn might abolish or reduce the rates of membrane fusion at the cis-Golgi, and thus block or reduce the rates of anterograde cargo transport. Taking into account that the *GOSR2*-PME mutations do not cause zygote or early embryonic lethality – otherwise these patients would not be alive – a complete trafficking interruption seems unlikely. Yet, if an anterograde cargo trafficking defect is indeed at the heart of the pathophysiology of *GOSR2*-PME, then we are facing the difficult challenge of explaining how this might disturb human physiology in a nervous system restricted manner. *GOSR2* is required for every cell's basic physiology and expressed throughout the human body to similar levels, yet patients present with a phenotype mostly restricted to the nervous system (Corbett et al., 2011; Su et al., 2004; Wu et al., 2016). If we assume a broad trafficking defect, why do these patients not present with immunodeficiency or exocrine pancreas insufficiency? After all, antibody secreting plasma cells and digestive enzyme secreting pancreatic acinar cells depend heavily upon the function of the secretory pathway (Farquhar and Palade, 1981; Palade, 1975). Therefore, the central aim of this PhD was to unravel the ‘neuronal bottleneck’ of this disorder, which promised to hold the key to understand the genotype-to-phenotype relationship of *GOSR2*-PME.

To achieve these aims I have used Sanger sequencing of a cohort of patients with PME-like phenotypes, and disease modelling in patient-derived fibroblasts and *Drosophila*. Chapter 2 will summarize how I have identified a novel K164del *GOSR2*-PME mutation. Chapter 3 will describe how the pathogenic Membrin mutations affect SNARE function and basic non-neuronal cell biology. Chapter 4 finally summarizes our investigations into how Membrin mutations impact neuronal development and function. To this end, I have introduced the disease mutations into *Drosophila* and thereby generated the first multicellular model of *GOSR2*-PME. In Chapter 5 I will

summarize our main insights into *GOSR2*-PME that are derived from these studies, their relevance to neuronal cell biology, and potential future research avenues related to this work.

Chapter 2. Expanding the mutational spectrum of *GOSR2* mediated progressive myoclonus epilepsy

2.1 Introduction

During my first 3 month PhD laboratory rotation I was working on the human genetics of a very severe set of neurological disorders – the progressive myoclonus epilepsies (PME). This is a broad group of diseases with similar core symptoms, i.e. epilepsy, myoclonus, ataxia, dementia and a progressive disease course (Michelucci et al., 2012). The initial aim was to assemble a cohort of patients with PME-like presentations from DNA samples stored at the National Hospital for Neurology and Neurosurgery and Institute of Neurology. Such a collection of patient DNAs could then be Sanger sequenced for target genes and ultimately subjected to next generation sequencing. Because the initial aim was to uncover novel variants and potentially broaden the phenotype of *SCARB2*, we loosely assembled a cohort around the phenotype of *SCARB2*-PME, which belongs to the group of PMEs without prominent dementia (Berkovic et al., 2008; Michelucci et al., 2012). The paradigmatic disorder of this PME subset is Unverricht-Lundborg disease (ULD), which is caused by mutations in the *CSTB* gene, most commonly by a dodecamer expansion in the promoter region (Crespel et al., 2016; Lalioti et al., 1997b). Other, much rarer forms of PME without gross cognitive decline are due to *PRICKLE1* and *GOSR2* mutations (Bassuk et al., 2008; Corbett et al., 2011). While all of the above are autosomal-recessive disorders, recently also a dominant form has been described, which is caused by mutations in the *KCNC1* potassium channel gene (Muona et al., 2015, Oliver et al., 2017). Because my initial sequencing of all 12 *SCARB2* exons in this cohort did not reveal any novel pathogenic mutations, I subsequently investigated the *GOSR2* gene for sequence alterations. Initially I focused on the only known *GOSR2*-PME associated c.430G>T (p.G144W) mutation and discovered one patient heterozygous for this mutation (Corbett et al., 2011; Praschberger et al., 2015). Because *GOSR2*-PME is an autosomal-recessive disorder this sequence alteration was not

sufficient to explain the phenotype. Given the phenotypic resemblance of this patients with other *GOSR2*-PME cases, we hypothesized that an additional mutation located in a different exon might be present in the second *GOSR2* allele. Indeed, I identified a novel c.491_493delAGA (p.K164del) mutation by screening the remaining exons in this patient. In the following chapter I detail the involved genetic screening that led to this discovery and outline the phenotype of this *GOSR2*-PME patient, who harbored the second *GOSR2* mutation currently associated with PME.

2.2 Statement of Contribution

I assembled the final cohort of patients screened in this study and performed the Sanger sequencing under the guidance of Niccolo Mencacci. Henry Houlden and Joshua Hersheson provided an initial selection of potential patients for this study. Bettina Balint and Kailash Bhatia contributed extensive clinical data and examinations for the compound heterozygous *GOSR2*-PME patient that we describe here. I also investigated the clinical phenotype of this patient based on medical records.

This work has already been published under the title ‘Expanding the Phenotype and Genetic Defects Associated with the *GOSR2* Gene’ (Praschberger et al., 2015).

2.3 Materials and Methods

2.3.1 Patient cohort

We assembled a cohort of 43 patients with a clinical presentation suggestive of progressive myoclonus epilepsy/ataxia. These patients were negative for mutations in *ATN1* and the 8344 and 3243 mutations in the mitochondrial lysine and leucine tRNA genes, respectively. DNA had previously been extracted and stored at the National Hospital for Neurology and Neurosurgery. The study was approved by the local ethical board and informed consent was given by all patients.

2.3.2 Sanger Sequencing

Oligonucleotide primers used in this study were designed with the Primer3 software (Koressaar and Remm, 2007; Untergasser et al., 2012) (Table 2 and Table 3). The *SCARB2* and exon 5 *GOSR2* primers were designed prior to my arrival to the project. The subsequent *GOSR2* primers were designed by myself.

Exon	Forward primer (5'-3')	Reverse primer (5'-3')
1	TCCCTCCTTGCAGTTGGATC	TGTAGCAGCAGGGATGGGAG
2	GATCTAGGAGGTCAGAATAGGGG	GAAAGTGTGCTCCCACACAG
3	TTGCTTATTAAAGTGGTGTC	ACTTAATGGCTCCTAAATG
4	CCCCTTTGCTATGGGGTAG	AGTTAATCTGGCTTGGGGTG
5	CTTCACCACACCATCTGGG	TGTTTTACCACCATCTTGATTTG
6	GACAGCTCCAGTTAAATCTTGC	TCCTCATGCTTTTGGTGGTC
7	TGCTAACTTGCGGATTTCG	AGCTGGGACTGTAGGTGTGC
8	CTTTAGGAACCAGGCTGTGG	CAGGACTAAACTGGTGAACAATG
9	GGACTACACAGAAATGGTGCTC	ACTCCTCCTGACATCAACCC
10	GTCTGTCCGGGAAAGTGTG	TTTTGCCCTTCTGTCATAACTTAC
11	GCTAACAGGAGGACATTCCC	AGCTGACAGCCCTTCAGTG
12	ACTCCCCACCCAAACTTTTC	CTTTCAACAGGCAACAAGCC

Table 2. *SCARB2* primers
These primers bind intronic regions flanking the exons of the *SCARB2* gene.

Exon	Forward primer (5'-3')	Reverse primer (5'-3')
1	CAACCACTGCTAGTAAGGCG	AAAACTCGGCCTCTACCCTG
2	GGACCTAAAGTGCCACATACA	AGAGTGCAGTCAGGAAGCC
3	ACAACATTTACGGCCTAACTTGA	AACATGTACGTTGGTTTTCAGAA
4	TCCTCAGTACAAAGCCTGGC	CAAAACAGATGGCGCTCAGA
5	AAGACAGAGCAGTGAGACCC	TCAAGGGCTCTGTCTTGTCA
6	GTTGGCAAAGCTCCATCTCC	AAACATTTCAAAAGGCGGCC
7	TCCATTACACACAGCACTGC	TCAAAGCCAACCACTGTCAAG

Table 3. *GOSR2* primers
These primers bind intronic regions flanking the exons of the *GOSR2* gene.

The PCR reaction mixture consisted of 50 ng of DNA, 0,5 μM of forward and reverse primer and 10 μl FastStart PCR Master (Roche) in a 20 μl reaction volume. 1 μl of DMSO was added to the PCR reaction in order to enable amplification of *GOSR2* exon 1. One of two touch-down PCR protocols was used – 65td55 (*SCARB2* exon 5 and 7) or 60td50 (*SCARB2* exon 1-4, 6, 8-12 and all *GOSR2* exons) (Korbie and Mattick, 2008) (Table 4).

	65td55	**60td50**
initial	94°C 5 min	94°C 5 min
8x	94°C 30 s	94°C 30 s
	65°C 30 s	60°C 30 s
	72°C 60 s	72°C 60 s
16x	94°C 30 s	94°C 30 s
	65°C* 30 s	60°C‡ 30 s
	72°C 60 s	72°C 60 s
16x	94°C 30 s	94°C 30 s
	55°C 30 s	50°C 30 s
	72°C 60 s	72°C 60 s
final	72°C 7 min	72°C 7 min

Table 4. PCR cycling conditions
The two above cycling protocols were trialed for each primer pair outlined in Table 2 and Table 3 with and without the addition of DMSO and one successful condition used for the screening. */‡ denotes that in each subsequent step the annealing temperature was reduced by 0.5/0.6°C.

After confirmation of successful PCR reaction via visualisation of amplification products on a 2% agarose gel, excess dNTPs and ssDNA were inactivated by the addition of Fast-AP (Thermo Fisher Scientific) and Exonuclease I (Thermo Fisher Scientific) and incubation for 30 min at 37°C and 15 min at 80°C. 3 µl of the cleaned PCR product was then mixed with 0,5 µl BigDye Terminator v.3.1 (Thermo Fisher Scientific), 2 µl Sequencing Buffer, 500 nM primer and subjected to thermal cycling (Table 5) in a 10 µl total volume. The resulting product was cleaned with Sephadex G-50 (Sigma) filled Corning FiltrEX plates (Sigma).

initial	94°C 1 min
16x	94°C 30 s
	50°C 15 s
	60°C 4 min

Table 5. Cycling condition for Sanger sequencing reaction

Capillary gel electrophoresis and fluorescent dye detection was performed on the ABI 3730 DNA Analyser (Life Technologies) and the resulting sequences where viewed with the Sequencher software (Gene Codes).

2.3.3 Repeat-primed PCR

To screen our PME cohort for the *CSTB* dodecamer expansion we utilized repeat-primed PCR (Lalioti et al., 1997b). This technique is designed to identify large DNA repeat expansions, which would otherwise be difficult to amplify (Warner et al., 1996). Therefore, the PCR reaction contains three primers, one flanking the expansion, one corresponding to the repeat sequence plus an additional overhang and a third primer recognizing this overhang. This combination allows for priming from multiple locations within the repeat expansion and subsequent amplification of these differently sized fragments. A fluorescent tag on one of the primers then allows for the visualization of the varying fragment sizes in this amplification reaction. The same repeat-primed PCR primers for the *CSTB* expansion were used as

previously described (Table 6) (Krysa et al., 2012). For thermal cycling, reactions contained 12 µl of Extensor Long PCR Master Mix (Thermo Fisher Scientific), 2 M betaine, 330 nM of the CSTB_R and P3R primers and 33 nM of the CSTB_rpF primer in a 25 µl total reaction volume.

Name	Primer sequence (5'-3')	Description
CSTB_R	[6FAM]GGCCGGGGAGGAGGCACT	Reverse primer flanking the expansion + 5' fluorescence tag
CSTB_rpF	TACGCATCCCAGTTTGAGACGCCCCGCCCCGCGCCCCGCCCCGCG	Forward primer recognising the expansion (underscore) + 5' overhang
P3R	TACGCATCCCAGTTTGAGACG	Additional reverse primer recognising the above overhang

Table 6. *CSTB* expansion repeat-primed PCR primers

Cycling condition were based on a previous protocol amplifying a different disease-associated expansion (Table 7) (Hantash et al., 2010).

Initial	98°C 10 min
10x	97°C 35 s
	53°C 2 min
	68°C 2 min
25x	97°C 35 s
	53°C 2 min
	68°C 2 min + 20 s/cycle
Final	68°C 10 min

Table 7. *CSTB* expansion repeat-primed PCR cycling conditions

2 µl of these PCR products where then mixed with 0.3 µl of Liz 500 (ABI) and 9.2 µl HiDi formamide (ABI), incubated at 95°C for 3 min and immediately afterwards placed on ice for a minimum of 5 min. Fragments were subsequently run on an ABI 3730 (ABI) and analysed with GeneMapper (ABI).

2.4 Results

In the present study we screened a cohort of 43 patients exhibiting a progressive myoclonus epilepsy/ataxia-like presentation for mutations in genes associated with this phenotype. Patients with previously established *CSTB* mutations and additional cases revealed by repeat-primed PCR accounted for 13 cases and were excluded from further analysis. The remaining 30 patients did not harbour pathogenic mutations in any of the 12 *SCARB2* exons or their adjacent splice sites, while four previously reported, heterozygous single nucleotide polymorphisms (SNPs) were detected (rs143655258, rs180948007, rs2228380 and rs143699909). When these 30 patients were also screened for the c.430G>T mutation in exon 5 of *GOSR2*, one patient was discovered, who carried this allele in the heterozygous state (Figure 3A, B). Given that *GOSR2* mediated PME is a recessive disease, this finding did not fully explain the patient's phenotype. We therefore sequenced the remaining *GOSR2* exons in this patient and discovered a novel, three base-pair deletion (c.491-494delAGA) in exon 6 resulting in the deletion of a lysine (p.K164del) in the functionally important and highly conserved SNARE domain of the encoded SNARE protein Membrin. None of the other 29 patients in the cohort harboured this variant. Because the patient's healthy son was heterozygous for c.491-494delAGA, but not for c.430G>T, we can infer that these mutations are on separate alleles and that the patient therefore is compound heterozygous for these defects in the *GOSR2* gene (Figure 3).

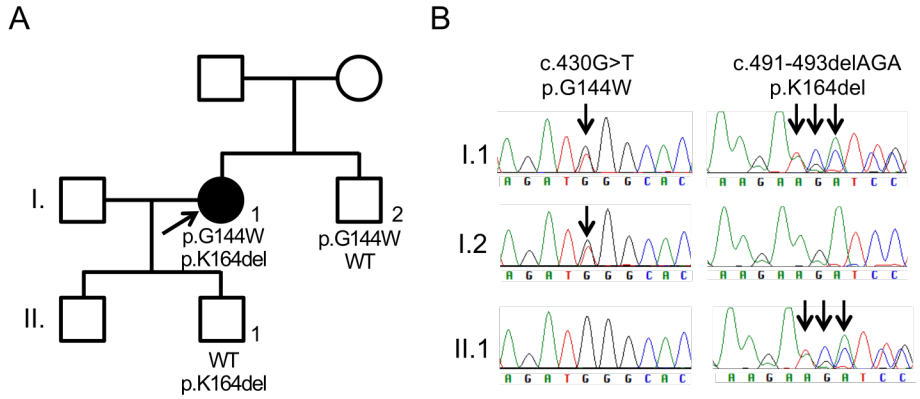

Figure 3. Chromatograms of the novel *GOSR2*-PME mutation
(A) Family tree depicting the patient's (arrow) healthy children and brother, who suffered from cervical dystonia.
(B) Chromatograms of one child and the brother indicate that the novel and previously described *GOSR2* mutations segregate independently and that the patient therefore carries them in the compound heterozygous state.

She also harboured a c.7C>T missense variant, encoding the substitution of a proline residue for a serine (p.P3S). This change is classified as benign by the *in silico* tools PolyPhen-2 and SIFT (Adzhubei et al., 2010; Kumar et al., 2009). Furthermore, an A/C polymorphism (rs12944167) – resulting in the similar P3T (both threonine and serine are characterised by a hydroxyl side chain) – has been reported in the 1000 Genomes Project phase 3 with a minor allele frequency of 1%, which further suggests that the P3S change in our patient is non-pathogenic.

The G144W-K164del compound heterozygous *GOSR2*-PME patient reported here was a British-Caucasian woman who passed away at 62 years of age. Prior to this this she lived in a care facility, largely bed-bound and fully supported for all activities of daily living. Her disease started with ataxia around age 2 with motor deterioration associated with infections and febrile episodes. Subsequently the patient developed myoclonus and the first seizure was reported at the age of 14. She was able to attend a normal school until 11 years of age and retained some fine motor tasks during her second decade of life. Owing to progressive motor deterioration she became fully wheelchair-bound around age 30.

Clinical examinations by Bettina Balint revealed that the patient's speech was interrupted by myoclonus and highly dysarthric. She also displayed other

signs consistent with ataxia, such as broken pursuit, gaze-evoked nystagmus and profound limb dysmetria. Myoclonus was very prominent, of cortical origin, worse under action, less pronounced at rest, stimulus sensitive and affected the patient's face, neck and upper limbs. Interestingly, she also displayed both areflexia and scoliosis, which have frequently been reported in *GOSR2*-PME. However, she did not have syndactyly or pes cavus, which have been reported in a minority of *GOSR2*-PME patients (Boissé Lomax et al., 2013; van Egmond et al., 2014). Cognitive function was largely preserved in this patient, with only a mild cognitive decline reported. However, brain imaging revealed cerebral and cerebellar atrophy (Figure 4).

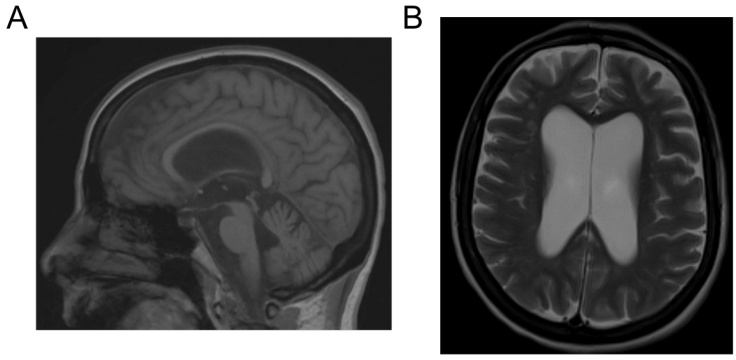

Figure 4. Brain imaging
(A) Sagital and (B) axial MRI images of the *GOSR2*-PME depicting cerebral and cerebellar atrophy.

While EEG revealed generalized, epileptiform activity, a photo-paroxysmal response and an overall slowed background, nerve conduction studies and EMG recordings were normal. The patient's serum creatine kinase levels were within normal limits, as opposed to several previous *GOSR2*-PME patients who displayed significant elevations (Boissé Lomax et al., 2013). Seizures were effectively supressed and myoclonus partially reduced with a combination of valproate, clonazepam, primidone and levetiracetam.

Prior to our finding of this novel *GOSR2* mutation several other genetic tests had been performed on this patient. No *CSTB* expansion could be detected, and sequencing of all *CSTB* exons did not reveal any mutation. Sequencing of the exons and the flanking intronic regions of *PRICKLE1* did not reveal any sequence alterations, and no expansion could be detected in *SCA1-3*.

No other family member was reported to suffer from a similar syndrome as the patient described here. Her brother suffers from primary cervical dystonia and he is heterozygous for the c.430G>T mutation but does not carry the novel c.491-494delAGA mutation. A maternal uncle was reported to suffer from ‘athetoid cerebral palsy’. The patient had two healthy sons. One of them was genetically tested and found to be heterozygous for c.491-494delAGA and not carry c.430G>T.

2.5 Discussion

In the present study I identified a novel c.491-494delAGA (p.K164del) *GOSR2* mutation in a patient suffering from progressive myoclonus epilepsy, who harboured the previously described c.430G>T (p.G144W) variant on her second *GOSR2* allele. Importantly, this is thus far the only variant besides the previously reported G144W mutation, which was homozygous in all *GOSR2*-PME patients described previously (Boissé Lomax et al., 2013; Corbett et al., 2011; van Egmond et al., 2014; 2015).

The clinical presentation of our patient recapitulates many characteristic features of *GOSR2*-PME, including an early disease onset around 2 years of age with ataxia, as well as areflexia, worsening of symptoms during febrile episodes and remarkably preserved cognitive function with only a mild deterioration later in the disease course. Other *GOSR2*-PME associated features were not present in the patient presented herein. She did not have elevated creatine kinase levels, nor EMG abnormalities, syndactyly or pes cavus. While MRI studies in previous *GOSR2*-PME cases were mostly unremarkable – except in two patients where atrophy of the cerebellar vermis or asymmetric cerebral and cerebellar atrophy was reported (Boissé Lomax et al., 2013) – the compound heterozygous patient described here displayed cerebral and cerebellar atrophy. This could not be solely attributed to her comparable high age, because these changes were already noted in her thirties. Our patient appears to have suffered from a milder disease course given that she lived up to 62 years and several other patients with this syndrome died around 30 years (Boissé Lomax et al., 2013). She was ambulant until her thirties and not wheelchair bound since the second decade of life as several other patients with this disease, which further suggests a less aggressive disease course. This might be due to normal variability within the phenotypic spectrum of *GOSR2*-PME. Alternatively, this could also be a consequence of the different mutation (K164del) that this patient carries in the compound heterozygous state with the original mutation (G144W). This possibility was addressed in experimental studies investigating the functional consequences of both disease associated mutations and is summarized in the following two chapters. However, solely

by a priori assessment of the location of both mutations, we would expect the novel c.491-494delAGA variant to confer more severe defects, not less. This mutation causes the deletion of one of two consecutive lysines (either K163 or K164) in Membrin's C-terminal half of the SNARE domain. Given that C-terminal SNARE zippering is critical for force generation, this change should result in more profound lipid fusion rate deficiencies as compared to G144W, a missense mutation in the N-terminal half of Membrin SNARE domain (Gao et al., 2012).

In summary, I discovered a novel PME associated *GOSR2* mutation, which further reinforces the relevance of this gene to PME and provides an additional allele in the quest to uncover the disease mechanism of this unresolved disorder.

Chapter 3. Investigating the pathophysiology of *GOSR2* mediated progressive myoclonus epilepsy in patient-derived fibroblasts

3.1 Introduction

Chapter 3 and Chapter 4 summarize the main project carried out during my PhD research, where we investigated *how* mutations in the Golgi SNARE protein Membrin – encoded by the *GOSR2* gene – cause the severe neurological syndrome progressive myoclonus epilepsy (PME). When I started my PhD, the G144W *GOSR2* mutation had been demonstrated to cause PME (Boissé Lomax et al., 2013; Corbett et al., 2011; van Egmond et al., 2014). In the first year of my research I identified a novel K164del *GOSR2* mutation associated with this syndrome (see previous chapter) (Praschberger et al., 2015). Yet *how* these mutations give rise to this complex neurological disorder was completely obscure. Thus, we set out to answer this question. At a first glance this question appears to be quite narrow. However, upon closer examination it turns out to be broad. This has its origins in the fact that a human disease phenotype always is a complex phenomenon where several cellular processes – downstream of the initial pathogenic 'insult' – interact to give rise to symptoms and clinical signs. Accordingly, we can understand and study any human disorder at varying degrees of magnification. As in microscopy, the most zoomed view will provide exquisite details but necessarily omit the wider context. Vice versa will a zoomed out perspective provide a high level understanding but overlook relevant details. Each of these levels of understanding will have their own disease *mechanisms* at heart, which together will ultimately provide a comprehensive explanation of an observed disease phenotype. Fortunately, we know which are the first causes of this form of progressive myoclonus epilepsy – they are sequence alterations in the *GOSR2* gene, which will eventually translate into SNARE domain mutant forms of the Golgi SNARE protein Membrin. Given that every molecule in a cell and every cell in a multicellular organism is embedded in a plethora of direct and indirect

interdependencies, these Membrin mutations (and every other pathogenic insult at the heart of different disorders) will have a wide range of molecular and cellular consequences. Some of these consequences will be directly relevant for the disorder at hand, others unimportant byproducts. This complexity and high degree of interdependency of physiological processes makes the study of their diseased states inherently blurry. Therefore, I want to rephrase our prime study aim and specify the levels of understanding we wished to achieve. The important paradox which needed to be resolved is how mutations in the *ubiquitously* important Golgi SNARE protein Membrin can give rise to a *selective* neurological syndrome with the core features of ataxia and hyperexcitability. Which aspect of the neuronal secretory pathway is special and sufficiently different to non-neuronal cell types such that a Golgi defect would show up almost exclusively in the nervous system? And how would such a defect broadly relate to a lack of coordination and an epileptic phenotype?

In order to comprehensively link the mutant *GOSR2* genotype with the PME phenotype we have to start with the most upstream cause and test how the Membrin mutations impact its ability to perform its role as a SNARE protein. From there we need to carry on and test how such alterations impact Membrin's function in facilitating anterograde cargo trafficking via the Golgi apparatus in a non-neuronal cell (this Chapter 3). After these steps, we have to enter *terra incognita* and unravel the 'neuronal bottleneck' of these mutations (Chapter 4). These investigations have the potential – if successful – to provide the key to resolve the seeming paradox of how mutations in an integral Golgi protein can give rise to a neurological disorder. They might thereby uncover the most critical disease mechanism underlying *GOSR2*-PME. After this step, we can aim to take our understanding of this disorder one level higher and try to provide a preliminary explanation how these neuronal abnormalities might impact a complex neuronal circuit in a way to give rise to ataxia and hyperexcitability.

3.2 Statement of contribution

The study summarized in Chapter 3 and Chapter 4 of this thesis is a collaborative effort with several scientists having made important contributions, both intellectually and experimentally. James Jepson was not only my primary supervisor but also a prolific experimenter on this project. He extensively characterized the effects of *membrin* mutations upon neuromuscular junction (NMJ) morphology and proteome, upon the distal axonal secretory pathway and also contributed to *Drosophila* stock generation. Nancy Malintan in James Rothman's lab performed liposome fusion assays to characterize the effects of the PME-associated Membrin SNARE motif mutations in the yeast Bos1 orthologue. She thereby provided key insight into the pathophysiology of *GOSR2*-PME at this 'highest resolution' perspective. Simon Lowe in James Hodge's and Maria Usowicz's labs performed a detailed analysis of the effects of the pathogenic Membrin mutations upon synaptic transmission at the L3 *Drosophila* neuromuscular junction (NMJ). He thus added crucial insights into the *GOSR2*-PME pathophysiology at a higher level. Carlo Giachello in Richard Baines' lab provided experimental evidence for seizure-like phenotypes of *GOSR2*-PME model *Drosophila*. Nian Patel studied the phenotypic consequences of wild-type and mutant Membrin overexpression in wild-type *membrin* animals as well as the consequences of global Membrin knock-down. Shyam Krishnakumar, Andreas Ernst and James Rothman have been critical in developing ideas and experimental strategies for this study. Several other scientists have contributed important guiding thoughts, either as a result of meetings or informal conversations.

My contributions to this project are several-fold. Being struck by the severity of the disorder during my human genetics work on *GOSR2*-PME (see above), I introduced it to the experimental neuroscience realm and assumed a leading role in intellectually and experimentally pushing towards unraveling a comprehensive disease mechanism. Experimentally, I performed the fibroblast work comprising of subcellular localization studies, Golgi trafficking assays and protein quantification. Furthermore, I generated the *GOSR2*-PME *Drosophila* models, analyzed their core organismal phenotypes (except

seizure-like behavior, see above) and uncovered the consequences of *membrin* mutations upon dendrite growth.

In the results section of this chapter I will primarily focus on my own work. However, for completeness, I will also include results from other researchers. When results were *not* obtained by myself, I will explicitly state the source of the experimental contribution. For an overview of the experimental figures, that are not based on results generated by myself, please refer to Table 8.

Figure 6	Nancy Malintan
Figure 27C, Figure 28A	Nian Patel
Figure 29C	Carlo Giachello
Figure 33D-G, Figure 36	James Jepson
Figure 37	Simon Lowe

Table 8. Experimental figures contributed by other researchers

Also, each of the respective figure legends contains a statement of the source of the contribution.

A complete and concise overview of the entire project has already been published under the title ‘Mutations in Membrin/*GOSR2* reveal stringent secretory pathway demands of dendritic growth and synaptic integrity’ (Praschberger et al., 2017).

3.3 Materials and Methods

3.3.1 Plasmids

Human *GOSR2* coding sequence (CDS of NCBI cDNA NM_004287.3) were custom synthesized by GeneArt (Thermo Fisher Scientific). A *cgac* Kozac's sequence is 5' of the initial ATG to facilitate efficient translation initiation. The start codon is directly followed by a FLAG tag coding sequence and therefore gives rise to N-terminal FLAG tagged Membrin isoforms. These constructs were 5'/3' flanked by NotI/KpnI restriction sites (for annotated sequences of the custom synthesized fragments, see Appendix) and delivered to us by the company in a pMA vector, which contains an ampicillin resistance gene. To enable transient overexpression of wild-type and mutant Membrin (encoded by the *GOSR2* gene) in mammalian cells these pMA_FLAG::*GOSR2*[WT]/[G144W]/[K164del] inserts were subcloned into pcDNA3.1(-), giving rise to pcDNA3.1(-)_FLAG::*GOSR2*[WT] /[G144W]/[K164del]. To this end, pMA_FLAG::*GOSR2*[WT]/[G144W]/[K164del] plasmids were transformed into chemically competent *E. coli* such as XL1-blue (Agilent) and amplified by overnight liquid bacterial culturing. The pcDNA3.1(-) backbone was derived from pcDNA3.1(-) mouse C/EBP beta (LAP) (Addgene plasmid #12557), which was provided as a bacterial stab culture and subsequently amplified by overnight liquid bacterial culturing. Plasmids where then extracted using the PureYield Plasmid Miniprep kit (Promega) and DNA concentrations determined with a NanoDrop 1000 spectrophotometer (Thermo Fisher Scientific). Approximately 1 µg of pMA_FLAG::*GOSR2*[WT]/[G144W]/[K164del] and pcDNA3.1(-) mouse C/EBP beta (LAP) plasmids where then double digested with NotI-KpnI (NEB) according to the manufacturers recommendations. Cut fragments were electrophoretically separated on a 1% agarose gel supplemented with [1/10000] GelRed (Biotium). After visualization on a Benchtop UV transilluminator (UVP), bands were manually excised and purified with the Wizard SV Gel and PCR clean-up kit (Promega). Subsequently, the inserts from the pMA plasmids were ligated into the cut pcDNA3.1(-) backbone with T4 ligase (Promega), transformed into chemically competent *E. coli*. and

individual colonies screened for successful subcloning by restriction digest. The presence of the correct open reading frame was then validated by Sanger sequencing with the forward (CMVF_pCDNA3: 5'-CAACGGGACTTTCCAAAATG-3') and reverse (bGH_R: 5'-TGTCCAATTATGTCACACCACAG-3') primers by Source Biosciences.

The Halo::FM4::hGH containing plasmid was previously cloned in the Rothman lab (Lavieu et al., 2013). GalT::RFP was a kind gift from Derek Toomre and encodes mTagRFP N-terminally fused to the first 82 amino acids of the human Beta-1,4-galactosyltransferase 1.

3.3.2 Bioinformatics

SNARE motifs in human and *Drosophila* Membrin, as well as yeast Bos1, were identified as described previously (Kloepper et al., 2007) and aligned with Clustal Omega (McWilliam et al., 2013). Conserved residues were highlighted using BoxShade.

3.3.3 Cell culture and transfections

Primary skin-derived fibroblasts from the first described *GOSR2*-PME patient were kindly shared by Mark Corbett (Corbett et al., 2011). As controls, we used fibroblasts from healthy individuals of either the same sex and similar age, or opposing sex and divergent age (control 1 = 23 year old female; control 2 = 60 year old male at time of biopsy; the G144W mutant Membrin fibroblasts were derived from a 32 year old female patient). Fibroblasts and HEK293T cells were grown in DMEM (Thermo Fisher Scientific) supplemented with 10% fetal bovine serum (FBS) (Thermo Fisher Scientific) at 37°C and humidified air with 5% CO_2. Fibroblast transfections were carried out with Lipofectamine 2000 (Thermo Fisher Scientific). In order to obtain a sufficient number of transfected cells of these hard to transfect cells, the following approach was taken. For paraformaldehyde (PFA) fixed analysis, 5000-7000 fibroblast cells were seeded onto 19 mm #1.5 barosilicate cover glasses (VWR) in 12-well plates and allowed to grow until 80% confluence. For live imaging, cells were seeded into 35 mm #1.5 CELLView glass bottom dishes (Greiner). 3 µg of plasmid DNA and 6 µl of Lipofectamine 2000 were

each diluted in 75 µl Opti-MEM, mixed and incubated for at least 5 min before addition to the cultures. To avoid excessive Lipofectamine toxicity complexes were removed after approximately 6-8.5 hours and washed with Dulbecco's phosphate buffered saline (DPBS) (Thermo Fisher Scientific). Human embryonic kidney (HEK293T) cells were transfected with Effectene (Qiagen).

3.3.4 Fibroblast imaging

3.3.4.1 Immuno-fluorescence microscopy

Cells were grown on 13/19 mm #1.5 glass coverslips (VWR) in 24/12-well plates and fixed in 4% PFA (Alfa Aesar) for 15 min followed by 3x phosphate buffered saline (PBS) washes and a 3 min permeabilization step in PBS supplemented with 0.3% NP40, 0.05% Triton-X 100 and 0.1% IgG free bovine serum albumin (BSA) (Sigma). Subsequently, cells were rinsed 3x in wash buffer (PBS + 0.05% NP40 + 0.05% Triton-X 100 + 0.2% IgG free BSA) and blocked for 45 min in blocking buffer (PBS + 0.05% NP40 + 0.05% Triton X-100 + 5% goat serum). Primary antibodies were diluted in blocking buffer and incubated overnight rocking at 4°C followed by 3x 5 min washes in washing buffer. Secondary antibodies were diluted in blocking buffer and incubated for 1 h rocking at room temperature. Before mounting in 2 µl SlowFade Gold (Thermo Fisher Scientific), cells were washed 3x in washing buffer for 5 min, then 3x briefly with PBS and finally immersed once in deionized water. The following antibodies were used: mouse anti-Membrin (clone 25, BD Biosciences; 1:500; this antibody was raised against Membrin residues 5-124 and therefore should not be affected by the G144W mutation.), mouse anti-FLAG (clone M2, Sigma; 1:1000), rat anti-FLAG (Agilent; 1:1000), rabbit anti-GPP130 (Cambridge Bioscience; 1:1000), rabbit anti-PDI (Sigma; 1:500), mouse anti-GM130 (clone 35, BD Biosciences; 1:1000), mouse anti-p230 (clone 15, BD Biosciences; 1:250), rabbit anti-ERGIC-53 (Sigma, 1:500) and goat anti-mouse/rabbit/rat Alexa Fluor 488/555/647 conjugated secondaries (Thermo Fisher Scientific; 1:500). Samples were imaged on inverted confocal Zeiss LSM710 or LSM880 microscopes with 63x 1.4NA oil immersion objectives.

3.3.4.2 hGH Golgi trafficking assay

For Golgi trafficking studies cells were loaded with HaloTag tetramethylrhodamin (TMR) Ligand (Promega) 24 h post transfection with Halo::FM4::hGH according to the manufacturer's protocol. Fibroblasts were incubated for 15 min with [1/1000] TMR ligand, subsequently washed with medium 3x and incubated for a further 30 min at 37°C to remove unbound ligand. Thereafter medium containing 1.5 µM D/D solubilizer (Clontech) was added in order to release the aggregated and therefore ER retained Halo-TMR::FM4::hGH cargo. Subsequently fibroblasts were PFA fixed. In order to microscopically correlate the cargo derived TMR signal with the cis-Golgi, I stained this compartment with an anti-GM130 antibody as outlined above. Imaging was carried out with a Plan-Apochromat 63x 1.4 NA oil immersion objective on a Zeiss confocal LSM880 microscope. Halo-TMR::FM4::hGH – GM130 Pearson's correlation coefficients (PCC) were extracted with the Coloc 2 ImageJ plugin.

3.3.4.3 GalT::RFP FRAP

For fluorescence recovery after photobleaching (FRAP) studies I imaged GalT::RFP transfected fibroblasts in 35 mm glass bottom dishes 24 h post transfection with a Plan-Apochromat 63x 1.4 NA oil immersion objective on a Zeiss confocal LSM880 microscope. The phenol red containing DMEM used for culturing these cells was exchanged for DMEM without this pH indicator (Thermo Fisher Scientific) in order to reduce background fluorescence. Temperature was maintained at 37°C throughout the experiment with an environmental chamber and a stage heater. The temperature of the imaging system was allowed to equilibrate for at least 30 min in order to warrant that all microscope parts in proximity to the cells – such as the objective – reached 37°C. In addition, the imaging chamber was perfused with humidified air supplemented with 5% CO_2. The pinhole was fully opened in order to also collect photons derived from Golgi resident GalT::RFP above and below the optical plane. Every 30 s one frame was acquired – 4 pre- and 40 post-bleach. To achieve effective focus correction and thereby remain in the intended optical plane over this comparably long acquisition time, Definite

Focus (Zeiss) was used. Photobleaching was carried out by scanning the entire Golgi resident GalT::RFP twice at 100% transmission of the 561 nm laser line, which decreased mean fluorescence intensity in this area by at least 84%. Only cells with low GalT::RFP expression levels were selected for these experiments. All image processing and analysis was carried out in Fiji.

3.3.5 Western blot

For western blot studies, fibroblasts were grown in 10 cm dishes and HEK293T cells in 6-well plates. 200/300 µl lysis buffer (HEPES-NaOH pH 7.5 20 mM, KCl 100 mM, glycerol 5%, EDTA 10 mM, Triton X-100 1%, 1x PhosSTOP™ phosphatase inhibitor cocktail (Roche), 1x cOmplete™ protease inhibitor cocktail (Roche)) was added to each 10cm dish/6-well of PBS washed fibroblasts or FLAG::*GOSR2*[WT] overexpressing or native HEK293T cells and incubated at -80°C for 1 min followed by resuspension. Lysed cells were centrifuged at 16 000 g, 4°C for 10 min and the liquid phase transferred to a fresh Eppendorf tube. Protein concentrations were quantified with the Pierce 660 nm Protein Assay (Thermo Fisher Scientific). Equal amounts of protein (5 µg for fibroblasts, 15 µg for HEK293T lysates) were used per lane of a 10-well, 1.5 mm NuPAGE Novex 4-12% Bis-Tris Protein Gel (Thermo Fisher Scientific). Prior to electrophoresis in a XCell SureLock Mini-Cell with 1x NuPAGE MOPS SDS running buffer and NuPAGE Antioxidant (Thermo Fisher Scientific), protein was denaturated for 10 min at 70°C in 1x NuPAGE LDS Sample Buffer (Thermo Fisher Scientific) supplemented with 50 mM DTT (Sigma). Protein was allowed to enter the gel at 80V for 10 min and then separated for 90 min at 160 V. The transfer onto an Immobilon-P PVDF (Millipore) membrane was carried out with the XCell II Blot Module (Thermo Fisher Scientific) in Tris-glycine-methanol transfer buffer (20 mM Tris, 150 mM glycine, 20% methanol) at 30 V for 90 minutes. Successful transfer was validated by visualizing protein bands with Ponceau S solution (Sigma). Remaining Ponceau S solution was removed by washing the membrane in tris buffered saline Tween 20 TBST (Tris HCl pH 7.5 10 mM, NaCl 140 mM, Tween 20 0.1%) and then blocked in a rotating 50 ml Falcon tube in TBST supplemented with 5% dried skimmed milk powder for 1 h at room temperature. Primary and secondary antibodies were diluted in

TBST+5% dried skimmed milk powder and incubated in a 50 ml rotating Falcon tube overnight 4°C and 2 h at room temperature respectively. The following antibodies were used: mouse anti-Membrin (clone 25, BD Biosciences; 1:2000), rabbit anti-Membrin (Synaptic Systems, 1:2500), rabbit anti-hamster Syntaxin-5 (Rothman lab; 1:1000; Orci et al., 2000), rabbit anti-Sec22b (Rothman lab; 1:1000; Volchuk et al., 2004), rabbit anti-rat Bet1 (Rothman lab; 1:1000; Volchuk et al., 2004), mouse anti-β-actin (clone AC-74, Sigma; 1:5000) and HRP-conjugated anti-mouse/rabbit secondaries (Jackson Immuno; 1:2500-8000). In case PVDF membranes were re-probed for proteins of similar molecular weight as previously tested proteins they were stripped with Restore Western Blot stripping Buffer (Thermo Fisher Scientific), followed by a 1 h blocking step and the above outlined antibody incubations. For semi-quantitative western blots, detection was carried out with SuperSignal West Pico Chemiluminescent Substrate (Thermo Fisher Scientific) and a ChemiDocTM Imaging system (Bio-Rad). Band intensities were extracted with Image Studio Lite (Li-cor). Alternatively, signal was detected with FUJI RX X-Ray films after incubation with SuperSignal West Pico Chemiluminescent Substrate (Thermo Fisher Scientific).

3.4 Results

3.4.1 *GOSR2*-PME mutations cause *partial* SNARE dysfunction

To assess the disease mechanism of *GOSR2*-PME at the highest possible resolution, we first have to turn our investigation towards the molecular changes encoded by the *GOSR2* mutations. Both pathogenic mutations result in amino acid changes within the evolutionarily conserved Membrin SNARE domain (Figure 5). Such alterations suggest impaired SNARE complex formation with its cis-Golgi partner SNAREs Bet1, Sec22b and Syntaxin-5. Physiologically this process is thought to occur via N- to C-terminal zippering along stereotypically spaced interacting layer amino acids (ranging from -7 to +8) within the respective SNARE domains (Figure 5) (Fasshauer et al., 1998; Gao et al., 2012). Both *GOSR2*-PME disease mutations – G144W and K164del – affect this critical layered structure, which directly suggests that cis-Golgi SNARE complex assembly might be impaired.

Figure 5. Membrin SNARE domain sequence alignment
SNARE domain alignment of *Homo sapiens* (*Hs*), *Drosophila melanogaster* (*Dm*) and *Saccharomyces cerevisiae* (*Sc*) Membrin (uniprot ID O14653-1), Membrin (Q9VRL2) and Bos1 (P25385) respectively. Conserved residues are highlighted in black, similar residues in grey. Layer amino acids critical for forming the tetrameric cis-Golgi SNARE complex are indicated in green. The disease-causing G144W and K164del (one of two consecutive lysines is deleted) and their *Drosophila* and *yeast* orthologous residues are highlighted in blue and red.

This hypothesis was tested by Nancy Malintan in James Rothman's lab and I will briefly summarize her key findings, as they represent the fundament of the experimental pyramid described in this thesis. Nancy Malintan performed liposome fusion assays with the wild-type and mutant Membrin yeast orthologue Bos1 and its respective yeast partner SNAREs (Bet1, Sec22 and Sed5). Yeast proteins where chosen because of inherent difficulties of working with purified mammalian Syntaxin-5 and because yeast Golgi

SNARE liposome fusion assays represent a well established experimental system (Parlati et al., 2000; 2002). Golgi SNARE proteins are conserved throughout eukaryotic evolution, which is why our experimental results derived from yeast will likely also be applicable to human (Kloepper et al., 2007). The validity of our approach is further reinforced by observations that mammalian and yeast Golgi SNARE can be functionally interchangeable in liposome fusion assays and living cells (Fischer von Mollard and Stevens, 1998; McNew et al., 1997; Varlamov et al., 2004). To determine the functional impact of Bos1/Membrin SNARE motif mutations Nancy Malintan introduced purified Bet1 into one liposome population, wild-type or G176W/D196del (orthologous to G144W/K164del in human Membrin) mutant Bos1, Sec22 and Sed5 in another population and read successful fusion after mixing of the two populations with a Förster resonance energy transfer (FRET) based approach. This readout is based on the de-quenching of the NBD-rhodamine FRET pair as a result of fusion induced spatial separation of the lipid tethered fluorophores (Struck et al., 1981). Consistent with the predictions Nancy Malintan found that both yeast orthologous Bos1 mutations caused reduced fusion rates, which were nevertheless larger than negative control, where Bet1 was omitted (Figure 6A, B).

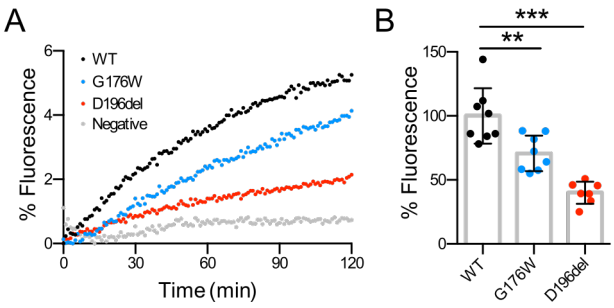

Figure 6. Reduced liposome fusion rates due to *GOSR2*-PME mutations
(A) Example traces showing increase in NBD fluorescence due to liposome fusion between wild-type and G176W/D196del mutant Bos1 containing liposome fusion reactions. Expressed as a fraction of maximal NBD fluorescence after addition of detergent.
(B) Endpoint (120 min) quantification of experiment as described in (A), normalized to wild-type. n = 8, 8, 7 for WT, G176W and D196del. Replicate values derived from repeat experiments, mean and SD are shown. **, *** represent $p < 0.01$, 0.001; ANOVA with Dunnett's multiple comparison test.
These experiments were performed and analysed by Nancy Malintan in James Rothman's laboratory.

These findings suggest that the *GOSR2*-PME mutations cause *partial*, and not complete loss of function. In addition, Nancy Malintan found that the effect size scaled with the nature of the change. The missense mutation (G176W) in the N-terminal half of the Bos1 SNARE domain had a more subtle effect, while the deletion mutation (R196del) in the C-terminal half of the Bos1 SNARE domain was more deleterious (Figure 6A, B). This is consistent with the critical importance of SNARE complex C-terminal zippering for force generation (Gao et al., 2012) and a probable misalignment of the C-terminal layers +3 to +8 as a result of the single amino acid deletion. In summary, we can infer from these yeast liposome fusion studies that the G144W and K164del Membrin mutations likely cause a partial decrease of cis-Golgi SNARE complex formation, and in turn reduced membrane fusion of ER-derived vesicles with the Golgi apparatus and ER-Golgi intermediate compartment (ERGIC).

3.4.2 Mutant Membrin retains the capability to localize to the cis-Golgi

Only Membrin localized to the Golgi and ERGIC will be capable of mediating ER-to-Golgi transport via fusing opposing lipid bilayers together with its partner SNAREs Bet1, Syntaxin-5 and Sec22b. Previous electron microscopy immuno-gold studies have established that Membrin physiologically localizes primarily to the cis-Golgi as well as to the ERGIC (Hay et al., 1998; Volchuk et al., 2004). Thus, in a first step – in order to serve as an internal control and to confirm these findings in the experimental system of this study – I have tested these findings with indirect immuno-fluorescence confocal microscopy in primary skin fibroblasts derived from a healthy human. It has to be noted however, that by doing so, we are pushing the boundaries of diffraction limited optics (maximum 200 nm resolution) and therefore will not be able to unambiguously distinguish between the ERGIC in Golgi proximity – as opposed to the peripheral ERGIC next to ER exit sites – as well as cis- from trans-Golgi. Nevertheless, this system is sensitive enough to evaluate whether Membrin is correctly localized within the Golgi area and if so, whether it is shifted towards the cis-Golgi/ERGIC or trans-Golgi/trans-Golgi network. At the light microscopy level I found a high degree

of colocalization of endogenous Membrin with the cis-Golgi marker GPP130, the ERGIC marker ERGIC-53 and a less colocalization with the trans-Golgi marker p230 (Figure 7A, B). These findings are consistent with the previously established predominant localization of Membrin in the cis-Golgi and ERGIC, and therefore confirm the validity of my imaging approach.

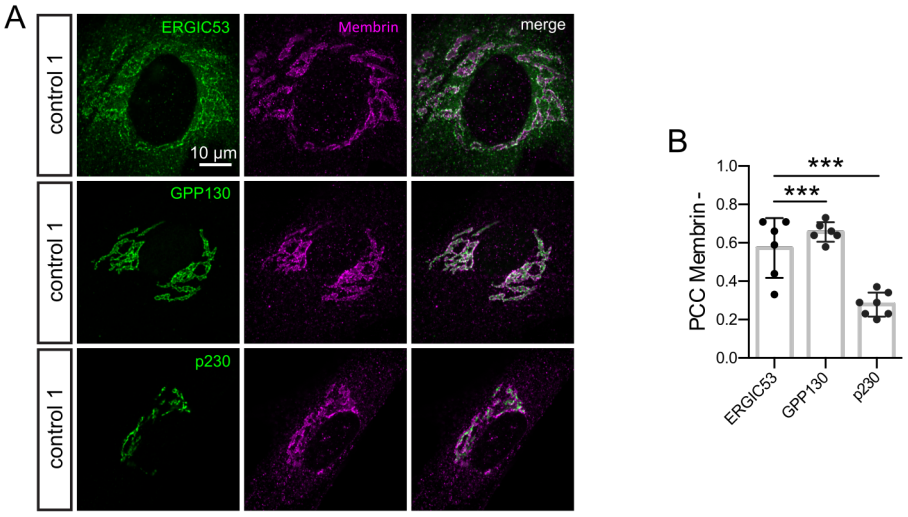

Figure 7. Subcellular localization of endogenous Membrin
(A) Example confocal slices of human control fibroblasts co-stained for Membrin and the ERGIC, cis- and trans-Golgi markers ERGIC53, GPP130 and p230 respectively.
(B) Pearson's correlation coefficients (PCC) of experiment as outlined in (A). N = 6, 6 and 7 for ERGIC53, GPP130 and p230. Replicate values derived from individual cells of one experiment, mean and SD are shown. *** represents $p < 0.001$; ANOVA with Dunnett's multiple comparison test.

Corbett et al. suggested that G144W mutant Membrin fails to localize to the Golgi apparatus (Corbett et al., 2011). This observation implies that the G144W Membrin mutation confers complete loss of function due to an absence from its target compartment, which however would not be compatible with organismal life. In addition, the partial membrane fusion defects observed in liposome fusion studies are only relevant for impacting ER-to-Golgi trafficking rates if mutant Membrin also localizes to its native site of action – the ERGIC and cis-Golgi. This is why we tested whether Membrin harboring the SNARE motif mutations could in principle localize to these sites. To this end I overexpressed wild-type or G144W/K164del mutant Membrin in primary human skin fibroblasts derived from a healthy control and assessed their subcellular localization with confocal microscopy. The

Membrin constructs were N-terminal fused to a FLAG tag in order to be able to distinguish the transgenically expressed Membrin from the endogenous protein. Overexpressed wild-type as well as mutant Membrin successfully exited the ER, which is apparent from confocal images where the FLAG staining did not overlap with the ER resident enzyme protein disulfide isomerase (PDI) (Figure 8A, B).

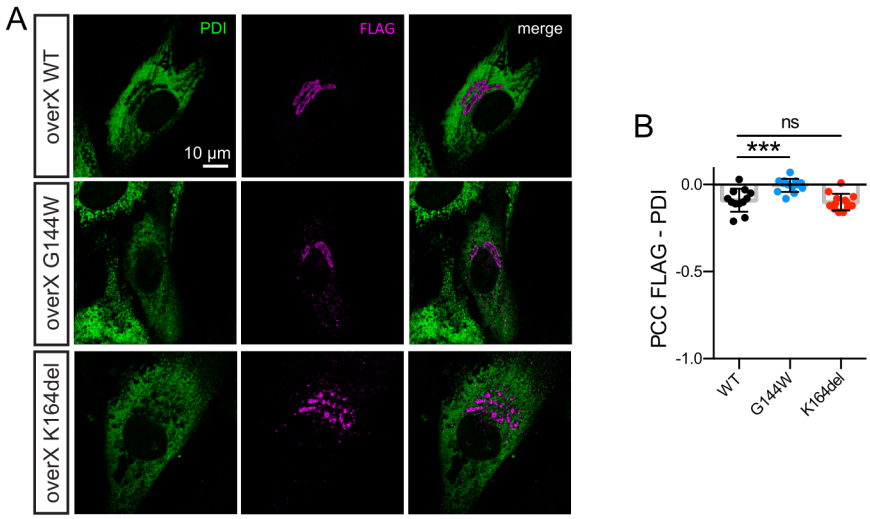

Figure 8. Mutant Membrin successfully exits the ER
(A) Example confocal slices of wild-type, G144W and K164del FLAG-tagged Membrin overexpressed in control fibroblasts. Cells were co-stained for FLAG and the ER resident protein PDI. Comparable results were obtained in HEK293T cells.
(B) Pearson's correlation coefficients (PCC) of experiment as outlined in (A). N = 12, 13, 13 for WT, G144W, K164del. Replicate values derived from individual cells of one experiment, mean and SD are shown. *** represents $p < 0.001$, ns = not significant ($p > 0.05$); ANOVA with Dunnett's multiple comparison test.

In contrast, overexpressed wild-type and mutant Membrin localized to the cis-Golgi, as colocalization of all FLAG::Membrin variants with the cis-Golgi marker GPP130 was apparent (Figure 9A). Nevertheless, a subtle but statistically significant decrease of colocalization was present in G144W and K164del compared to wild-type Membrin when Pearson's correlation coefficients were extracted (Figure 9B). I speculate that this finding might be explained by a decrease of cis-Golgi entry of mutant Membrin due to SNARE defects and a consecutive build-up of mutant Membrin containing vesicles adjacent to the cis-Golgi. To confirm this idea immuno-gold electron

microscopy would have to be carried out, which however surpasses the scope of these experiments.

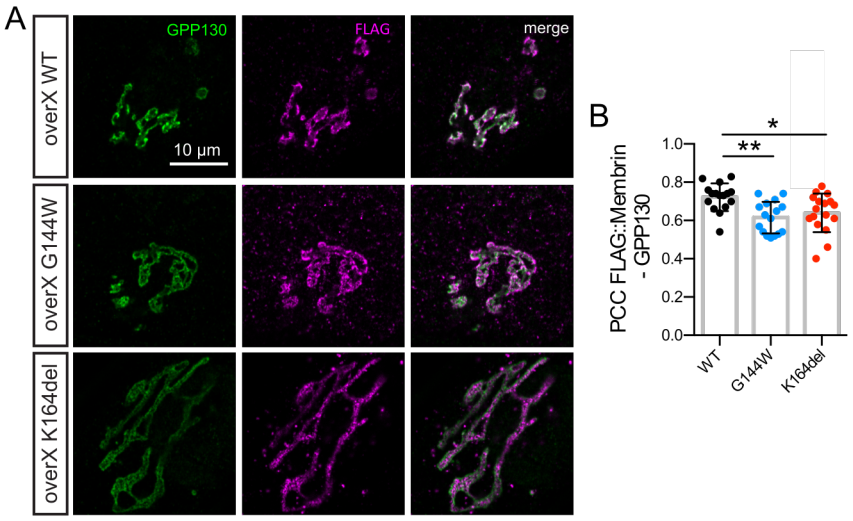

Figure 9. Mutant Membrin localizes to the cis-Golgi
(A) Example confocal slices of wild-type, G144W and K164del FLAG-tagged Membrin overexpressed in control fibroblasts. Cells were co-stained for FLAG and the cis-Golgi resident protein GPP130. Comparable results were obtained in HEK293T cells.
(B) Pearson's correlation coefficients (PCC) of experiment as outlined in (A). N = 16, 16, 17 for WT, G144W, K164del. Replicate values derived from individual cells of one experiment, mean and SD are shown. *, ** represent $p < 0.05, 0.01$; ANOVA with Dunnett's multiple comparison test.

To test whether also endogenous G144W mutant Membrin could localize to this compartment, we re-examined the patient fibroblasts from the original *GOSR2*-PME study (Corbett et al., 2011). Prior to performing experiments with these fibroblasts, which where kindly shared by Mark Corbett, I confirmed the presence of the *GOSR2* gene alteration that gives rise to G144W mutant Membrin by means of Sanger sequencing (Figure 10).

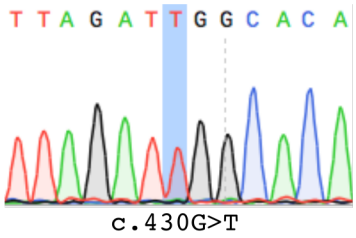

Figure 10. Sequence confirmation of G144W mutant Membrin fibroblasts
Fibroblasts derived from a *GOSR2*-PME patient were sequenced prior to performing experiments in order to confirm the presence of the pathogenic c.430G>T nucleotide alteration in exon 5 of the *GOSR2* gene. This change gives rise to G144W mutant Membrin.

Next, I examined the specificity of commercially available anti-Membrin antibodies. A mouse monoclonal Membrin antibody purchased from BD Biosciences appeared specific in western blot, as it detected a band around the expected 25 kDa molecular weight (Figure 11A). Also, in immuno-fluorescence microscopy it clearly recognized the overexpressed protein (Figure 11B). This antibody was used for western blot quantifications and immuno-fluorescence microscopy presented in this thesis. Exceptions to this are the anti-p230 co-staining (Figure 7), which required a non-mouse anti-Membrin antibody and one control western blot (Figure 13D). For these experiments I used a Synaptic Systems polyclonal rabbit anti-Membrin antibody, which detected Membrin in western blot and recognized the overexpressed protein in immuno-fluorescence microscopy (Figure 11C, D).

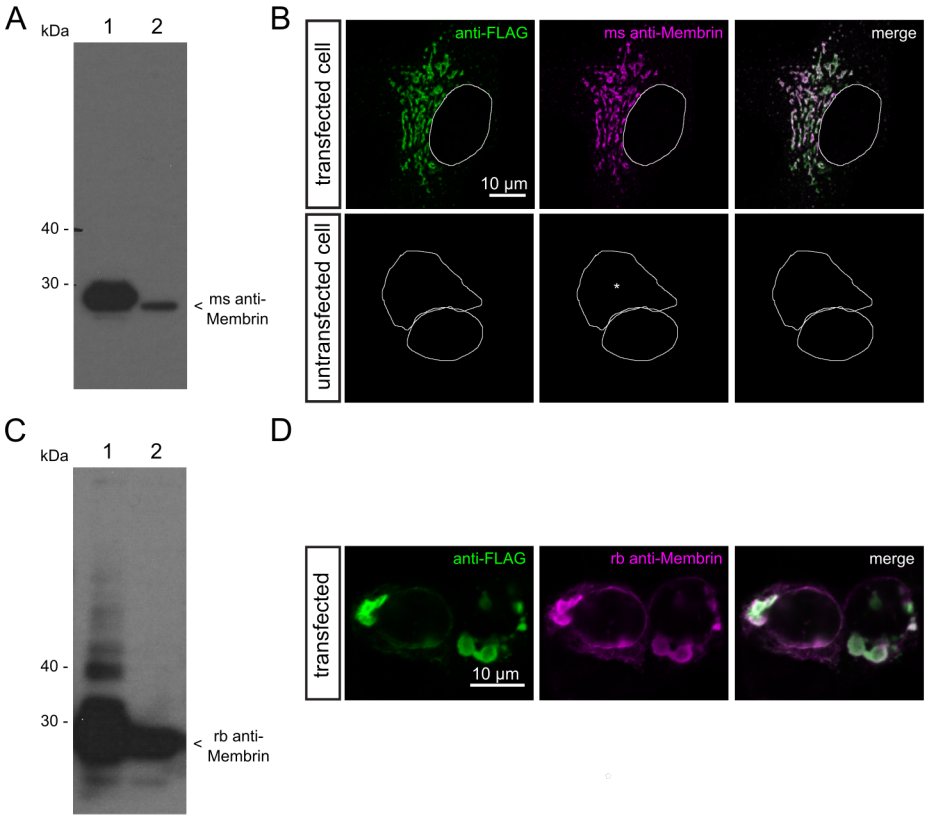

Figure 11. Anti-Membrin antibody validation
(A) The mouse (ms) monoclonal Membrin antibody used in this study exhibits specificity in western blot. Only one band around the expected molecular weight of approximately 25 kDa is apparent. Equal total protein amounts of HEK293T cell lysate (lane 2) or HEK293T cells overexpressing WT FLAG::Membrin (lane 1) were probed.
(B) The mouse monoclonal Membrin antibody used in this study recognizes wild-type FLAG::Membrin overexpressed in control fibroblasts and processed with the same immuno-fluorescence protocol. Top row shows an overexpressing cell, where Membrin and FLAG signal clearly colocalize. At identical settings, endogenous Membrin cannot be seen in an untransfected cell. Boundaries of nuclei and Golgi region (*), as seen by Membrin signal at much higher contrast settings, are outlined.
(C) Western blot of HEK293T cell lysate (lane 2) or HEK293T cells overexpressing WT FLAG::Membrin (lane 1) with the rabbit (rb) polyclonal Membrin antibody, which was used in this study. One strong band around the expected molecular weight of approximately 25 kDa is apparent. Also, one lower molecular weight band and several of higher molecular weight are visible, albeit of much weaker signal intensity.
(D) Two HEK293T cells overexpressing WT FLAG::Membrin are shown, where FLAG and rabbit anti-Membrin staining colocalise.

Utilizing this validated antibody, Membrin could clearly be detected at the cis-Golgi of G144W mutant fibroblasts (Figure 12A, B) and did not appear to accumulate in the ER (Figure 12C), thereby confirming our overexpression results also in patient cells harboring endogenous G144W mutant Membrin.

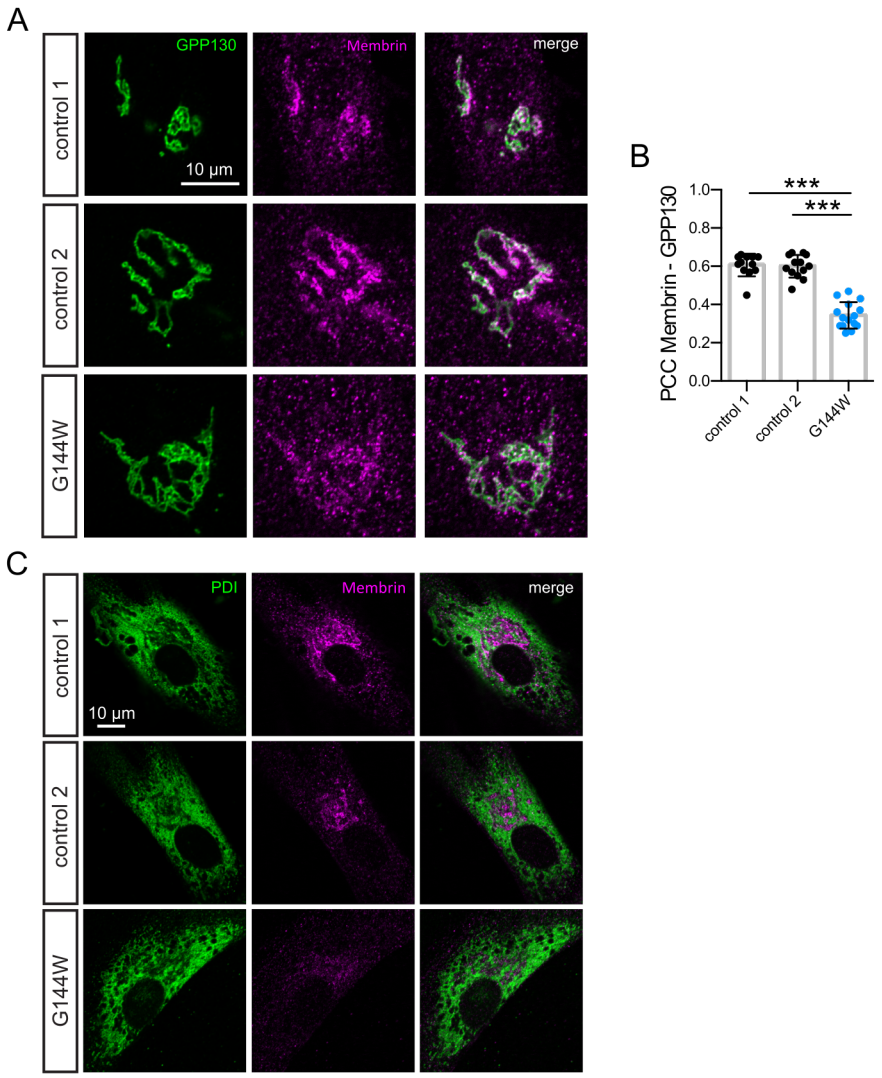

Figure 12. Endogenous G144W mutant Membrin localizes to the Golgi
(A) Example confocal slices of control and G144W mutant Membrin fibroblasts co-stained for Membrin and GPP130. Membrin in control and G144W mutant fibroblasts localized to the Golgi apparatus. However, G144W Membrin levels in the Golgi area was greatly reduced as compared to both controls. This was also seen in several repeat anti-Membrin stainings.
(B) Pearson's correlation coefficients between endogenous Membrin and GPP130 signals of the experiment described in (A) are shown. N = 12, 13, 15 for control 1, control 2, G144W. Replicate values derived from individual cells of one experiment, mean and SD are shown. **, *** represent $p < 0.01$, 0.001, ANOVA with Dunnett's multiple comparison test.
(C) Example confocal slices of control and G144W mutant Membrin fibroblasts co-stained for the ER resident protein PDI.

Taken together our subcellular localization experiments suggest that both the G144W and K164del mutant forms of Membrin retain their intrinsic capability to localize to their cis-Golgi target compartment. This suggests that the partial SNARE domain deficiencies as found in liposome fusion assays by

Nancy Malintan are likely also relevant in determining lipid bilayer fusion rates at the cis-Golgi in a living cell.

3.4.3 Reduced levels of G144W mutant Membrin

While overexpressed and endogenous G144W mutant Membrin could also be detected at the cis-Golgi, Membrin levels in the Golgi area of G144W mutant fibroblasts were significantly decreased when compared to controls as measured by quantitative immuno-fluorescence (Figure 13A). Western blots confirmed an overall reduction of Membrin levels in mutant fibroblasts (Figure 13B, C). Because Corbett et al reported unchanged Membrin levels in the same cell line, I utilized an independent rabbit polyclonal antibody to confirm this finding (Figure 13D).

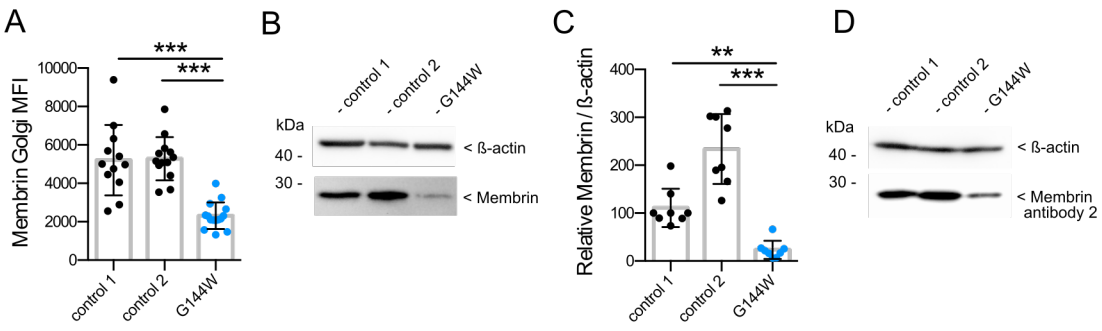

Figure 13. Reduced Membrin levels in G144W mutant fibroblasts
(A) Membrin mean fluorescence intensity in the Golgi region as demarcated by GPP130 of experiment as described in Figure 12A. N = 12, 13, 15 for control 1, control 2, G144W. Replicate values derived from individual cells of one experiment, mean and SD are shown.
(B) Western blot of lysates from control and G144W Membrin fibroblasts is shown.
(C) Quantification of experiment as described in (B). N = 8 replicate values, derived from three independent lysates per genotype and immunoblotted twice/three times. Mean and SD are shown.
(D) Western blot of lysates from control and G144W Membrin fibroblasts is shown utilizing a different anti-Membrin antibody as in (B).
Replicate values, mean and SD are shown. **, *** represent $p < 0.01$, 0.001, ANOVA with Dunnett's multiple comparison test.

If fewer cis-Golgi SNARE complexes are formed, either due to a SNARE domain defect or the presence of fewer Membrin molecules at the cis-Golgi, Membrin's partner SNAREs might also be present at different levels. I tested this notion with western blot, where Bet1, Syntaxin-5 and Sec22b levels

appeared grossly unchanged between G144W mutant fibroblasts and either control (Figure 14).

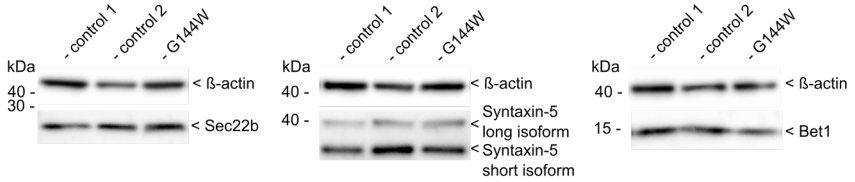

Figure 14. Western blot of Membrin's partner SNAREs
Equal amounts of lysates derived from healthy control or G144W mutant Membrin fibroblasts were loaded into each lane. Immuno-detection was carried out with anti-Bet1, Syntaxin-5 and Sec22b antibodies. β-actin served as a loading control. Note that Syntaxin-5 exists as a long and a short isoform. Similar results were obtained with three independent lysates using each of the depicted antibodies.

In summary, we found reduced Membrin levels in G144W fibroblasts, while the relative amounts of its partner SNARE proteins remained largely unchanged. The availability of fewer G144W mutant Membrin molecules at the ERGIC and cis-Golgi could provide an additional mechanism – besides the SNARE dysfunction as observed in liposome fusion studies – of delaying membrane fusion at the ERGIC/cis-Golgi.

3.4.4 Intact ER-to-Golgi trafficking in G144W fibroblasts

To assess how SNARE dysfunction – and potentially how reduced amounts of G144W mutant Membrin at the cis-Golgi – affect ER-to-Golgi transport in a non-neuronal cell, I performed Golgi trafficking assays in control and G144W mutant Membrin fibroblasts. Therefore I overexpressed human growth hormone (hGH) fused to four FM domains and a Halo-tag. The FM domains self-aggregate in the absence of a solubilizing drug and thus do not allow ER exit of this model cargo (Rivera et al., 2000; Rollins et al., 2000). When D/D solubilizer is added, this chimeric protein disaggregates and enters the secretory route, where it can be optically visualized after addition of a Halo-tag TMR ligand.

I co-stained for the cis-Golgi resident protein GM130 in order to be able to test the colocalization of the cargo with this compartment as a function of time. To obtain quantitative information I assessed the degree of TMR-

GM130 covariance in the Golgi region by computing Pearson's correlation coefficients (PCC). The validity and interpretation of this measure of colocalization critically depends upon well controlled image acquisition conditions (Dunn et al., 2011), which is particularly important when trying to assess small effect sizes such as are expected in our case. Therefore I performed technical controls prior to commencing the extensive image acquisition for this experiment. No substantial chromatic shift between the two acquisition channels – green and red – were detected with 0.5 and 0.1 µm TetraSpeck beads (Figure 15A). In addition, the full width at half maximum of the X-Y point spread function for both channels indicated adequate resolving capabilities for the employed confocal system (Figure 15B) (Cole et al., 2011).

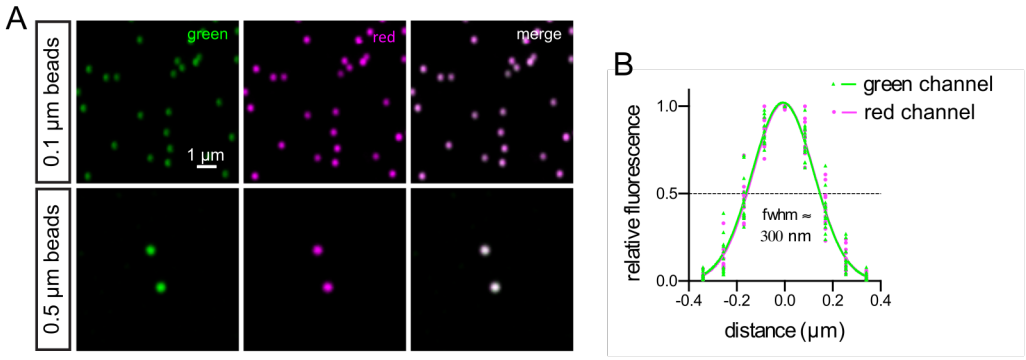

Figure 15. Optical properties of the imaging setup
(A) Confocal slices of 0.1 or 0.5 µm TetraSpeck beads acquired with green and red acquisition settings as used for the TMR-GM130 colocalization studies (see Figure 17).
(B) X-Y point spread function derived from 0.1 µm TetraSpeck beads as shown in (A). Normalized pixel values (circles and triangles), Gaussian fit (lines) and full width at half maximum (fwhm) are depicted. N = 13 beads from one experiment.

Finally, I evaluated the prediction that 'perfect' colocalization should yield a PCC of 1, while no colocalization should yield 0. To this end I stained control fibroblasts with a rabbit anti-GPP130 primary antibody and two anti-rabbit secondary antibodies – one conjugated with an Alexa Fluor 488 and the other one with Alexa Fluor 555 (Figure 16A). Indeed, this yielded a PCC of approximately 1 (Figure 16B). If one channel was turned by 90° and therefore a purely random relationship modeled, the PCC dropped to approximately 0 (Figure 16B). In addition, bleed-through or potential dye

cross-reactivity between the green and red acquisition channels were not present in my sample preparation and imaging settings (Figure 16C). In summary, these technical controls suggested that the experimental system was thoroughly calibrated and therefore capable of delivering meaningful quantitative results.

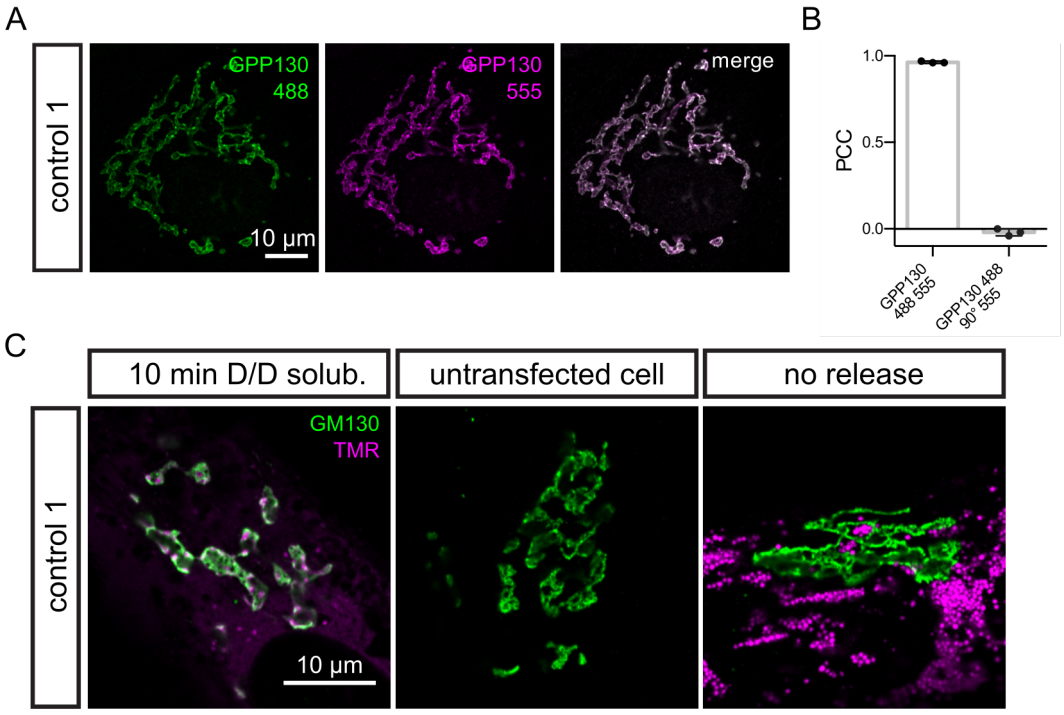

Figure 16. PCC and bleed through controls
(A) Healthy control fibroblasts were stained with an anti-GPP130 antibody and colocalization of Alexa Fluor 488 and 555 tagged secondary antibodies detected in single confocal slices.
(B) Pearson correlation coefficients (PCC) of experiment (A) were computed either in the original acquisition image orientation, or with one channel rotated by 90° in respect to the other channel. N = 3 individual cells from one experiment. Mean and SD are shown.
(C) Confocal control images showing no bleed-through or dye cross-reactivity between the green and red acquisition channels. Control fibroblasts were stained with anti-GM130 (cis-Golgi) and Halo-tag TMR ligand. They were imaged with identical laser intensities and gain settings and are shown with the same contrast settings. Image one depicts an experimental image as analysed in Figure 17, were the artificial secretory pathway cargo Halo::FM4::hGH was transfected and released from the ER via the addition of D/D solubilizer (see below). Colocalisation between the GM130 and TMR signals is apparent. Image two depicts a cell that was not transfected with Halo::FM4::hGH but loaded with TMR. Only green, but no red fluorescence can be observed. Image three shows a cell where Halo::FM4::hGH was transfected but not released from the ER. Thus, GM130 and TMR anti-localise and no green fluorescence can be seen in the regions were red signal is detected.

After completion of the above technical validations and thereby gained confidence into the accuracy of my imaging set-up I imaged G144W mutant and control fibroblasts with no release and 10, 20 and 30 min after cargo release. By 10 min after the addition of D/D solubilizer cargo appeared accumulated in the cis-Golgi (Figure 17A). After 20 and 30 min cargo accumulated adjacent to the cis-Golgi and colocalization with GM130 was reduced compared to the 10 min time point (Figure 17A). In addition, vesicular structures became apparent, consistent with cargo that has successfully transitioned the Golgi apparatus and is now being distributed via the trans-Golgi network towards the plasma membrane. Remarkably, the pattern of prominent TMR-GM130 colocalization after 10 min of D/D solubilizer incubation, and a decrease by 20 and 30 min, was very similar in G144W mutant fibroblasts. This qualitative observation indicates that ER-to-Golgi trafficking in G144W fibroblasts is not grossly abnormal.

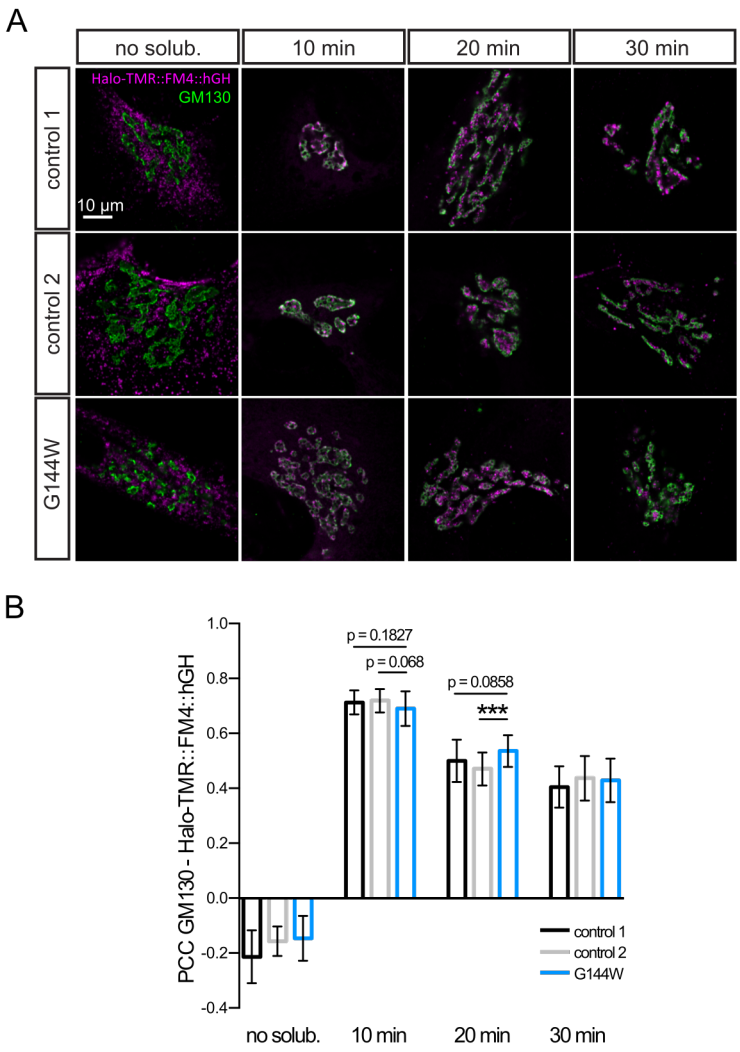

Figure 17. ER-to-Golgi trafficking in G144W mutant Membrin fibroblasts
(A) Example confocal slices of control 1 & 2 and G144W mutant Membrin fibroblasts overexpressing the artificial Halo::FM4::hGH cargo loaded with TMR. When no D/D solubilizer was present the cargo remained in the ER due to aggregation of the FM domains. 10 min after solubilization significant colocalization with the cis-Golgi marker GM130 was apparent, which decreased after 20 and 30 min of solubilization. Remarkably, also G144W mutant fibroblasts appeared to traffic this cargo efficiently. This was also observed in a small pilot experiment, where G144W mutant and control 1 cells were studied.
(B) Quantification of experiment as described in (A). Pearson's correlation coefficients of Halo-TMR::FM4::hGH and GM130 were calculated for each time point. Number of individual cells of one experiment quantified for control 1 & 2 and G144W are as follows: no solubilizer – 23, 21, 23; 10 min – 27, 28, 27; 20 min – 26, 29, 28; 30 min – 27, 26, 28. Mean and SD are shown. *** represents $p < 0.001$, ns = not significant ($p > 0.05$); one-way ANOVA with Dunnett's multiple comparison test.

PCCs at each time point quantitatively confirmed these observations. With no D/D solubilizer present, the ER retained hGH cargo and the cis-Golgi marker GM130 were negatively correlated (Figure 17B). 10 min after solubilization

PCCs rose to approximately 0.7, and subsequently significantly decreased to approximately 0.5 and 0.4 by 20 and 30 min respectively. Importantly, ER-to-Golgi trafficking in G144W fibroblasts was quantitatively almost indistinguishable from both controls (Figure 17B). Only a very subtle decrease in colocalization of the cargo with GM130 was apparent after 10 min of disaggregation. Conversely, after 20 min, a trend towards increased PCCs was measured in G144W fibroblasts. Collectively, these effect sizes were marginal and did not consistently reach statistical significance. Nevertheless, their *pattern* suggests a very subtle rate change of cis-Golgi entry. In such a scenario we expect the peak of TMR-GM130 colocalization to appear later than in the controls and therefore to maintain high PCCs until later time points.

To complement the hGH data I performed fluorescence recovery after photobleaching (FRAP) experiments as an additional ER-to-Golgi transport readout. To this end I overexpressed a chimeric reporter construct consisting of an N-terminal portion of a trans-Golgi resident galactosyltransferase and a RFP tag (GalT::RFP). Thereafter I photobleached the entire pool of Golgi resident GalT::RFP in control and G144W fibroblasts in order to assess its recovery through ER-to-Golgi transport of non-bleached molecules (Figure 18A) (Sengupta et al., 2015; Zaal et al., 1999). To minimize bleach-artefact as a result of acquiring 44 frames in this approximately 20 min live imaging experiment, I collected photons with a highly sensitive Gallium arsenide phosphide (GaAsP) detector, which enabled me to use a very low 561 nm excitation laser power. Indeed, these acquisition settings resulted in comparably stable GalT::RFP fluorescence in non-bleach control acquisitions (Figure 18B). GalT::RFP fluorescence recovered by approximately 50% in the Golgi area following experimental photo-bleaching by scanning this region twice with 100% transmission of the 561 nm laser (Figure 18B). Recovery kinetics were remarkably similar between G144W and control fibroblasts. Only a trend towards reduced recovery in G144W was apparent. However, no statistically significant difference after 10 or 19.5 min recovery times could be detected. These data are consistent with our hGH trafficking results and might be the consequence of a minor trafficking delay in G144W

fibroblasts, which is too small to conclusively be demonstrated with these common ER-to-Golgi trafficking assays.

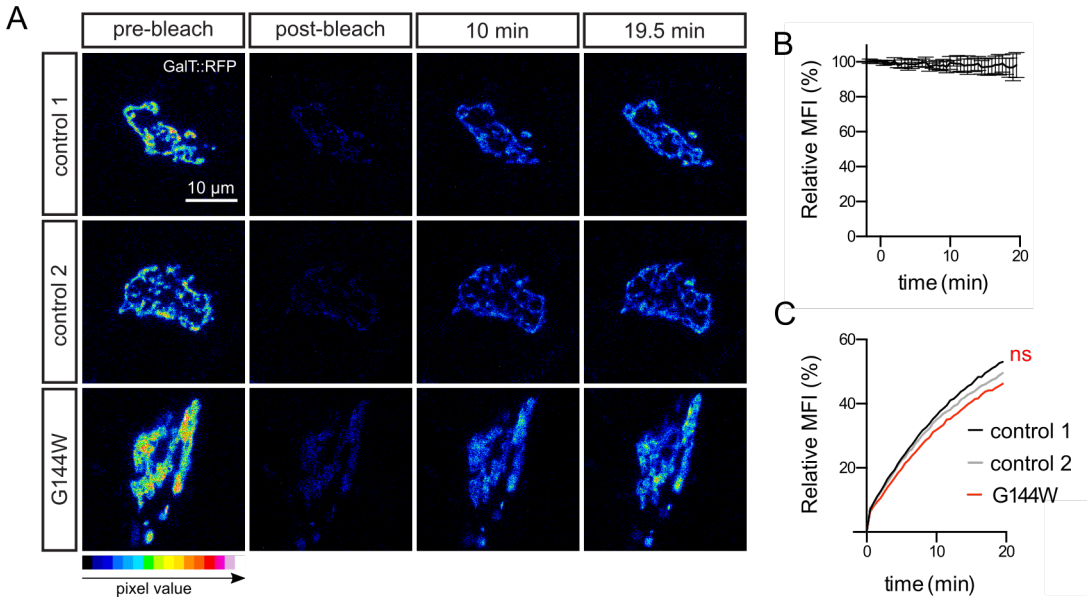

Figure 18. Golgi FRAP
(A) GalT::RFP in the entire Golgi region of control and G144W mutant Membrin fibroblasts was photo-bleached and recovery assayed over the course of 19.5 min. Example images of pre-bleach, immediately post-bleach, 10 and 19.5 min recovery time points are shown in successive order for each genotype.
(B) Control acquisition with the same settings as (A) and (C), however without experimental photo-bleaching. Mean fluorescence intensity (MFI) in the Golgi area of two individual control 1 and one control 2 cells are shown. Graph represents mean and SD for each time point.
(C) Quantification of experiment as described in (A). MFIs of the Golgi region were extracted, expressed as relatives to baseline fluorescence and corrected for post-bleach residual fluorescence. Mean recovery of controls and G144W are shown. N = 16, 16, 13 individual cells from five independent imaging sessions for control 1, control 2, G144W. ns = not significant ($p > 0.05$) after 10 and 19.5 min of recovery; ANOVA with Dunnett's multiple comparison test.

Taken together, these ER-to-Golgi trafficking studies with an artificial cargo that is synchronously released from the ER, as well as our GalT::RFP FRAP studies, demonstrate remarkably preserved Golgi entry kinetics in G144W fibroblasts. This finding in a non-neuronal cell type is consistent with the observation that *GOSR2*-PME almost exclusively affects the nervous system and does not manifest as a broad multi-system disorder as one might expect from a Golgi disorder (Freeze and Ng, 2011). It further reinforces the importance of studying the pathophysiology of *GOSR2*-PME in neurons, which might display differential vulnerability to subtle Golgi trafficking

alterations owing to their very large secretory demands (Horton and Ehlers, 2004; Pfenninger, 2009).

3.5 Discussion

3.5.1 Necessary steps for *understanding GOSR2*-PME

To gain an overarching, multi-level insight into how mutations in the Golgi SNARE protein Membrin ultimately give rise to PME, we have to trace the effects of the pathogenic sequence alterations from protein to organism. In this directional endeavour we have to first establish a solid fundament and thus start at the protein and basic cellular levels – which is summarized in this chapter. Given that a physiological function has previously been established for Membrin, we can directly test how this function changes as a consequence of the *GOSR2*-PME mutations. Only then will we move on to the neuronal and organismal levels (Chapter 4), which deal with phenomena more distant of the *first cause* of *GOSR2*-PME – i.e. *GOSR2* sequence alterations. However, functional roles for Membrin are not well established at these remote levels. The current literature does not comprise studies detailing the relationship of Membrin and *neuronal* cell biology or Membrin and its impact upon neural circuits. Thus, it is the more important to start with a fixed stepping stone in proximity of the first cause of *GOSR2*-PME and in the realm of the *known* and gradually ascend into the unknown that is also further downstream of the initial pathogenic insults.

Previous research has established that Membrin is a SNARE protein, which largely acts at the ERGIC and cis-Golgi and thereby mediates anterograde cargo trafficking in the early secretory pathway (Hay et al., 1997; Volchuk et al., 2004). SNARE proteins have been shown to represent the minimal machineries responsible for fusing opposing lipid bilayers via the formation of tight hetero-tetrameric SNARE complexes along conserved SNARE motifs (Südhof and Rothman, 2009). The known role of Membrin is thus summarized by its function of enabling ERGIC/cis-Golgi cargo deposition via SNARE complex mediated membrane fusion. Central to this process is the structural integrity of Membrin's SNARE motif, which is necessary to form the cis-Golgi SNARE complex. Intriguingly, both pathogenic disease mutations alter Membrin's SNARE domain. These changes thus directly suggest impaired SNARE complex formation and resulting alterations in secretory

trafficking. We therefore set out to test these predictions with liposome fusion assays and Golgi trafficking studies. We also tested whether mutant Membrin localizes to the ERGIC/Golgi – a prerequisite for its physiological function.

3.5.2 SNARE defects

Prior to my PhD research only one *GOSR2* mutation had been associated with PME, i.e. G144W. I discovered the novel K164del mutation, which gave rise to PME in the compound heterozygous state with G144W. Having a second disease allele at hand for the investigation of the pathophysiology of this severe neurological condition promised to be a useful tool and a valuable internal control. After all, both alleles are expected to display effects with the same directionality. They are both expected to *decrease* Membrin function, because *GOSR2*-PME is an autosomal-recessive disorder. However, their effect sizes might vary, particularly if we consider the precise location and nature of the mutations within Membrin's SNARE domain. G144W is a missense mutation in the N-terminal half of Membrin's SNARE domain, K164del a single amino acid deletion in its C-terminal half. Because the C-terminal half of SNARE domains is thought to generate the force critical to membrane fusion and because the K164 deletion likely causes the misalignment of several interacting residues in this part of the SNARE complex, we were expecting to see more dramatic consequences upon SNARE function in this mutant (Gao et al., 2012; Zhang, 2017). Indeed, this is what Nancy Malintan's liposome fusion assays revealed. Bos1 (the yeast Membrin orthologue) carrying either mutation was capable of fusion, yet both mutations caused decreased rates of liposome fusion mediated by yeast cis-Golgi SNARE proteins. Furthermore, the effect size of this reduction was larger in the D196del allele (orthologous to K164del). These experiments established the furthest *upstream* disease mechanism due to the pathogenic *GOSR2*-PME mutations, i.e. membrane fusion deficits as a result of the SNARE motif disruptions.

3.5.3 Mutant Membrin at the cis-Golgi

To study the physiological consequences of the *in vitro* established SNARE defects in a living cell, I utilized healthy control and *GOSR2*-PME patient-derived skin fibroblasts. In a first step, I wanted to know whether the pathogenic Membrin mutations caused abnormalities of its subcellular localization, which was suggested in previous work from Corbett et al. (Corbett et al., 2011). Such a defect would be physiologically relevant, as only Membrin localized to the ERGIC/cis-Golgi is capable of mediating membrane fusion at this site. In addition, Membrin localizing to different subcellular compartments might interfere with resident proteins and thereby contribute to the disease phenotype. Therefore, we transiently overexpressed N-terminal FLAG tagged wild-type and mutant Membrin in healthy control fibroblasts and studied its subcellular localization with confocal microscopy. Both mutants clearly exited the ER and localized to the cis-Golgi in a pattern comparable to wild-type Membrin. While there was a clear positive correlation between G144W/K164del mutant Membrin and the cis-Golgi marker GPP130, it was nevertheless significantly decreased by a small amount compared to wild-type Membrin. Such a result is not surprising considering that Membrin is required for proteins to enter the Golgi. If mutant Membrin is overexpressed it presumably enriches in the ERGIC/Golgi, which itself might cause a partial membrane fusion deficit and therefore a peri-ERGIC/Golgi enrichment of mutant Membrin enriched membranes. Nevertheless, because of the observed high correlation between mutant Membrin and GPP130 we conclude that the G144W and K164del disease mutations do not impair Membrin's capability to localize to the Golgi by a large degree. From this it follows that the lipid fusion deficits as found in liposome fusion assays likely have a direct impact upon the cargo entry kinetics at the ERGIC/Golgi.

While we found that overexpressed G144W mutant Membrin could clearly localize to the cis-Golgi, Corbett et al. reported that *endogenous* G144W mutant Membrin failed to localize to this compartment in patient-derived fibroblasts (Corbett et al., 2011). This finding has far-reaching implications, as it suggests that the G144W mutation – even though it only partially

impairs the Membrin SNARE domain – could be a true null allele as a consequence of its inability to localize to its physiological site of action. We therefore sought to repeat the finding of Corbett et al. using the same patient cells harboring a homozygous G144W Membrin mutation. However, we used a different antibody, which we thoroughly validated before commencing with these experiments. Under our experimental conditions we could clearly detect Membrin at the cis-Golgi of these cells, but to significantly decreased levels. It appears conceivable that under low contrast conditions this decrease might be misinterpreted as an absence of the protein, which could be an explanation for the discrepant conclusions of Corbett et al. and our own. This significant decrease of G144W mutant Membrin at the Golgi apparatus might either be the consequence of localization to a different subcellular compartment or an overall reduction, possibly due to increased protein turn-over. Because G144W mutant Membrin did not appear accumulated in the ER nor strikingly enriched elsewhere within mutant fibroblasts, the latter notion appeared more likely. We addressed this hypothesis with western blot studies and found significantly decreased G144W mutant Membrin levels in patient fibroblasts when compared to healthy controls. Also this finding is in disaccord with the study of Corbett et al., who reported unchanged Membrin levels in G144W fibroblasts (Corbett et al., 2011). The fact that we used a thoroughly validated antibody for our studies, plus an additional independent antibody and furthermore that also our immuno-fluorescence microscopy studies confirmed decreased G144W Membrin levels, argues for the validity of our results. Whether this decrease is functionally relevant is presently unclear, especially in the light of substantial Membrin level fluctuations that we observed also between both healthy controls (Figure 13B) and the availability of only a single patient fibroblast line in this study. Of note, Bethani et al. showed that 10% of the physiological endosomal SNARE levels were often sufficient for unaltered endosomal trafficking, lending support to the idea that some SNARE proteins might be more abundantly expressed than required (Bethani et al., 2009). Such a scenario could also be true for the cis-Golgi SNARE proteins, in which case our finding of reduced G144W Membrin would likely not contribute to the disease phenotype. If however this change is disease

relevant, then its effect is expected to further aggravate the partial loss of function nature of the G144W mutation.

Unfortunately, we were not able to obtain fibroblasts from the G144W – K164del compound heterozygous patient reported in this thesis (Praschberger et al., 2015). This fibroblast line would have served as an additional validation platform of our studies, although disentangling the relative contribution of either mutation would have been difficult.

3.5.4 Unimpaired ER-to-Golgi trafficking in a non-neuronal cell

Nancy Malintan's liposome fusion assays revealed SNARE defects caused by the *GOSR2*-PME mutations and my subcellular localization studies suggested that the disease mutations do not prevent Membrin from reaching its site of action – the ERGIC and cis-Golgi. As a result, lipid fusion rates of ER-derived, cargo loaded COPII vesicles with these compartment is expected to be reduced in a Membrin mutant cell. To test whether such a lipid fusion deficit leads to reduced cis-Golgi cargo entry rates I performed two independent sets of ER-to-Golgi trafficking assays in G144W mutant Membrin fibroblasts. In one experiment, I synchronously released ER-retained model cargo into the secretory pathway and assayed its arrival time in the cis-Golgi. In a complementary approach, I measured the ER-to-Golgi recycling rates of a fusion construct between RFP and a portion of a Golgi enzyme (Sengupta et al., 2015; Zaal et al., 1999). Both experiments revealed remarkably convergent results, as they showed Golgi entry comparable to two fibroblast lines derived from healthy control subjects, with only a subtle trend towards reduced rates. This finding appears surprising at first glance, considering the pathogenic SNARE motif defects. Of note however, the G176W Bos1 mutation (orthologous to the G144W Membrin mutation) exhibited very mild effects in liposome fusion studies. Equivalent changes in lipid fusion kinetics at the ERGIC/cis-Golgi of a living cell might be below the detection limit of the employed trafficking assays. In addition, this subtle SNARE defect might possibly be absorbed by the physiological presence of supernumerous Membrin molecules and the compensatory engagement of 20% more cis-Golgi SNARE complexes. Maybe such partial SNARE defects

are only physiologically relevant under conditions of very large trafficking rates, while not being functionally relevant for providing a basic ER-to-Golgi cargo flux as required by most cell types. Importantly, the finding of unimpaired early secretory pathway trafficking in a G144W mutant non-neuronal cell model provides a likely explanation why most tissues – apart from the nervous system – do not exhibit symptoms in *GOSR2*-PME, despite the disease-causing mutation affecting a ubiquitously important protein.

3.5.5 Considerations about the fibroblast studies

Due to limited availability, I was only able to obtain one *GOSR2*-PME patient-derived fibroblast line. *GOSR2*-PME is a very rare disorder with only 18 patients worldwide reported and thus biological material is scarce. Therefore, the interpretation of the observed results is more difficult. Given that we are comparing results from one patient-derived fibroblast line with fibroblasts derived from two different healthy controls, we are comparing cells which not only differ in the pathogenic mutation, but also in the presence of thousands of unrelated SNPs. Therefore, the observed cellular phenomena might also be influenced by this genetic heterogeneity. Further disease cell lines would thus increase the confidence of attributing observed effects to the disease mutation and rule out the possibility that the effects are caused by unrelated SNPs. In addition, subtle effects, such as those that are expected for the ER-to-Golgi traffic rate change due to G144W, might be overshadowed by natural variation in the kinetics of this process. These changes might only become fully apparent by comparing several *GOSR2*-PME fibroblast lines with healthy controls. To circumvent these intrinsic difficulties, future studies into the cell biology of *GOSR2*-PME would greatly benefit from the generation of G144W/K164del mutant Membrin knock-in cell lines utilizing the CRISPR/Cas9 genome editing technology (Cong et al., 2013; Mali et al., 2013). The unedited cell line would then be the perfect control, as it would contain the same genetic background.

3.5.6 The importance of a neuronal model

The experiments at the protein and basic cellular levels outlined in this Chapter have provided solid foundations for our quest to shed light upon the pathophysiology of *GOSR2*-PME. They have not yet, however, touched upon the cardinal point related to our investigation, i.e. how neurons are exquisitely sensitive to Membrin mutations. In fact, the apparent lack of ER-to-Golgi trafficking impairment in a non-neuronal mutant Membrin model cell has consolidated the spotlight that was already directed toward the nervous system because of the almost exclusive neurological symptomatology of *GOSR2*-PME patients. This is why we developed *Drosophila* models of this disorder, which not only allows for the study of Membrin mutant neurons grown in their natural environment, but also provides an organismal read-out of the disease mutations. The summary of our *Drosophila* investigations into *GOSR2*-PME are detailed in the following Chapter.

Chapter 4. Investigating the pathophysiology of *GOSR2* mediated progressive myoclonus epilepsy in novel *Drosophila* models of the disorder

4.1 Introduction

The previous Chapter has established the impact of the *GOSR2*-PME mutations upon SNARE-mediated membrane fusion and ER-to-Golgi trafficking in a non-neuronal cell. While the G176W/R196del Bos1 mutations (orthologous to human G144W/K164del Membrin mutations) both decreased lipid fusion in a cell free reconstitution assay and G144W/K164del mutant Membrin correctly localized to their ERGIC/cis-Golgi, G144W mutant Membrin fibroblasts appeared to traffic cargo to the Golgi in rates comparable to healthy controls. This finding might explain why tissues other than the nervous system are not symptomatically affected in *GOSR2*-PME and further reinforced the idea that neurons might be selectively vulnerable to these partial loss of function Membrin mutations. To investigate which aspects of neuronal cell biology might be affected and how such changes could affect neural circuits in a way to give rise to ataxia and hyperexcitability, we introduced the disease mutations into *Drosophila*. These *GOSR2*-PME models exhibited severe motor, seizure-like and early lethality phenotypes. Dendritic growth was highly impaired in the presence of Membrin mutations, presumably due to restrictions in ER synthesized, and therefore ER-to-Golgi trafficking and Membrin dependent, lipid supplies, which are required for plasma membrane expansion. Intriguingly, also synaptic morphological and physiological abnormalities, such as reduced trans-synaptic stability and hyperactive neurotransmission, were detectable at the experimentally highly accessible neuromuscular model synapse. These findings collectively show that dendritic growth and synaptic integrity depend upon tightly controlled trafficking rates. Our neuronal findings in *Drosophila* outlined in this Chapter thereby provide the missing key to understand how the *GOSR2*-PME mutations result in nervous system dysfunction.

4.2 Statement of contribution

Please refer to the ‘Statement of contribution’ section in Chapter 3 for a detailed account of my contribution to our collaborative investigations into the pathophysiology of *GOSR2*-PME. Experimental results from other researchers than myself are included also in this section to facilitate a more holistic view of the project. The respective sources are clearly identified in the text and figure legends.

4.3 Materials and Methods

4.3.1 Plasmids

Drosophila melanogaster *membrin* CDS (of NCBI cDNA NM_139703.4) with and without the G147W and K166del mutations were custom synthesized by GeneArt (Thermo Fisher Scientific) according to the same design as outlined in 'Materials and Methods' of Chapter 3 for the *GOSR2* constructs, giving rise to pMA_FLAG::*membrin*[WT]/[G147W]/[K166del] (annotated sequences of the custom synthesized fragments can be found in the Appendix).

In order to create wild-type and mutant *GOSR2*/*membrin* transgenic flies the inserts of the pMA plasmids were subsequently cloned via NotI and KpnI (NEB) into pUASTattB (Bischof et al., 2007), giving rise to pUASTattB_FLAG::*GOSR2*[WT]/[G144W]/[K164del] and pUASTattB_FLAG::*membrin*[WT]/[G147W]/[K166del] according to the subcloning protocol as outlined in 'Materials and Methods' of Chapter 3. Subcloning of FLAG::*GOSR2*[WT] was carried out by Kofan Chen. The presence of the correct open reading frame was validated by Sanger sequencing with the primers pUASTattB_F2 (5'-GCAACCAAGTAAATCAACTGCA-3') and pUASTattB_R2 (5'-TGTCCAATTATGTCACACCACAG-3') by Source Biosciences.

4.3.2 *Drosophila* stocks

4.3.2.1 *membrin*^{1524}

A *membrin* null (*membrin*^{1524}) allele was previously generated in an EMS screen investigating tube morphogenesis and kindly shared by Mark Krasnow (Ghabrial et al., 2011). These flies harbor a c.255C>T mutation in the *membrin* gene, which gives rise to a premature stop codon causing termination of translation 47 amino acids prior to membrin's critical SNARE domain. To control for potential genetic background effects, we outcrossed *membrin*^{1524} for five generations into the isogenised *white* mutant (*white*^{1118}) strain iso31 by following an AccI (NEB) restriction site that is introduced by the nonsense mutation. To this end individual females – either *w*[1118]; +; *membrin*^{1524}/+ or *w*[1118]; +; +/+ – where crossed to iso31 males. After egg

laying and hatching of L1 larvae, mother animals were removed, frozen at -20°C and subsequently ground in 40 µl of 'dirty genomic prep buffer' (Proteinase K 0.32 U, 10 mM Tris-HCl pH 7.6, 1 mM EDTA, 25 mM NaCl). Samples were subsequently incubated for 30 min at 37°C followed by Proteinase K heat inactivation at 95°C for 10 min. The mixture was spun down for 30 s at 14000 g and 2 µl of the supernatant used as the template for PCR with 0.8 µM of forward (mem1524_OUTF1: 5'-GTGGTAAAGGACATCGAGCG-3') and reverse (mem1524_OUTR1: 5'-CCACCACTCCTCCGATGAAT-3') primers and 12.5 µl GoTaq G2 Green Master Mix (Promega) in a 25 µl final volume. Initial denaturation at 95°C for 2 min was followed by 35 cycles of 95°C 30 s, 60°C 30 s, 73°C 60 s and a final extension at 73°C for 5 min. 5 µl of this PCR product was digested with 5 U of AccI in Cutsmart Buffer (NEB) for 2 h at 37°C, separated by 1% agarose gel electrophoresis and visualized with UV light and GelRed [1/10000] (Biotium). A double band around 350/300 basepairs indicated the desired genotype, where *membrin*^{1524} was present in the heterozygote state (Figure 19).

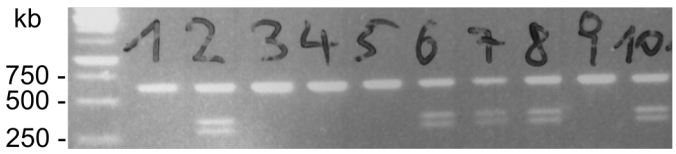

Figure 19. Diagnostic digest during outcrossing of the *membrin*^{1524} allele
A double band of the expected size in lanes 2, 6, 7, 8 and 10 indicates that these F2 females, which were previously individually crossed to iso31 males, carried the *membrin*^{1524} allele in the heterozygous state. Therefore, their offspring virgin females were selected for further backcrossing and diagnostic AccI digest.

The presence of the c.255C>T *membrin*^{1524} was also confirmed by Sanger sequencing. Therefore, the same fragment as above was PCR amplified with Q5 high-fidelity DNA polymerase (NEB), cleaned up with the Wizard SV Gel and PCR clean up system (Promega) and sequenced with mem1524_OUTF1 and mem1524_OUTR1 by Source Biosciences.

4.3.2.2 Generation of wild-type and mutant *GOSR2* and *membrin* transgenic flies

Transgenic fly lines under the control of the UAS-enhancer (Brand and Perrimon, 1993) were generated by microinjection of pUASTattB_FLAG::*GOSR2*[WT]/[G144W]/[K164del]/pUASTattB_FLAG::*membrin*[WT]/[G147W]/[K166del] into *y*[1] M{vas-int.Dm}ZH-2A *w**; M{3xP3-RFP.attP'}ZH-51C embryos (Cambridge fly facility). Because the pUASTattB plasmid harbors an attB sequence and this fly line a specific attP landing site, it allows for site-specific integration into this locus in germline cells via the action of phiC31 integrase, which is transgenically provided via the *vasa* promoter (Bischof et al., 2007). This approach has the advantage of ensuring that all transgenes are integrated precisely in the same genomic localization and hence observed differences in phenotypes can be attributed to the respective mutations rather than differences in transcription due to integration into transcriptionally silent regions of the genome. The ZH-51C landing platform was chosen, as in the current gene annotation (FlyBase release FB2017_03) it is clearly localized between genes and not in exons, introns or UTRs, which makes it less likely to cause insertional mutagenesis (see Figure 20).

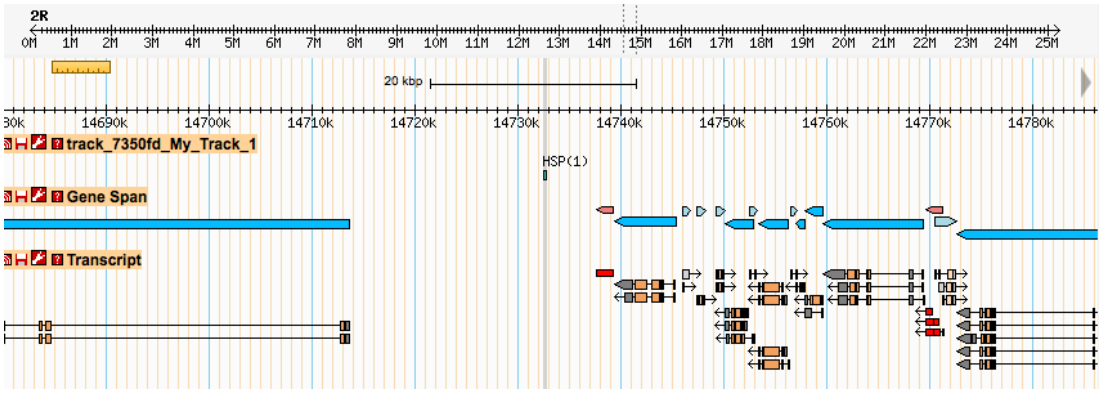

Figure 20. Intergenic localisation of the ZH-51C landing platform
HSP(1) indicates the position of this transgene integration site on the right arm of chromosome two. Screen shot is taken from FlyBase release FB2017_03 after performing BLAST with the flanking sequence of ZH-51C provided at the flyc31.org website.

Additionally, the light orange eye color of pUASTattB (which also contains a mini-*white* gene) transgene insertions in this site facilitates selection for

additive mini-*white* effects when crossed to other transgenic flies. Furthermore, ZH-51C is localized on the second chromosome, which allows to readily combine these transgenic flies with the *membrin*^{1524} allele, which is localized on the third chromosome. After removal of the integrase from the X-chromosome, balanced transformants were provided to us by the Cambridge Fly Facility. Thereafter UAS-FLAG::*GOSR2*[WT]/[G144W]/[K164del] or UAS-FLAG::*membrin*[WT]/[G147W]/[K166del] flies were backcrossed for five generations into iso31.

4.3.2.3 Assembly of model stocks

In order to express wild-type or mutant *GOSR2* or *membrin* in *membrin* null flies we generated two stocks that then need to be crossed to each other – one of them containing the transgenes plus the *membrin* null allele, the other one the *membrin* null allele plus a global driver.

To generate the transgene half of the 'model cross', I first balanced second chromosome transgenic flies for the third chromosome and *membrin*^{1524} flies for the second chromosome. The resulting *w*[1118]; UAS-FLAG::*GOSR2*[WT]/[G144W]/[K164del]/+; TM2/TM6B-Tb or UAS-FLAG::*membrin*[WT]/[G147W]/[K166del]/CyO; MKRS/TM6B-Tb were crossed with *w*[1118]; CyO/Sco; *membrin*^{1524}/TM6B-Tb and Curly, non-Sco, non-*ebony*/non-MKRS bearing, mini-*white* males and virgin females were selected to establish the stocks, which were subsequently homozygosed for the second chromosome transgene. This crossing gave rise to the first half of the 'model cross' (I.): *w*[1118]; UAS-FLAG::*GOSR2*[WT]/[G144W]/[K164del]; *membrin*^{1524}/TM6B-Tb or *w*[1118]; UAS-FLAG::*membrin*[WT]/[G147W]/[K166del]; *membrin*^{1524}/TM6B-Tb.

In order to obtain the driver half of the 'model cross', *membrin*^{1524} was combined with the *daughterless*-Gal4 (*da*-Gal4, Bloomington stock centre #55850) driver, which was outcrossed for 5 generations into iso31 prior to stock generation by members of the Jepson lab. *w*[1118]; +; *membrin*^{1524} and w[1118]; +; *da*-Gal4 were combined by selecting for meiotic recombinants. Therefore, *w*[1118]; +; *membrin*^{1524}/*da*-Gal4 transheterozygote virgin females were crossed to *w*[1118]/Y; +; TM2/TM6B-Tb. In the next generation mini-

white expressing males over TM6B-Tb were selected and individually crossed to virgins *w*[1118]; +; TM2/TM6B-Tb. After egg laying and hatching of L1 larvae the presence of *membrin*^{1524} in the father animals was tested by PCR and diagnostic digest with AccI as described above. Where AccI restriction sites were detected, stocks were established from their offspring by crossing mini-*white* expressing males and virgin females over TM6B-Tb with each other. The full genotype of the resulting second half of the 'model cross' is (II.): *w*[1118]; +; *membrin*^{1524}, *da*-Gal4/TM6B-Tb.

In order to express wild-type or mutant *GOSR2* or *membrin* in *membrin* null flies the following 'model cross' is required:

I.

w[1118]; UAS-FLAG::*GOSR2*[WT]/[G144W]/[K164del]; *membrin*^{1524}/TM6B-Tb

or

w[1118]; UAS-FLAG::*membrin*[WT]/[G147W]/[K166del]; *membrin*^{1524}/TM6B-Tb

X

II.

w[1118]; +; *membrin*^{1524}, *da*-Gal4/TM6B-Tb

Three of the four possible genotypes of this cross are theoretically viable (homozygosity for the third chromosome balancer TM6B-Tb is known to be lethal) and the absence of the Tubby allele indicates the presence of the desired genotype (a) (*X* = any of the *GOSR2* or *membrin* transgenes):

a) ***w*[1118]; UAS-FLAG::*X*/+; *membrin*^{1524}, *da*-Gal4/*membrin*^{1524}**

b) *w*[1118]; UAS-FLAG::*X*/+; *membrin*^{1524}/TM6B-Tb

c) *w*[1118]; UAS-FLAG::*X*/+; *membrin*^{1524}, *da*-Gal4/TM6B-Tb

Because mutant human Membrin did not rescue *membrin* null animals to the L3 stage and wild-type human Membrin rescue yielded severely impaired adults, we based our experiments on more physiological *Drosophila* Membrin rescue models. In order to increase readability of the full genotypes of these flies I used Mem-WT, Mem-G147W and Mem-K166del as abbreviations throughout this thesis (Table 9).

Mem-WT	*w*[1118]; UAS-FLAG::*membrin*[WT]/+; *membrin*^{1524}, *da*-Gal4/membrin^{1524}
Mem-G147W	*w*[1118]; UAS-FLAG::*membrin*[G147W]/+; *membrin*^{1524}, *da*-Gal4/membrin^{1524}
Mem-K166del	*w*[1118]; UAS-FLAG::*membrin*[K166del]/+; *membrin*^{1524}, *da*-Gal4/membrin^{1524}

Table 9. Full genotypes of *GOSR2*-PME model *Drosophila*

To genetically label the highly elaborate class IV dendritic arborization (da) neurons – which comprise of one ddaC, one v'ada and one vdaB neuron per hemisegment (Grueber et al., 2002) – for dendritic analysis (see below), the *w*[1118]; *ppk*-CD4::tdGFP (Bloomington stock centre #35842) stock was used. This fly line is an optimized expression system comprising of one EGFP plus one GFP fused to the CD4 transmembrane domain downstream the *pickpocket* (*ppk*) promoter (Grueber et al., 2003; Han et al., 2011). James Jepson combined *w*[1118]; ppk-CD4::tdGFP with *w*[1118]; +; *membrin*^{1524} *da*-Gal4/TM6B-Tb according to standard *Drosophila* mating schemes (Roote and Prokop, 2013). The resulting stock is the driver half of the 'model cross' with an additional *ppk*-CD4::tdGFP transgene with the following genotype – *w*[1118]; *ppk*-CD4::tdGFP; *membrin*^{1524}, *da*-Gal4/TM6B-Tb. These flies need to be crossed to (I.) (see above) and non-Tubby animals selected for further analysis.

4.3.2.4 *emp*-GFP knock-in

In the course of this PhD project I also generated an endogenously GFP-tagged *emp* allele, which is the *Drosophila* orthologue of the PME-gene *SCARB2* (Berkovic et al., 2008). However, time constraints precluded me from undertaking further investigation into *SCARB2*-PME utilizing these flies. The *emp*-GFP knock-in fly was generated by recombination-mediated cassette exchange of a MiMIC insertion (Mi12296, Bloomington stock centre #57917) between exon 1 and exon 2 of the *emp* gene. The plasmid pBS-KS-attB1-2-PT-SA-SD-1-EGFP-FlAsH-StrepII-TEV-3xFlag was injected by the Cambridge Fly Facility, who provided us with five independent flies with successful cassette exchange. Diagnostic PCR confirmed that in three lines the EGFP coding sequence had inserted into the correct strand. Details of this technique are described in (Venken et al., 2011).

4.3.2.5 Additional *Drosophila* stocks utilized in this study

To evaluate the lethal phase of *membrin*^{1524} at the L1 and L2 larval stages, I rebalanced this allele over the fluorescent TM3 *Kr* > GFP balancer chromosome (Casso et al., 2000), which was also backcrossed to iso31 for 5 generations. For nervous system overexpression of Membrin, *nsyb*-Gal4 (Bloomington stock centre #51635) was used, which was previously backcrossed to iso31 for 5 generations by members of the Jepson lab. *w*[1118]; +; *ppk*-Gal4 (#32079; previously backcrossed to iso31 for 5 generations by members of the Jepson lab), *w*[1118]; +; UAS-*RedStinger* (#8547), *w*[*]; +; nsyb::eGFP (#6922), *w*[*]; *nompC*-Gal4 (derived from #36361) were from Bloomington stock centre. Membrin RNAi transgene was from the Vienna Drosophila Research Center (GD 44535) and backcrossed for 5 generations into iso31 (Dietzl et al., 2007).

4.3.3 Fly husbandry

Flies were reared on solid fly food (1 w/v% agar, 1.5 w/v% sucrose, 3.3 w/v% glucose, 3.5 w/v% yeast, 1.5 w/v% corn meal, 1.5 v/v% soy flour, 3 w/v% treacle, 1 w/v% wheat germ, 0.1 w/v% nipagin, 0.5 v/v% propionic acid) in polystyrene tubes. Experimental flies were incubated at 25°C with a 12 h

light-dark cycle unless specified otherwise. Stocks were maintained either at room temperature or 18 °C.

4.3.4 Viability experiments

To evaluate the lethal phase of the disease-causing *membrin* mutations I crossed 20 virgin females *w*[1118]; +; *membrin*^{1524}, *da*-Gal4/TM6B-Tb with 30 males *w*[1118]/Y; UAS-FLAG::*membrin*[WT]/[G147W]/[K166del]; membrin^{1524}/TM6B-Tb and collected embryos overnight with dedicated embryo collection cages (FlyStuff, Dutscher) and apple juice-sucrose agar plates containing yeast paste. These crosses were allowed to lay eggs for several consecutive nights onto fresh plates and set up twice. During the day egg/embryos were mobilized with a paintbrush, rinsed with water, counted and transferred to standard food tubes. After 10 days of incubation at 25°C (11 days after initiation of egg-laying) non-Tubby pupae were counted. Given that theoretically only one quarter of the collected eggs/embryos are of the correct genotype, we used the following formula to calculate egg/embryo to pupa viability: non-Tubby pupae/(total eggs/4). The resulting fraction was normalized to wild-type because we found a considerable reduction with consecutive egg-lays, presumably reflecting decreasing fertilization. Eclosion rates were determined 11 days (for *GOSR2*-PME 'model crosses') and 12 days (for *nsyb*-Gal4 and *da*-Gal4 x UAS-*membrin* crosses (the latter experiment was carried out by Nian Patel)) after onset of egg laying, a time point where under our conditions non-eclosion was equal to death or imminent death in the pupal case. The eclosion data were pooled as the eclosion rates did not change over consecutive egg-lays.

In mutant *GOSR2* rescue animals no non-Tubby pupae or L3 larvae were observed. Therefore only eclosion rates of *w*[1118]; UAS-FLAG::*GOSR2*[WT]/+; *membrin*^{1524}, *da*-Gal4/*membrin*^{1524} animals were determined. Furthermore, I counted non-Tubby and Tubby pupae of the respective 'model cross', in order to screen for large deviations from the expected Mendelian ratios.

4.3.5 Larval crawling assay

To test for motor defects of *GOSR2*-PME model larvae, we quantified locomotion in non-Tubby third instar larvae from the 'model cross' as described above. Larvae were removed from their standard food tubes by an approximately 10 min incubation with 20% sucrose solution. This caused larvae to emerge from the food and to float on the surface (Bhatt and Neckameyer, 2013). Thereafter L3 larvae were selected, rinsed with deionized water and transferred to sucrose-agar plates (2 w/v% agar, 4 w/v% sucrose). Individual animals were then picked up with a paintbrush, briefly dried with a Kimwipe and placed in the center of a 9 cm diameter sucrose-agar dish residing above a 4 mm grid. Larvae were allowed to orient themselves for 30 s and filmed for the next 60 s. A minimum total of 19 larvae per genotype in two independent experiments were recorded and grid breaks in 60 s were scored offline.

4.3.6 Developmental delay assay

Egg-laying of the *membrin* 'model crosses' was allowed overnight on apple juice agar plates as outlined above. The following day yeast paste was removed and fresh paste added. Plates were then incubated at 25 degrees for 24 hours to allow hatching of L1 larvae and movement into the centrally located yeast paste. The following day the yeast paste containing L1/L2 larvae were transferred to fresh apple juice agar plates, fresh yeast paste was added and the plates were again incubated overnight. On day three yeast paste and apple juice agar plates were thoroughly rinsed and animals collected in 70 µm Falcon Cell Strainers. Late L2 and early L3 non-Tubby larvae were then transferred into standard food tubes and every day for 5 consecutive days the appearance of pupae counted. Four batches of animals derived from consecutive overnight egg-lays of the same parents were pooled. Counted pupae for each day were expressed as percentages of the overall counted pupae of the respective genotype.

4.3.7 Dendritic analysis

To study dendrites of mutant *membrin* animals the 'model cross' was carried out with the *ppk*-CD4::tdGFP containing driver line and non-Tubby L3 larvae of the following genotypes were selected:

1) *w*[1118]; UAS-FLAG::*membrin*[WT]/*ppk*-CD4::tdGFP; *membrin*^{1524}, *da*-Gal4/membrin^{1524}
2) *w*[1118]; UAS-FLAG::*membrin*[G147W]/*ppk*-CD4::tdGFP; *membrin*^{1524}, *da*-Gal4/membrin^{1524}
3) *w*[1118]; UAS-FLAG::*membrin*[K166del]/*ppk*-CD4::tdGFP; *membrin*^{1524}, *da*-Gal4/membrin^{1524}

Alternatively, wild-type or mutant Membrin was selectively overexpressed in class IV da neurons with the *ppk* promoter. Therefore the driver line *w*[1118]; *ppk*-CD4::tdGFP; *ppk*-Gal4 was generated according to standard *Drosophila* mating schemes and crossed to *w*[1118]; UAS-*membrin*[WT]/[G147W]/[K166del] as well as to iso31 and *w*[1118]; +; UAS-*RedStinger*.

Throughout the following experiments either the left or right ddaC neuron in abdominal segment 5 of L3 larvae was imaged (Grueber et al., 2002).

4.3.7.1 Dendritic morphology of *GOSR2*-PME model neurons

In order to avoid movement artefacts L3 larvae were heat-killed (70°C for approximately 5 s) and mounted under a #1.5 glass coverslip prior to imaging. Z-stacks of ddaC neurons were obtained with a Zeiss confocal LSM710 microscope and a N-Achroplan 10x 0.25 NA objective. To extract total dendrite length and to serve as a template for the ImageJ Sholl Analysis plugin, dendrites were semi-manually traced with the ImageJ NeuronJ plugin (Ferreira et al., 2014; Meijering et al., 2004). Terminal branches were manually counted on dendrite tracings with the ImageJ multi-point tool.

4.3.7.2 Dendritic baseline fluorescence of *GOSR2*-PME model neurons

The same prep as outlined above for the dendritic morphology analysis was used to obtain baseline CD4::tdGFP fluorescence in proximal dendrites and axons of *GOSR2*-PME model neurons. Z-stacks were acquired with a Zeiss confocal LSM510 microscope and a Plan-Neofluar 20x 0.5 NA objective and a 150 x 150 µm field of view. After maximum intensity projection of z-stacks in Fiji, a region of interest (ROI) of axons and major dendrites contained in a 37.5 µm radius ddaC soma enclosing circle was manually drawn and mean-fluorescence intensities extracted and background subtracted (Figure 21).

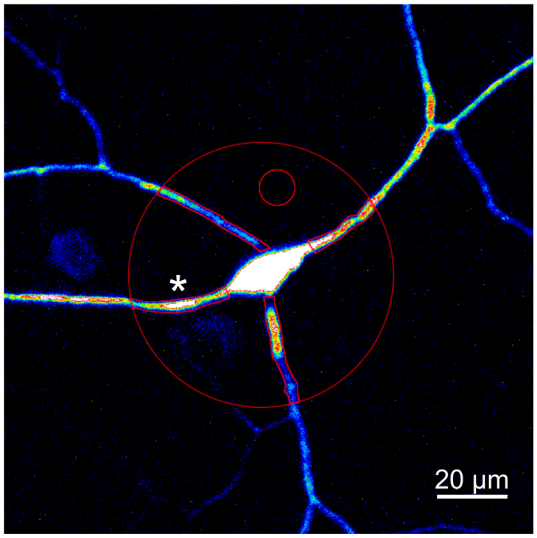

Figure 21. ddaC baseline fluorescence analysis
Regions of interest around axon (*) and major dendrites contained within a 37.5 µm circle around the ddaC abdominal segment 5 soma were drawn. Mean fluorescence intensities of these regions were background (small circle) corrected.

4.3.7.3 Dendritic FRAP of *GOSR2*-PME model neurons

For FRAP experiments, L3 larvae were fillet-prepped in HL3 saline without Ca^{2+} (70 mM NaCl, 5 mM KCl, 20 mM $MgCl_2$, 10 mM $NaHCO_3$, 5 mM trehalose, 115 mM sucrose, 5 mM HEPES-NaOH pH 7.2). Animals were opened along the anterior midline to maintain the integrity of the dorsal body wall, where ddaC neurons are located. Fillets were transferred to a #1.5 glass bottom dished and submerged in fresh HL3 saline with a custom-made platinum wire anchor with the interior body wall facing the solution. Imaging

was carried out on an inverted Zeiss confocal LSM510 with a Plan-Neofluar 20x 0.5 NA objective. A z-stack was taken every 30 s – 2 pre- and 60 post-bleach. Bleaching of a 50 μm^2 area encompassing major primary dendrites directly adjacent to the soma was carried out by scanning for 200 iterations with 100% transmission of the 488 nm Argon laser at a tube current of 6 A. Prior to extracting fluorescence intensities, z-stacks were maximum intensity projected for each time point and each resulting projection image aligned to the first time point with the TurboReg ImageJ plugin, in order to compensate for x-y optical drift during the approximately 30 min acquisition period (Thévenaz et al., 1998). Mean fluorescence intensity of a small dendritic region contained in a 5 µm diameter circle 25 µm from the bleach border adjacent to the soma served as a read-out (Figure 22), which was background corrected in each frame. This is the most distant dendritic region from either bleach margin and thus the contribution to fluorescence recovery from lateral diffusion of dendrite surface localizing CD4::tdGFP is minimized. Bleach depth in this region was consistently greater than 87%.

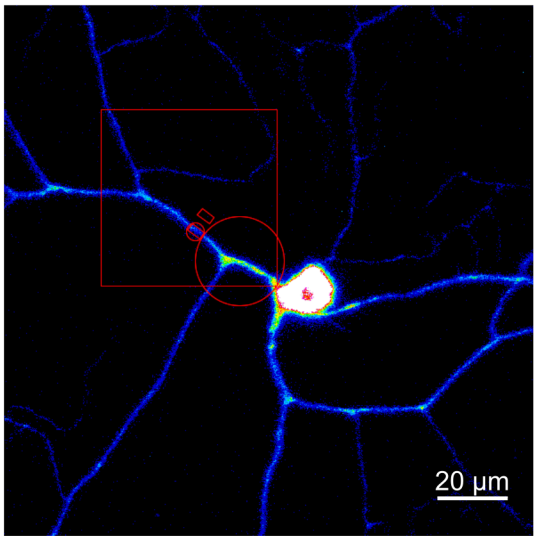

Figure 22. Dendrite FRAP analysis
Mean fluorescence intensity of a small dendritic fragment contained in a 5 µm circle, 25 µm (large circle) from the soma bleach margin was extracted over the time course and background subtracted for each frame (small ROI adjacent to dendrite). Depicted is the first maximum projected z-stack, prior to photobleaching of a 50 μm^2 area (square).

4.3.7.4 Class IV da neuron overexpression studies

L3 larvae overexpressing wild-type or mutant Membrin or control animals were heat-killed and mounted as described above. Z-stacks were acquired with an inverted Zeiss confocal LSM710 with a Plan-Apochromat 20x 0.8 NA objective. To facilitate rapid quantification of the observed qualitative differences, a previously validated protocol was used, where Sholl analysis is performed directly on binary images (Ferreira et al., 2014). Therefore, all image z-stack were first maximum intensity projected. Then, the same thresholds (10000 – 65535 for these 16-bit images) were applied to all images, which yielded binary images with clearly visible dendrites and only occasional background pixels. The Sholl analysis ImageJ plugin was then used to compute total intersections with 1 pixel increasing radii starting at the center of the cell soma (Ferreira et al., 2014). 400 µm was chosen as the ending radius to cover the majority of the abdominal segment 5 ddaC dendrite arbor. Because these neurons are tightly surrounded by tiling neighbouring class IV da neurons, some of the more distal Sholl circles also intersect with these dendrites. Specifically, these Sholl settings also yield intersections with some distal branches of the contralateral abdominal segment 5 and the ipsilateral abdominal segment 3 and 6 ddaC neurons as well as the ipsilateral abdominal segment 5 v'ada neuron. However, these additional intersections do not render the experiment less powerful, because these neurons have similarly large dendritic arbors, which thus will be equally vulnerable to the Membrin mutations.

4.3.8 *Drosophila* brain immuno-fluorescence microscopy

Dissection and immuno-staining of adult fly brains largely followed a published protocol (Wu and Luo, 2006). Flies were anaesthetized with CO_2, immersed in 70% ethanol, dissected with sharp forceps in phosphate buffer Triton X-100 (PBT; 100 mM phosphate buffer pH 7.2 plus 0.3% Triton X-100) and fixed in 4% PFA (Alfa Aesar) at room temperature for 15 min under constant agitation. Remaining fixative, as well as primary and secondary antibodies were removed by 3 short and 3 x 10 min washes with PBT. Prior to antibody labeling, brains were blocked in PBT + 5% goat serum. Primary

and secondary antibodies were diluted in PBT + 5% goat serum and incubated at 4°C overnight. The following antibodies and respective dilutions were used: mouse anti-FLAG (clone M2, Sigma; 1:1000), rat anti-FLAG (Agilent; 1:1000), mouse anti-GFP (clone 3E6, Thermo Fisher Scientific; 1:1000), rabbit anti-*Drosophila* Membrin (cusMEM4; custom polyclonal production by Biomatik (see below); 1:500), goat anti-mouse/rabbit/rat Alexa Fluor 488/647 (Thermo Fisher Scientific, 1:500-1000). Stained fly brains were mounted in SlowFade Gold antifade (Thermo Fisher Scientific) with the brain's anterior facing a #1.5 glass coverslip and between #1.5 glass coverslip bridges, in order to preserve the structure of the whole brain. Z-stacks were acquired with an inverted Zeiss confocal LSM710 with a Plan-Apochromat 20x 0.8 NA objective.

4.3.9 Western blot

Drosophila western blots were carried out according to the same protocol as used for mammalian cultured cells (described in 'Materials and Methods' of Chapter 3). To lyse *Drosophila* L3 larvae, 5 animals were placed in an Eppendorf tube containing 50 or 100 µl of the above lysis buffer and ground for 10 s with Pellet pestles (Kimble Kontes). For immuno-detection mouse anti-FLAG (clone M2, Sigma; 1:2000), rabbit anti-*Drosophila* Membrin (cusMEM4; custom polyclonal production by Biomatik (see below); 1:500), mouse anti-β-actin (clone AC-74, Sigma; 1:2000) and HRP-conjugated anti-mouse/rabbit secondaries (Jackson Immuno; 1:1000-5000) were used.

4.3.10 Antibody production

Polyclonal anti-*Drosophila* Membrin antibodies were custom produced by Biomatik for this study. To this end they synthesized two peptides corresponding to two independent regions of *Drosophila* Membrin. Both peptides were injected into two rabbits (Table 10). Thereafter, antibodies were affinity purified from the rabbit's sera, lyophilized and shipped to us.

MESLYHQTNNVVKDIERDFQRLSQLSAQESLDVENGIQLKITQANANCDRLDVLLYKVPPSQRQSSKL RVDQLKYDLRHLQTSLQTARERRQRRMQEISEREQLLNHRFTANSAQPEETRLQLDYELQHHTQLGNA HRGVDDMIASGSGILESLISQRMTLGGAHKRIQAIGSTLGLSNHTMKLIERRLVEDRRIFIGGVVVTL LIIALIIYFLVL				
Peptide ID	465774		465775	
Animal ID	RB6725	RB6726	RB6725	RB6726
Short name	cusMEM1	cusMEM2	cusMEM3	cusMEM4

Table 10. Summary of custom anti-*Drosophila* Membrin antibodies
Two rabbits were immunized with independent peptides corresponding to *Drosophila* Membrin (uniprot Q9VRL2), giving rise to four variants of custom rabbit polyclonal anti-*Drosophila* Membrin antibodies.

I reconstituted these antibodies with deionized water to a final 1 mg/ml concentration and screened each of the four different rabbit polyclonal anti-*Drosophila* Membrin antibodies for specificity in immuno-fluorescence microscopy of *Drosophila* brains. While cusMEM3 and 4 clearly recognized transgenically expressed FLAG::*membrin*[WT] in adult Mem-WT *Drosophila* brains, cusMEM1 and 2 barely did (Figure 23A and data not shown).

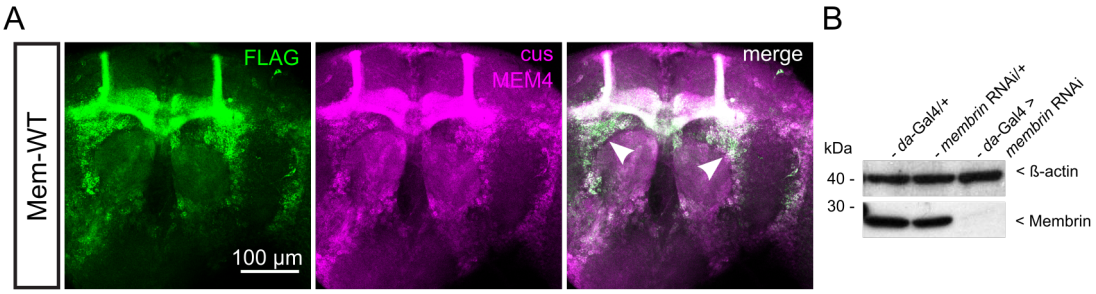

Figure 23. Custom anti-*Drosophila* Membrin antibody validation
(A) Confocal slices through an adult *Drosophila* Mem-WT brain, co-stained with an anti-FLAG and the custom anti-*Drosophila* Membrin antibody cusMEM4. Prominent colocalization between the two channels in somatic areas, such as adjacent to the antennal lobes (arrowheads) indicates that the custom antibody has the capability of recognizing Membrin in an immuno-fluorescence preparation.
(B) Western blot of L3 larvae lysates probed with cusMEM4. The band around approximately 25 kDa appears to represent *Drosophila* Membrin, as it is greatly reduced upon RNAi mediated global Membrin knock-down. 15 µg of total protein was loaded into each lane and equal loading confirmed with an anti-β-actin antibody.

However, none of these custom antibodies yielded a robust perinuclear staining – as expected for an antibody targeting a Golgi protein – in *Drosophila* brains with physiological Membrin levels (data not shown). Because of its superiority in immuno-fluorescence studies, cusMEM4 was further validated in western blot. There it recognized a band around the expected 25 kDa size, which disappeared almost entirely upon Membrin RNAi mediated knock-down (Gasteiger et al., 2003) (Figure 23B). This result not only suggests that the observed band around 25 kDa indeed represents *Drosophila* Membrin, but also that the GD 44535 *membrin* RNAi line induces efficient knock-down of Membrin levels. Thus, cusMEM4 represents a good tool for western blot and might also be useful for immuno-fluorescence studies, should an optimization of the immuno-staining protocol provide increased sensitivity towards endogenous Membrin expression levels.

4.4 Results

4.4.1 A novel *Drosophila* model of *GOSR2*-PME

In order to investigate the pathophysiological consequences of the *GOSR2*-PME mutations in our primary cell type of interest – neurons – as well as in an entire organism, we developed the first in vivo model of this disorder. Because Golgi SNARE proteins are highly conserved throughout evolution (Kienle et al., 2009a; 2009b; Kloepper et al., 2008; 2007), we chose the comparably simple yet genetically powerful *Drosophila melanogaster* as our experimental model. *Drosophila* harbors a single *GOSR2* orthologue, which is termed *membrin*. We obtained a *membrin* null strain (*membrin*^{1524}) for this study, which was previously generated in an EMS screen for defective trachea morphogenesis and kindly shard by Mark Krasnow (Ghabrial et al., 2011). This fly harbors a c.253C>T mutation in *membrin*, which gives rise to a premature stop codon (Q85X) upstream Membrin's critical SNARE and transmembrane domains and is therefore a null allele. The presence of this mutation was confirmed by Sanger sequencing in our lab (Figure 24A).

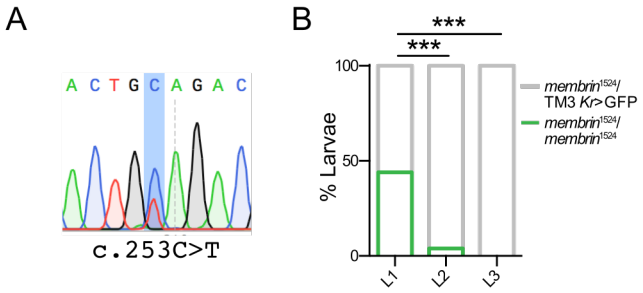

Figure 24. The *membrin* null allele *membrin*^{1524}
(A) Chromatogram depicting the heterozygous c.253C>T *membrin* sequence alteration in *w*[1118]; +; *membrin*^{1524}/TM6B-Tb.
(B) *membrin*^{1524} was balanced over the fluorescently labeled TM3 *Kr*>GFP chromosome to discern heterozygote animals. Homozygosity for *membrin*^{1524} caused largely L1 lethality, as at the L2 stage hardly any non GFP-positive larvae could be detected. N = 50, 53, 56 quantified larvae at the L1, 2, 3 stages; *** represents $p < 0.001$; Fisher's exact test and Bonferroni correction.

Homozygosity for *membrin*^{1524} caused pre-L3 lethality, as only Tubby L3 larvae could be observed in *Drosophila* stock where this allele is balanced over TM6B-Tb. To further investigate the lethal phase of this allele I rebalanced this stock over the fluorescent TM3 *Kr*>GFP chromosome, which

allows to discern heterozygous from homozygous animals from the germ band extension embryonic stage onwards (Casso et al., 2000). These investigations revealed that homozygosity for *membrin*^{1524} is largely lethal between the L1 and L2 larval stages (Figure 24B). This finding is surprising if we consider Membrin's essential role in mediating ER-to-Golgi trafficking and the observation that *BOS1* null yeast are incapable of mitotic growth (Shim et al., 1991). An explanation of this extended viability in *Drosophila* might be maternal Membrin mRNA and/or protein deposition into the embryo, which could rescue homozygous *membrin*^{1524} to the L1 stage. This notion was not experimentally tested as it goes beyond the central aim of our investigation, which aimed to unravel how partial loss of function Membrin alleles cause neuronal disease.

To investigate the consequences of G144W and K164del *GOSR2* or G147W and K166del *membrin* mutations in *Drosophila* we first generated wild-type and mutant UAS-*GOSR2*/UAS-*membrin* transgenes, which harbor an N-terminal FLAG tag. Each of these transgenes was inserted into the same genomic localization by ΦC31 integrase mediated site-specific integration, thus enabling similar expression levels between the different alleles (Bischof et al., 2007). To activate the otherwise inert UAS-transgenes the global *daughterless*-Gal4 (*da*-Gal4) driver was used (Brand and Perrimon, 1993). Finally, after backcrossing UAS-*GOSR2*/UAS-*membrin*, *da*-Gal4 and *membrin*^{1524} into the *w*[1118] mutant isogenic iso31 strain to control for genetic background effects, we combined all components in a way to enable expression of wild-type or mutant *GOSR2*/*membrin* in a *membrin* null background.

To assess functional conservation, I tested whether *Drosophila membrin* could be replaced by human *GOSR2*. Indeed, I found that global expression of wild-type *GOSR2* was capable of partially rescuing homozygous *membrin*^{1524} animals – which otherwise would die between the L1 and L2 larval stages – to the pupal and adult stages (Figure 25A, B). This experiment provides evidence supporting the otherwise bioinformatically determined conservation between human *GOSR2* and *Drosophila membrin*.

It therefore validates our approach of studying *GOSR2*-PME in this model organism. Furthermore, this observation illustrates that our genetic setup is functional and that the N-terminal FLAG tag does not abolish Membrin's function. It has to be noted, however, that these *GOSR2* rescue animals appeared slow and weak at the adult stage and usually died within three days after eclosion. Thus, human *GOSR2* is only capable of partially rescuing *membrin* null animals. Furthermore, G144W and K164del mutant *GOSR2* were not capable of rescuing homozygous *membrin*^{1524} animals to the pupal stage, as only Tubby L3 pupae were observed from the respective 'model crosses' (Figure 25A).

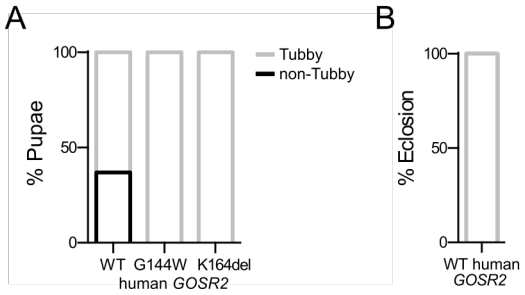

Figure 25. Wild-type human *GOSR2* enables early developmental viability of membrin null *Drosophila*
(A) Wild-type and mutant human *GOSR2* was globally expressed with the *daughterless*-Gal4 driver in a *membrin* null genetic background. Early developmental viability was assessed at the pupal stage. Non-Tubby pupae indicate the desired genotypes resulting from the necessary genetic cross as described in the Methods section. No obvious shift from the expected Mendelian ratios was observed in WT, while G144W/K164del mutant *GOSR2* failed to rescue to the pupal stage. N = 139, 87, 115 quantified total WT/G144W/K164del pupae.
(B) All scored WT *GOSR2* non-Tubby animals managed to eclose from their pupal cases. N = 51 quantified non-Tubby pupae.

We therefore shifted our focus to UAS-*membrin* transgenes, which are closer to the normal physiology of *Drosophila*. Expressing wild-type or G147W/K166del mutant Membrin in a *membrin*^{1524} background yields two *GOSR2*-PME model mutant fly lines and one control. Their full genotypes are abbreviated Mem-G147W, Mem-K166del and Mem-WT in this thesis (Figure 26).

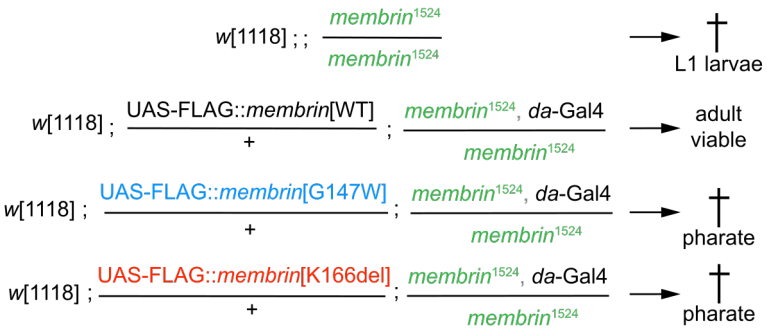

Figure 26. Genetics of the *GOSR2*-PME model used in this study
Genotypes of the *GOSR2*-PME *Drosophila* model used in this study. Four components – two *membrin* null alleles (*membrin*^{1524}), the global *da*-Gal4 driver and UAS-*membrin* transgenes – are combined by a single genetic cross (See 'Materials and Methods' for details).

4.4.2 Early phenotypes in mutant Membrin *Drosophila*

To investigate whether mutant Membrin causes *Drosophila* phenotypes that are informative for the investigation of the *GOSR2*-PME pathophysiology, I carefully assessed the resulting organismal consequences. Global expression of wild-type as well as G147W and K166del mutant Membrin was capable of rescuing homozygous *membrin*^{1524} animals to the pupal stage, which indicates that both mutations do not render the protein completely un-functional (Figure 27A). Both mutants exhibited subtle reductions in egg to pupa viability rates when compared to Mem-WT, which reached statistical significance only in Mem-K166del (Figure 27A). While these effects where mild, we observed a striking clustering of lethality of *GOSR2*-PME mutant *Drosophila* at the young adult stage. While Mem-WT successfully managed to eclose from their pupal cases and emerged as freely moving adults, we observed that Mem-G147W/Mem-K166del frequently died as fully developed pharate adults within their pupal cases (Figure 27B). When surgically freed from their pupal cases they appeared weak and uncoordinated. While 98% of Mem-WT animals managed to eclose, only around 10% of Mem-G147W and 33% of Mem-K166del did (Figure 27B). Those mutant animals that succeeded in freeing themselves from the pupal cases often got stuck in the food and died within a few days. This aggregation of early lethality at the pharate adult stage might be because eclosion represents a considerable hurdle, which might be too big to overcome for motor impaired Mem-G147W

or Mem-K166del animals. Given that G147W and K166del mutant Membrin was only *partially* able to rescue lethality arising from homozygosity for a *membrin* null allele, we present organismal data that support the liposome fusion assay derived notion that the *GOSR2*-PME mutations confer *partial* loss of Membrin function. Further experimental evidence supporting this idea stems from global Membrin knock-down via RNA-interference, which also resulted in pharate stage lethality (Figure 27C, quantified by Nian Patel).

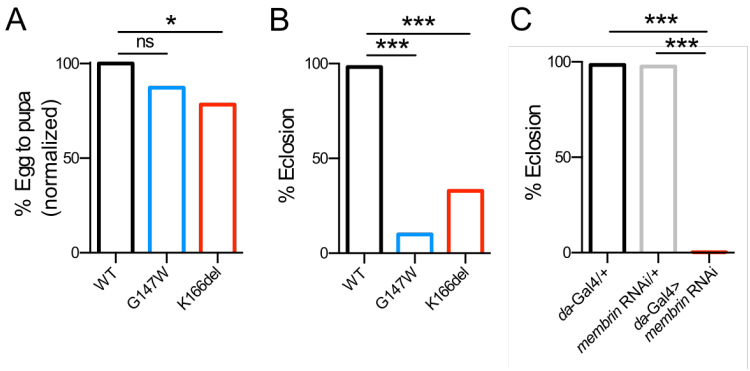

Figure 27. Membrin mutations cause early lethality
(A) Global expression of WT, G147W and K166del mutant Membrin rescues *membrin* null homozygous animals to the pupal stage. A subtle decrease in egg to pupa viability is apparent in Mem-K166del when compared to Mem-WT. Data expressed as relatives to Mem-WT. N = 1222, 1308, 1260 counted total eggs/embryos for Mem-WT/-G147W/-K166del crosses. Statistical analysis was performed based on the theoretically determined number of eggs/embryos of the desired genotype, i.e. N = 306, 327, 315 for Mem-WT/-G147W/-K166del.
(B) Mem-G147W and Mem-K166del frequently die as fully developed pharate adults within their pupal cases as shown by a drastic decrease in eclosion rates compared to Mem-WT. N = 120, 112, 97 individual non-Tubby pupae scored for Mem-WT/-G147W/-K166del.
(C) Global RNAi mediated Membrin knock-down with the *da*-Gal4 driver resulted in pharate stage lethality. N = 378, 162, 313 individual pupae scored for the *da*-Gal4 driver, *membrin* RNAi only and knock-down genotypes. Data were obtained and analysed by Nian Patel.
*, *** represent $p < 0.05$, 0.001, ns = not significant ($p > 0.05$); Fisher's exact test with Bonferroni correction.

Also global overexpression of mutant Membrin in a wild-type *membrin* background resulted in substantial pharate stage lethality (Figure 28A – quantified by Nian Patel), presumably by outcompeting endogenous wild-type Membrin. If the overexpressed mutant Membrin isoform is far more concentrated in the cis-Golgi, then we can easily imagine a scenario where it is preferentially integrated into the cis-Golgi SNARE complex instead of the endogenous wild-type protein. Because endogenous Membrin is still present

and likely still contributes to membrane fusion in this setting, the eclosion deficits are reduced compared to those observed in Mem-G147W and Mem-K166del (compare Figure 28A with Figure 27B).

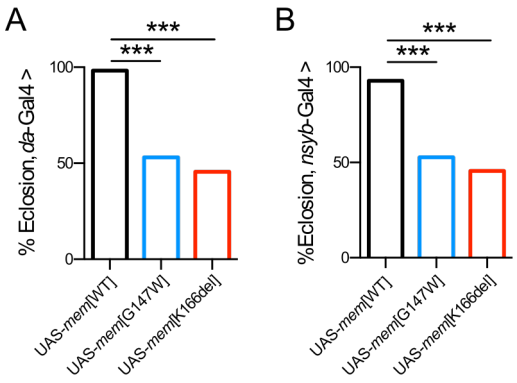

Figure 28. Global and nervous system overexpression of mutant Membrin
(A) Global overexpression of mutant UAS-*membrin* in wild-type *membrin* animals with *da*-Gal4 resulted in reduced eclosion rates due to pharate adult lethality. N = 284, 514, 403 individual pupae scored for UAS-*membrin*[WT]/[G147W]/[K166del]. This experiment was performed and analysed by Nian Patel.
(B) Nervous system specific overexpression of mutant UAS-*membrin* in wild-type *membrin* animals with *nsyb*-Gal4 resulted in reduced eclosion rates due to pharate adult lethality. N = 616, 491, 618 individual pupae scored for UAS-*membrin*[WT]/[G147W]/[K166del].
*** represent $p < 0.001$; Fisher's exact test with Bonferroni correction.

Nevertheless, this experiment suggested to us that the genetically simple approach of overexpressing mutant Membrin in an otherwise wild-type *membrin* animal could serve as a tool to test whether the observed lethality phenotypes in Mem-G147W/Mem-K166del are derived from neuronal abnormalities. Indeed, when we selectively overexpressed G147W or K166del mutant Membrin in the nervous system of *Drosophila* with the *nsyb*-Gal4 driver line we observed pharate adult stage lethality (Figure 28B), with a relative severity comparable to global overexpression with *da*-Gal4. These findings suggest that expression of mutant Membrin in neurons is *sufficient* to cause the lethality phenotypes observed in Mem-G147W and Mem-K166del. They therefore reinforce the notion that the *GOSR2*-PME phenotype can arise from selective vulnerability of neurons to the respective Membrin mutations.

Next I tested whether *GOSR2*-PME model *Drosophila* also exhibited organismal phenotypes prior to their premature death as young adults, which occurred either within the pupal cases or soon after eclosion. Interestingly, *membrin* mutant animals appeared to be developmentally delayed. I quantified this effect by selecting late L2/early L3 Mem-WT, Mem-G147 and Mem-K166del larvae, transferring them to fresh food tubes and counting the appearance of pupae daily for the next five days. Onset of pupation was observed two days after selection of larvae. While 31% of Mem-WT rescue animals pupated by this day, only around 8% of Mem-K166del and none of Mem-G147W were observed to reach this developmental stage (Figure 29A). By day three almost all Mem-WT and Mem-K166del animals were pupae whereas only approximately 21% of Mem-G147W animals pupated and it took this group of animals until day five for all animals to initiate pupation.

Given that *GOSR2*-PME is a severe epilepsy syndrome and movement disorder, we wanted to find out whether *GOSR2*-PME *Drosophila* exhibited signs of motor abnormalities. I therefore quantified larval locomotion by counting 4 mm grid crosses within 60 s. Mem-WT crossed on average 10 grids in 60 s (Figure 29B), whereas Mem-G147W and Mem-K166del only approximately 7.5 grids. This finding illustrates clear motor defects in these mutants, which otherwise appear morphologically grossly normal.

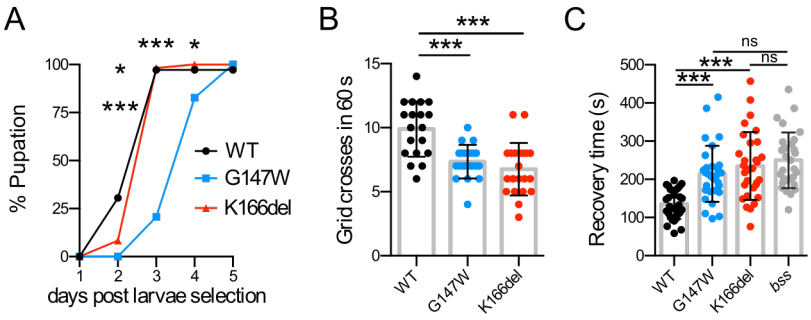

Figure 29. Developmental delay, locomotor deficits and seizure-like behavior in *GOSR2*-PME model larvae
(A) Mem-WT, Mem-G147W and Mem-K166del larvae were transferred to fresh food tubes at the late L2/early L3 developmental stages. Onset of pupation was subsequently scored for 5 consecutive days and expressed as a fraction of total pupae. N = 36, 58, 59 individual pupae were counted for Mem-WT/-G147W/-K166del.
(B) Freely moving Mem-G147W and Mem-K166del L3 larvae crossed fewer 4 mm grids in 60s than Mem-WT. Replicate values derived from individual L3 larvae, mean and SD are shown. N = 19, 20, 21 for Mem-WT/-G147W/-K166del.
(C) Recovery time after a 30 V electroshock to the central nervous system of L3 larvae was quantified as an indirect readout of seizure severity/duration. A significant increase in Mem-G147W and Mem-K166del is apparent when compared to Mem-WT. Both mutants are comparable to the seizure mutant *bang-senseless* (*bss*). Replicate values derived from 30 larvae per genotype, mean and SD are shown. This experiment was carried out and analysed by Carlo Giachello in Richard Baines' lab.
*, *** represent $p < 0.05$, 0.001, ns = not significant ($p > 0.05$); Fisher's exact test with Bonferroni correction (A), ANOVA with Dunnett's multiple comparison test (B), Kruskal-Wallis test with Dunn's post-hoc test (C).

Because *GOSR2*-PME is a severe epilepsy syndrome, we wanted to know whether also Mem-G147W and Mem-K166del had hyperexcitability phenotypes. Indeed, Carlo Giachello in Richard Baines' lab found that Mem-G147W and Mem-K166del L3 larvae exhibit seizure-like phenotypes, with a relative severity comparable to the *bang-senseless Drosophila* seizure model (Figure 29C) (Giachello and Baines, 2015; Parker et al., 2011). They displayed significantly larger recovery times from electro-shock induced seizures when compared to Mem-WT, which is thought to be a consequence of increased seizure severity and/or persistent epileptiform activity in mutant *membrin* animals (Giachello and Baines, 2015). *GOSR2*-PME *Drosophila* therefore not only exhibit ataxia-like locomotor deficits but also seizure-like phenotypes, which are correlates of two core neurological features observed in the human disorder.

Collectively, these phenotypes are thought to arise from a decrease in ERGIC/cis-Golgi lipid fusion rates due to partial Membrin SNARE defects. In order to test whether also reductions in G147W mutant Membrin levels could contribute to the observed phenotypes – as is suggested by decreased G144W mutant Membrin levels in patient fibroblasts – I performed semi-quantitative western blot with Mem-WT, Mem-G147W and Mem-K166del L3 larvae lysates (Figure 30A). These studies revealed similar Membrin levels in Mem-G147W and Mem-K166del when compared to Mem-WT, with only a subtle reduction in Mem-G147W (Figure 30B).

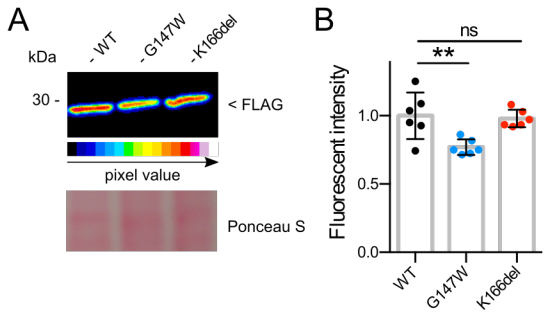

Figure 30. Membrin levels in *GOSR2*-PME *Drosophila* models
(A) Western blot of Mem-WT, Mem-G147W and Mem-K166del L3 larvae lysates. Animals were raised at 25°C and shifted overnight to 18°C prior to lysis, in order to reduce Gal4 expression and therefore facilitate unmasking of potentially reduced protein stability of G147W Membrin (Duffy, 2002). 5 µg of total protein was loaded into each lane and equal loading verified with Ponceau S staining.
(B) Quantification of experiment as described in (A). Normalized to Mem-WT. N = 6 replicate values, derived from three independent lysates per genotype and immunoblotted twice. Mean and SD are shown. ** represents $p < 0.01$, ns = not significant ($p > 0.05$); ANOVA with Dunnett's multiple comparison test.

This indicates that the observed phenotypes in our *Drosophila* models can solely be attributed to the SNARE defects and not to reductions in mutant Membrin levels. One possible explanation for the discrepancy between high G147W Membrin levels in our *Drosophila* models and a large reduction of G144W mutant Membrin in fibroblasts (Figure 13) might be that the expression levels in our model are artificially high and therefore largely mask G144W mutant Membrin proteostasis alterations. Alternatively, this result might further indicate that the fibroblast data are rather due to individual variations in Membrin levels – as is suggested by Membrin level variations

between the healthy controls – and thus do not represent changes incurred by the G144W mutation. To further investigate whether G144W causes Membrin protein instability it would be revealing to overexpress wild-type and mutant Membrin fused to a Halo or SNAP tag in HEK cells. These constructs could then be pulse labelled, which would enable to determine whether protein turnover rates are increased due to the G144W mutation.

In summary, I have developed the first *GOSR2*-PME in vivo models by utilizing *Drosophila*. These models exhibit severe and early phenotypes, which recapitulate key aspects of human patients. By demonstrating partial functional inter-changeability of human *GOSR2* and *Drosophila membrin* I have further confirmed the validity of our choice of model organism. Furthermore, our phenotypic data suggest partial loss of Membrin function due to *GOSR2*-PME mutations, which likely results in the observed organismal phenotypes due to *neuronal* abnormalities.

4.4.3 Profound dendrite growth deficits in *GOSR2*-PME model neurons

Important clues towards the mechanism underlying neuronal dysfunction due to Membrin mutations stemmed from studies investigating neuronal consequences of mutations in other ER-to-Golgi trafficking proteins. Overexpression of GTP-locked Arf1[Q71L] in developing cultured hippocampal neurons led to severely impaired dendritic growth (Dascher and Balch, 1994; Horton et al., 2005). Similarly, Ye et al. found in a *Drosophila* forward genetic screen that mutations in Sec23, Sar1 and Rab1 cause dendritic growth deficiencies (Ye et al., 2007). The explanation for this observation is that an early secretory pathway block likely prevents ER-derived lipids and proteins from reaching the surface of a growing neuron, which poses immense demands on such supplies due to its very large area (Hanus and Ehlers, 2008).

However, in contrast to Arf1[Q71L] and the truncated Sar1, which was studied due to organismal lethality in mosaic animals (Dascher and Balch, 1994; Horton et al., 2005; Ye et al., 2007), the G144W and K164del Membrin

mutations will not cause a complete block of anterograde trafficking. After all, yeast liposome fusion studies and *Drosophila* phenotypes of the orthologous mutations suggested *partial* and not complete loss of Membrin function. In addition, ER-to-Golgi trafficking in G144W mutant Membrin fibroblasts was efficient (Figure 17 and Figure 18). Thus, we tested whether even such a partial decrease might be sufficient to impair dendritic growth. To this end we utilized a set of highly elaborate sensory neurons within the larval body-wall neurons termed class IV dendritic arborization (da) neurons, which we genetically labeled with the *ppk* promoter and a membrane tagged – and therefore secretory pathway dependent – CD4::tdGFP reporter (Grueber et al., 2003; Han et al., 2011). This is a well established and widely used dendritogenesis model because these neurons have highly sophisticated, tiled dendritic arbors that branch in 2D and they are unambiguously polarized into a single axon and multiple dendrites (Figure 31A; arrowhead indicates the single axon, the remaining processes are dendrites) (Grueber et al., 2002). Amongst the three class IV da neurons, which are labeled in each hemisegment by the *ppk* promoter, we imaged a particular subtype termed ddaC neuron (the other *ppk*-positive larval body wall neurons are termed v'ada and vdaB) in abdominal segment 5 of Mem-WT, Mem-G147W and Mem-K166del L3 larvae (Figure 31A).

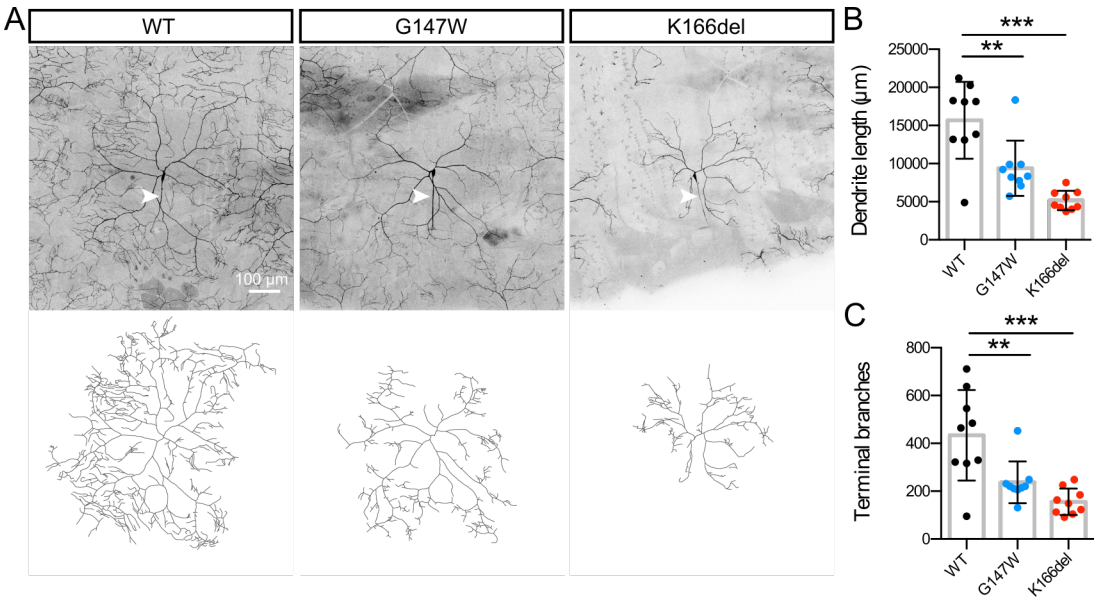

Figure 31. Membrin mutations cause dendritic growth deficits
(A) Maximum intensity projections of ddaC abdominal segment 5 neurons genetically labeled with *ppk* > CD4::tdGFP in Mem-WT/-G147W/-K166del. Respective tracings of the dendritic arbors are shown below. Arrowheads indicate axons. 9 abdominal segment 5 ddaC neurons from 7/7/8 different L3 larvae for Mem-WT/G147W/-K166del were traced and analyzed in (B, C) and Figure 32.
(B) Total dendritic length extracted from tracings as shown in (A). Replicate values derived from individual ddaC neurons, mean and SD are shown.
(C) Number of terminal branches of ddaC A5 neurons as shown in (A). Replicate values derived from individual ddaC neurons, mean and SD are shown.
, * represent $p < 0.01, 0.001$; one-way ANOVA with Dunnett's multiple comparison test.

The unique advantage of this approach is that we were able to image exactly the same identifiable neuron across different genotypes and thus reduced intrinsic variation of dendritic size to a minimum. Strikingly, both mutations caused substantial dendritic growth deficiencies. Mean reduction of total dendritic length amounted to approximately 40% in Mem-G147W and 67% in Mem-K166del when compared to Mem-WT (Figure 31B). Similarly, the average number of terminal dendritic branches was decreased in Mem-G147W and Mem-K166del by 45% and 64% respectively (Figure 31C). In addition, Sholl analysis revealed a clearly reduced elaboration of dendritic arborization in both mutants from approximately 100 µm away from the soma (Figure 32A) and a significant decrease of overall dendritic intersections (Figure 32B).

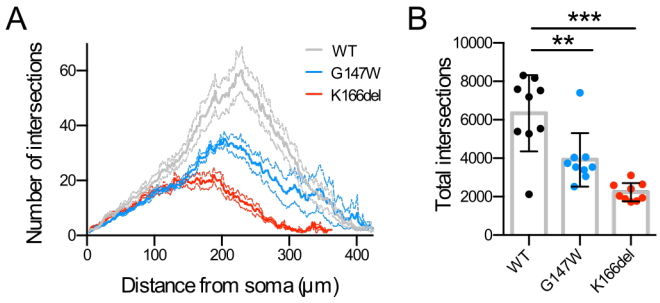

Figure 32. Sholl analysis
(A) Number of intersections of dendritic tracings (Figure 31A) with concentric circles with 2 pixel/circle increasing radii. Mean and SEM of 9 abdominal segment 5 ddaC neurons are shown for each genotype.
(B) Total intersection of Sholl analysis as described in (A). Replicate values derived from individual ddaC neurons, mean and SD are shown. **, *** represent $p < 0.01, 0.001$; one-way ANOVA with Dunnett's multiple comparison test.

Taken together we found that the partial loss of function G147W and K166del Membrin mutations exert a substantial effect upon neuronal growth in *Drosophila* model neurons. This may be the consequence of a subtle delay in the early secretory pathway, thus limiting the availability of plasma membrane, which can be added to the growing dendritic arbor.

To test whether a secretory pathway deficit is the cause of the observed dendrite growth deficits, I quantified the steady state levels of the secretory pathway dependent CD4::tdGFP model cargo in proximal dendrites of *GOSR2*-PME model *Drosophila* (Figure 33A). Indeed, mean fluorescence intensity of this cargo was significantly decreased in proximal dendrites of Mem-K166del (Figure 33A, B). Similarly, CD4::tdGFP levels were significantly reduced in proximal ddaC axons of Mem-K166del (Figure 33A, C). It has to be noted, however, that we did not distinguish between cell surface and intracellular fluorescence in this experiment. Thus, an accumulation of pre-Golgi CD4::tdGFP – which might be the result of the Membrin mutations – might be contributing to the fluorescence signal and therefore subtle effects could be masked. A way to circumvent this issue would be to selectively antibody stain the extracellularly located GFP tag of cell surface localizing CD4::tdGFP by omitting detergent in the staining protocol. Another potential pitfall is that I quantified neurites in proximity to the somatic Golgi, which might not be sensitive enough to detect a smaller

effect size, such as we would expect in Mem-G147W. Indeed, James Jepson found that distal axonal/synaptic CD4::tdGFP was significantly reduced both in Mem-K166del *and* Mem-G147W, which was not significantly different to Mem-WT proximally in neither axons nor dendrites (Figure 33). James Jepson also found that the endogenous synaptic cargo cysteine string protein (CSP) was significantly reduced at the neuromuscular junction (NMJ) of Mem-G147W and Mem-K166del L3 larvae when compared to Mem-WT (Figure 33F, G).

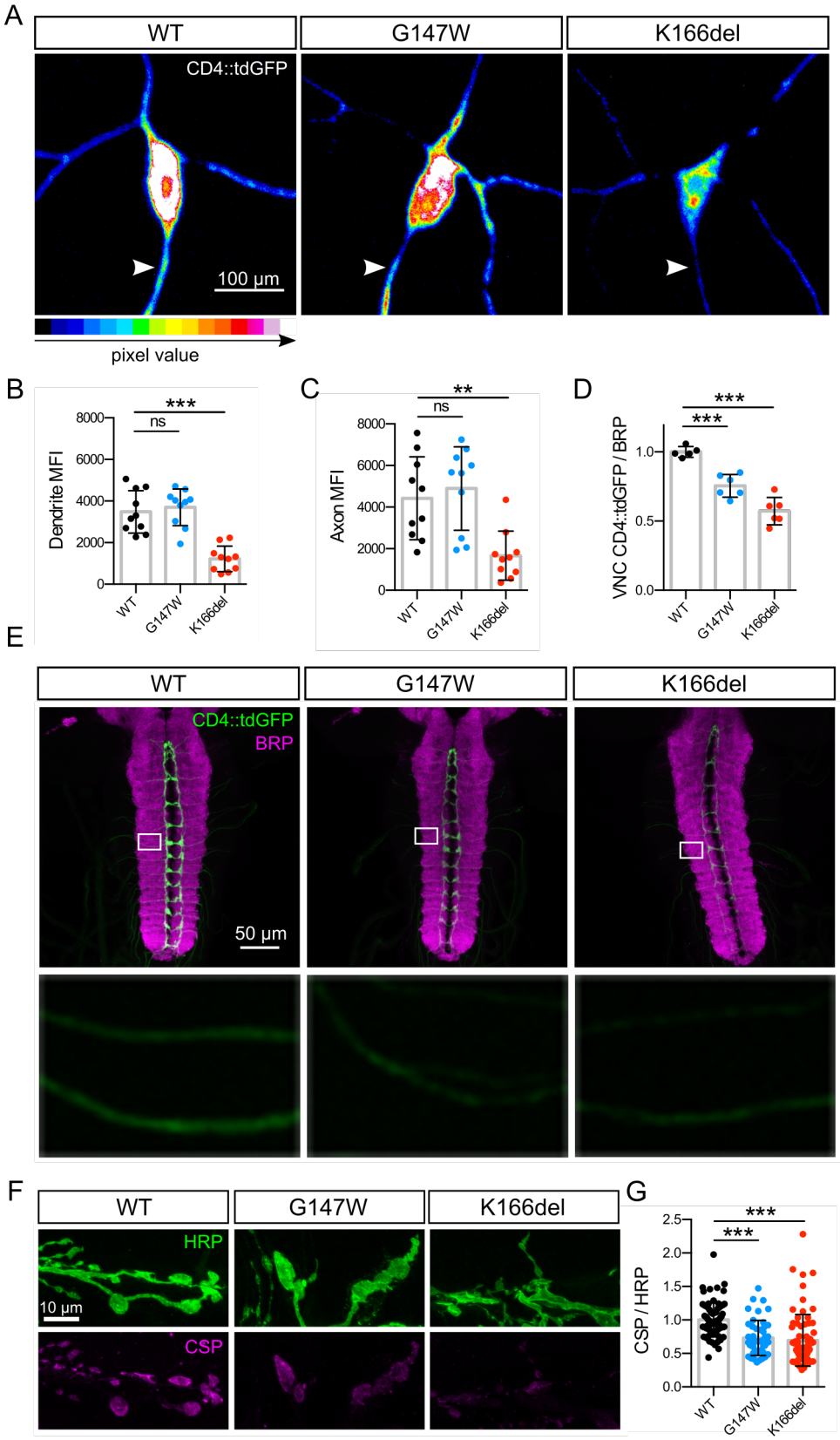

Figure 33. Steady-state dendritic, axonal and synaptic secretory pathway deficits

(A) Maximum intensity projections of abdominal segment 5 ddaC neurons in Mem-WT, Mem-G147W and Mem-K166del L3 larvae expressing the secretory pathway dependent CD4::tdGFP model cargo. Arrowheads indicate axons.

(B) Mean fluorescence intensity (MFI) in major dendrites within 37.5 µm distance from the soma center of neurons as described in (A). Replicate values were derived from 10 ddaC neurons per genotype (5 L3 larvae each). Mean and SD are shown.
(C) Mean fluorescence intensity (MFI) in the axon within 37.5 µm distance of the soma center of neurons as described in (A). Replicate values were derived from 10 ddaC neurons per genotype (5 L3 larvae each). Mean and SD are shown.
(D) Quantification of CD4::tdGFP fluorescence in *ppk* neuron axons and synapses in the L3 larval VNC, normalized to BRP, as shown in (E). N = 5, 6, 6 for Mem-WT/-G147W/-K166del. Replicate values derived from different larval brains, mean and SD are shown.
(E) Maximum intensity projections of distal *ppk* neuron axons/synapses reveal reduced levels of CD4::tdGFP in the VNC of Mem-G147W and Mem-K166del compared to Mem-WT. Neuropil is stained with anti-BRP.
(F) NMJs were stained with anti-CSP and anti-horseradish peroxidase (HRP) antibody, which labels neuronal membranes due to crossreactivity with certain surface glycans (Fabini et al., 2001). A significant reduction of CSP levels is apparent in Mem-WT as compared to Mem-G147W and Mem-K166del.
(G) Quantification of experiment as shown in (F). CSP levels were normalized to HRP and expressed relative to Mem-WT. N = 77/47/72 synaptic boutons from 9/8/7 L3 larvae for Mem-WT/-G147W/-K166del. Replicate values derived from individual synaptic boutons, mean and SD are shown.
, * represent $p < 0.01$, 0.001, ns = not significant ($p > 0.05$); one-way ANOVA with Dunnett's multiple comparison test (B-D); Kruskal-Wallis test with Dunn's post-hoc test (G).
Experiments and analysis shown in (D-G) were carried out by James Jepson.

Importantly, a CD4::tdGFP secretory pathway transport deficit might not be apparent at steady state but only when its trafficking is dynamically studied. In theory, we could imagine that an ER-to-Golgi trafficking deficit would result in the availability of fewer post-Golgi carriers, which are transported from the trans-Golgi network to the dendritic surface and thereby enable its growth. Thus, to visualize the trafficking of CD4::tdGFP I photo-bleached abdominal segment 5 ddaC soma adjacent major dendrites. A large dendritic region – contained within a 50 μm^2 bleach area – was photo-bleached and the recovery measured in a small dendritic region 25 µm from the soma (Figure 34A). This approach was chosen in order to minimize the contribution of lateral diffusion of cell surface localized CD4::tdGFP into the quantified region. After all, the signal of interest is not surface localized cargo per se but CD4::tdGFP molecules which are trafficked via the secretory pathway to the dendritic surface. As a control for my imaging settings I also quantified fluorescence in non-bleached dendrites, which remained stable over the approximately 30 min time course (Figure 34B). Consistent with more profound SNARE and secretory trafficking defects in Mem-K166del we could

detect a clear reduction in fluorescence recovery after experimental photo-bleaching in this mutant and only a non-significant trend towards reduced recovery in Mem-G147W when compared to Mem-WT (Figure 34C).

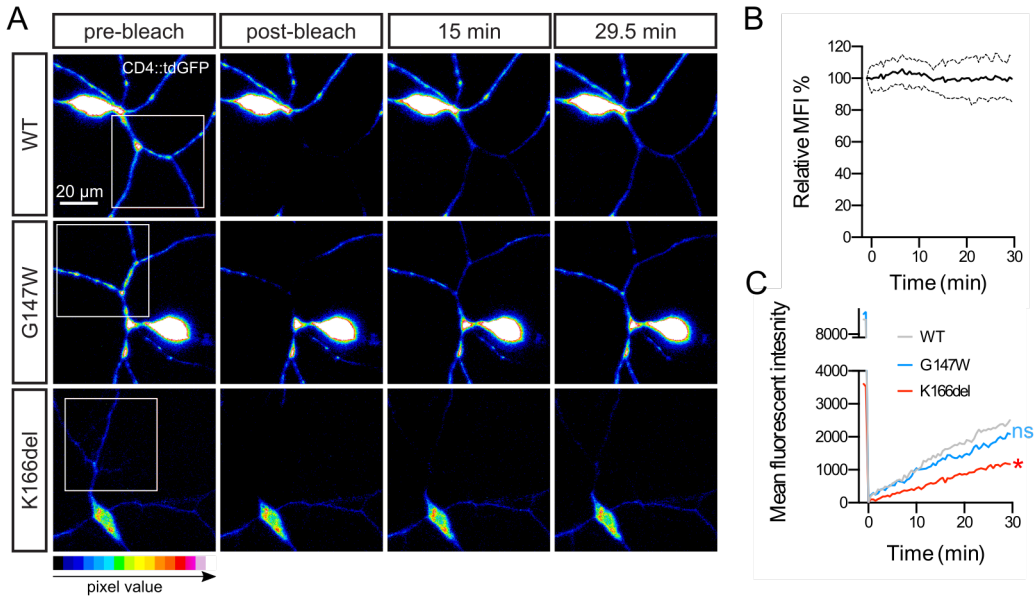

Figure 34. Dendritic FRAP in Membrin mutant ddaC neurons
(A) CD4::tdGFP in large segments of major ddaC A5 dendrites adjacent to the soma were photobleached with a 50 µm^2 region of interest (large square in first column) and fluorescence recovery quantified 25 µm from the soma proximal bleach margin for 29.5 min.
(B) Non-bleach control measurements of unbleached dendrites. Mean fluorescence intensities (MFI) in non-bleached regions of interest of 5 ddaC neurons, from 5 different L3 larvae per genotype were pooled in this graph. Mean and SD are shown.
(C) Average FRAP traces of experiment as described in (A). Means of 9/8/9 abdominal segment 5 ddaC neurons, from 9/8/9 different L3 larvae for Mem-WT/-G147W/-K166del are shown. */ns indicate endpoint comparison after 29.5 min recovery. * represents $p < 0.05$, ns = not significant ($p > 0.05$); one-way ANOVA with Dunnett's multiple comparison test.

In summary, I found reduced dendritic growth in Mem-G147W and Mem-K166del, which is likely caused by reduced cargo trafficking into growing dendrites as a result of partially decreased ER-to-Golgi trafficking rates.

4.4.3.1 Overexpression of mutant Membrin in class IV da neurons causes dendrite growth deficits

Previous organismal data suggested that mutant Membrin could be overexpressed in otherwise wild-type *membrin Drosophila* to recapitulate aspects of *GOSR2*-PME in a genetically more simple and versatile way than

our models permit. To validate the idea that mutant Membrin transgenes could serve as tools, I sought to also study their effects on the neuronal level. Therefore, I overexpressed wild-type and mutant Membrin in class IV da neurons of wild-type *membrin* Drosophila. To visualize ddaC neurons in abdominal segment 5, CD4::tdGFP was expressed with the *ppk* promoter (as described above). This experiment revealed that also simple overexpression of mutant Membrin – when compared to wild-type Membrin overexpression – is sufficient to result in less elaborate dendrites (Figure 35A).

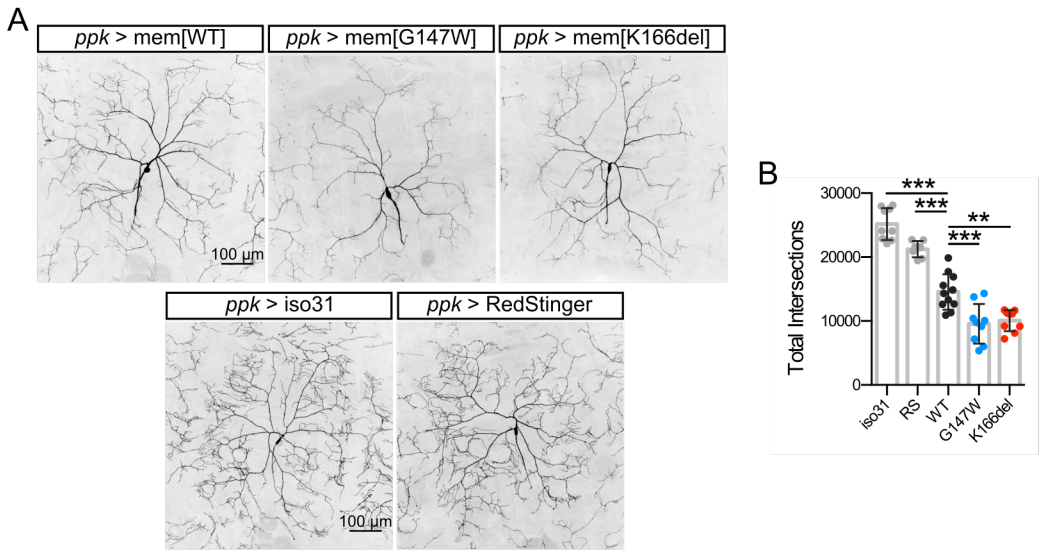

Figure 35. Overexpression of mutant Membrin in ddaC neurons
(A) Maximum intensity projections of ddaC, abdominal segment 5 neurons. *w*[1118]; *ppk*-CD4::tdGFP; *ppk*-Gal4 were crossed to *w*[1118]; UAS-*membrin*[WT]/[G147W]/[K166del], iso31 or *w*[1118]; +; UAS-*RedStinger*.
(B) Sholl analysis of experiment as described in (A). N = 9, 7, 11, 9, 9 ddaC neurons from 9/7/11/9/9 different L3 larvae for iso31, UAS-*RedStinger*, UAS-*membrin*[WT]/[G147W]/[K166del]. Replicate values derived from individual ddaC neurons, mean and SD are shown. **, *** represent $p < 0.01, 0.001$; one-way ANOVA with Tukey's multiple comparison test.

To rapidly retrieve quantitative results from these neurons, I performed Sholl analysis directly from thresholded images (Ferreira et al., 2014). This revealed a significantly decreased number of total intersection for G147W and K166del when compared to wild-type (Figure 35B). Because the mutations only affect the class IV da neurons in this experiment, it provides evidence that the dendrite growth deficits as observed in *GOSR2*-PME *Drosophila* is due to a cell autonomous deficiency and not due to e.g. a lack of trophic factors from other cell types in the larval body wall. Given the tight

connection between the secretory pathway and plasma membrane expansion, a primarily cell autonomous deficit was a priori most likely, which was hereby also experimentally confirmed. The relative severity of the dendritic growth deficits was lower in the overexpression setting when compared to the *GOSR2*-PME models. This is expected and consistent with less severe organismal phenotypes, when endogenous Membrin is present (compare Figure 28A, Figure 27B). Of note, also overexpression of wild-type Membrin in ddaC neurons induced dendrite growth deficiencies, thereby suggesting that increased Membrin levels can partially impair secretory trafficking, potentially by interfering with the trans-Golgi SNARE complex as an inhibitory (i-) SNARE (Varlamov et al., 2004). This is apparent when we compare wild-type Membrin overexpressing ddaC neurons with ddaC neurons where only CD4::tdGFP and Gal4 is present and those, with additional expression of an unrelated RFP and a nuclear localization sequence (Figure 35A, B). In summary, these experiments further suggest that mutant Membrin transgenes can readily be used for the study of *GOSR2*-PME. Furthermore, it highlights how increased Membrin levels in itself are sufficient to partially impair dendritic growth and confirmed that Membrin mutation induced dendrite growth deficits are due to cell autonomous defects.

4.4.4 Morphological and physiological abnormalities at mutant Membrin synapses

While dendritic length of *ppk* labelled ddaC neurons was greatly reduced in *GOSR2*-PME model Drosophila, James Jepson found that *ppk* labelled class IV da neuron axon bundles (comprising of one ddaC, v'ada, vdaB axon per hemisegment) reached their target synaptic regions in the center of the ventral nerve cord (Figure 33E) (Grueber et al., 2007). This finding clearly illustrates that axonal length is preserved in class IV da sensory neurons of *GOSR2*-PME *Drosophila*. These cells have elaborate dendrites *and* long axons, which therefore points towards a preferential vulnerability of dendrites due to Membrin mutations. Thus, our finding underscores results from Ye et al., who suggested that axonal growth is less vulnerable to early secretory pathway defects than dendritic growth (Ye et al., 2007). Nevertheless, James

Jepson found a clear secretory pathway deficit in distal axons, as steady state levels of CD4::tdGFP levels were significantly reduced in Mem-G147W and Mem-K166del when compared to Mem-WT (Figure 33D). Because synaptic development and function are highly orchestrated processes, where many proteins must be provided in the right quantity at the right time via the secretory pathway, we speculated that synaptic integrity might be altered as a result of the pathogenic Membrin mutations. In order to evaluate potential synaptic morphological abnormalities in *GOSR2*-PME *Drosophila*, James Jepson studied the NMJ of L3 larvae. These are glutamatergic contacts between motoneurons and body wall muscles, which have been widely used as model synapses due to their large size and ease of experimental manipulation (Harris and Littleton, 2015). Strikingly, James Jepson found a host of abnormalities at mutant Membrin NMJs, including elongated protrusions reminiscent of collapsed boutons, synaptic retraction, and cytoskeletal abnormalities (Figure 36A-D and data not shown).

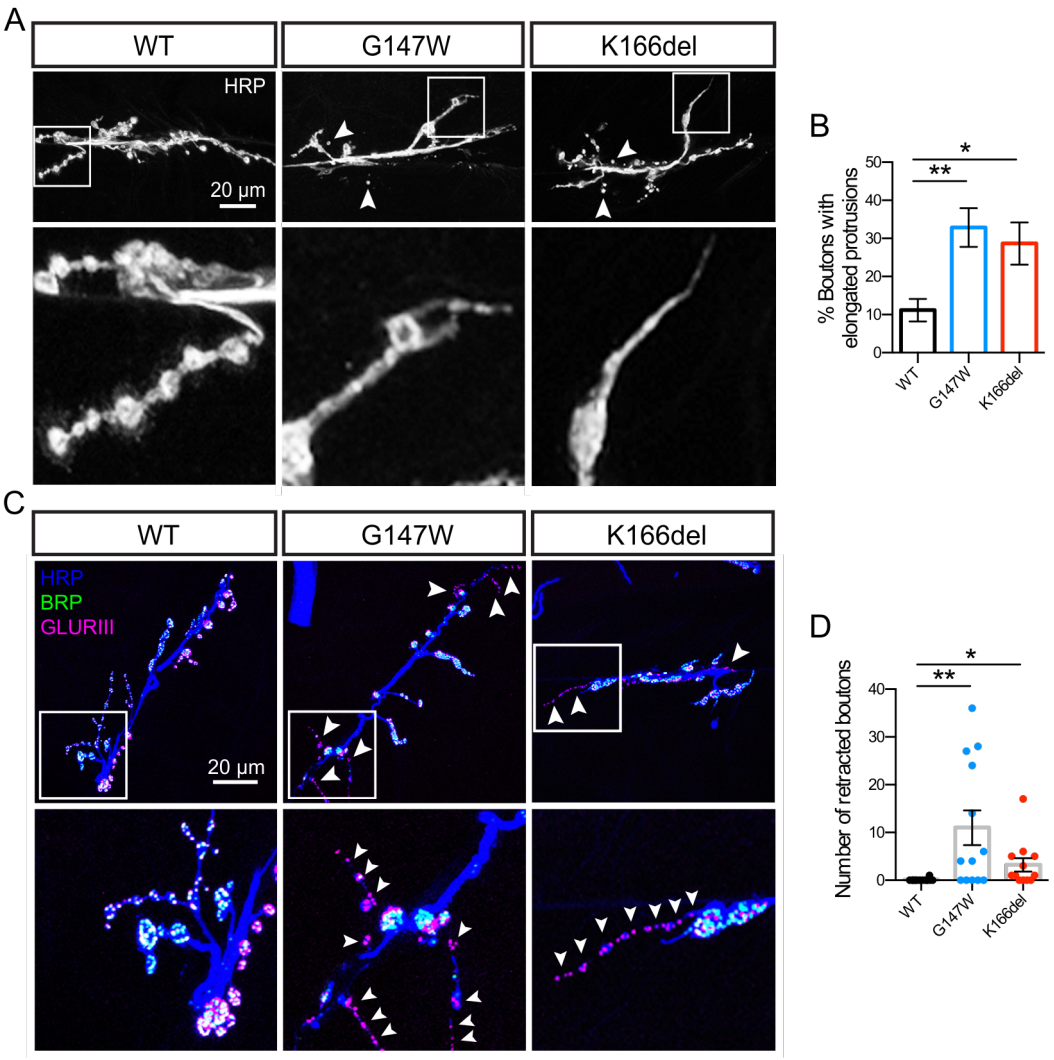

Figure 36. Structural abnormalities at *GOSR2*-PME model NMJs
(A) Muscle 6/7, abdominal segment 3 NMJs were stained with an anti-HRP. Maximum intensity projections of confocal z-stacks show rounded boutons in Mem-WT and elongated terminal protrusions in Mem-G147W and K166del. Arrowheads indicate isolated boutons, which are indications of synaptic retraction and was was further investigated in (C) and (D).
(B) Quantification of experiment as described in (A). N = 32, 31, 31 scored NMJs from 21/19/20 different L3 larvae for Mem-WT/-G147W/-K166del. Mean and SEM are shown.
(C) Apposition between pre- and postsynaptic membranes was evaluated by co-staining the presynaptic active zone protein Bruchpilot (BRP) and the postsynaptic glutamate receptor (GLURIII). Arrowheads indicate synaptic retraction, where GLURIII lacks its presynaptic active zone.
(D) Quantification of experiment as described in (C). N = 14, 13, 12 NMJs from 9/8/9 L3 larvae for Mem-WT/-G147W/-K166del. Replicate values derived from individual NMJs, mean and SEM are shown.
*,** represent $p < 0.05, 0.01$; Kruskal-Wallis test with Dunn's post-hoc test.
These experiments were carried out and analysed by James Jepson.

These morphological changes in *GOSR2*-PME *Drosophila* and the fact that human patients suffering from this disorder are profoundly hyperexcitable

suggested to us that also synaptic physiology might be altered. This is why Simon Lowe extended these morphological studies by evaluating synaptic transmission at this NMJ model synapse. He found a significant decrease in spontaneous neurotransmitter release in mutant animals (Figure 37A, B). In addition, Mem-G147W and Mem-K166del displayed a striking effect of hyperactive evoked synaptic transmission. Muscular responses to supra-threshold stimulation of the innervating nerve frequently resulted in dysmorphic and broadened excitatory postsynaptic potentials (EPSPs), which was particularly striking under 10 Hz repetitive stimulation (Figure 37C, D).

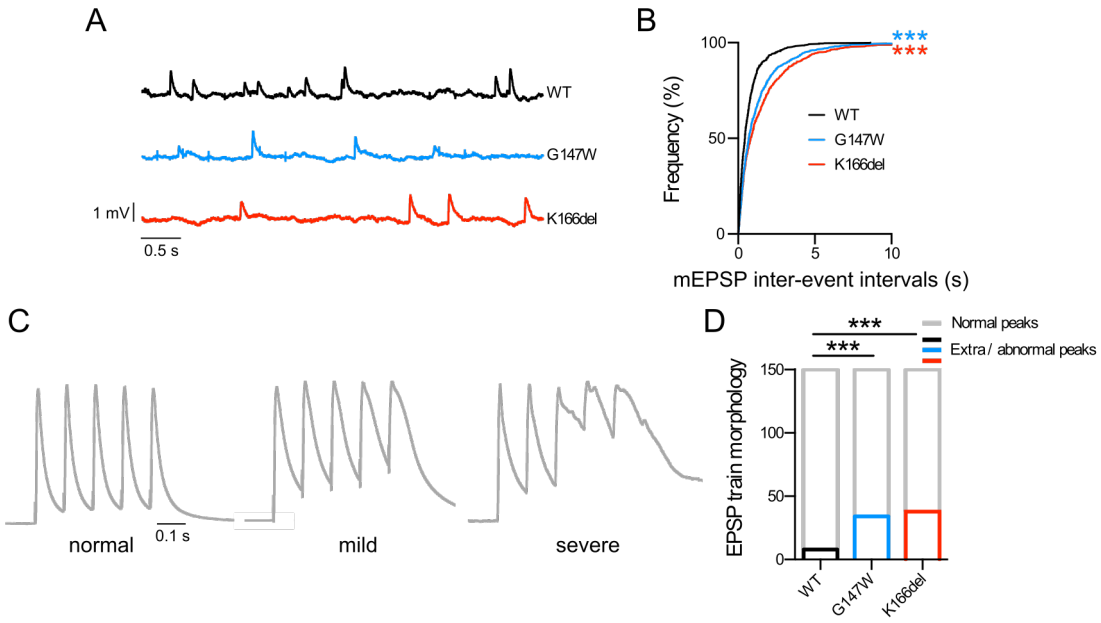

Figure 37. Hyperactive *GOSR2*-PME model NMJs
(A) mEPSP traces of Mem-WT/-G147W/-K166del recorded from muscle 6, abdominal segments 2-4.
(B) Cumulative frequency of mEPSP inter-event interval times of recordings as shown in (A). 800 mEPSPs from 8 animals per genotype were analysed.
(C) EPSPs, evoked by 5 stimuli at 10 Hz, were recorded from muscle 6, abdominal segments 2-4. Example traces are shown, ranging from normal to severely distorted shapes. Traces are normalized to the peak amplitude.
(D) EPSP train morphology was classified by a blinded observer. 10 animals per genotype were recorded and for each of them 15 EPSP trains analyzed.
*** represents $p < 0.001$; Kolmogorov-Smirnov test and Bonferroni correction (B), Fisher's exact test and Bonferroni correction (D).
These experiments were carried out and analysed by Simon Lowe in James Hodge's and Maria Usowicz's lab.

Thus, the PME causing Membrin mutations not only significantly disturbed dendritic development in our *Drosophila* models, but also caused

morphologically and physiologically abnormal synapses. This finding not only contributes to our understanding of how Membrin mutations cause a hyperexcitable nervous system but also suggests a tight dependence of synaptic integrity upon efficient secretory trafficking.

Interestingly, I have also detected overexpressed Membrin in axons and synapses of *Drosophila* neurons (Figure 38A, B).

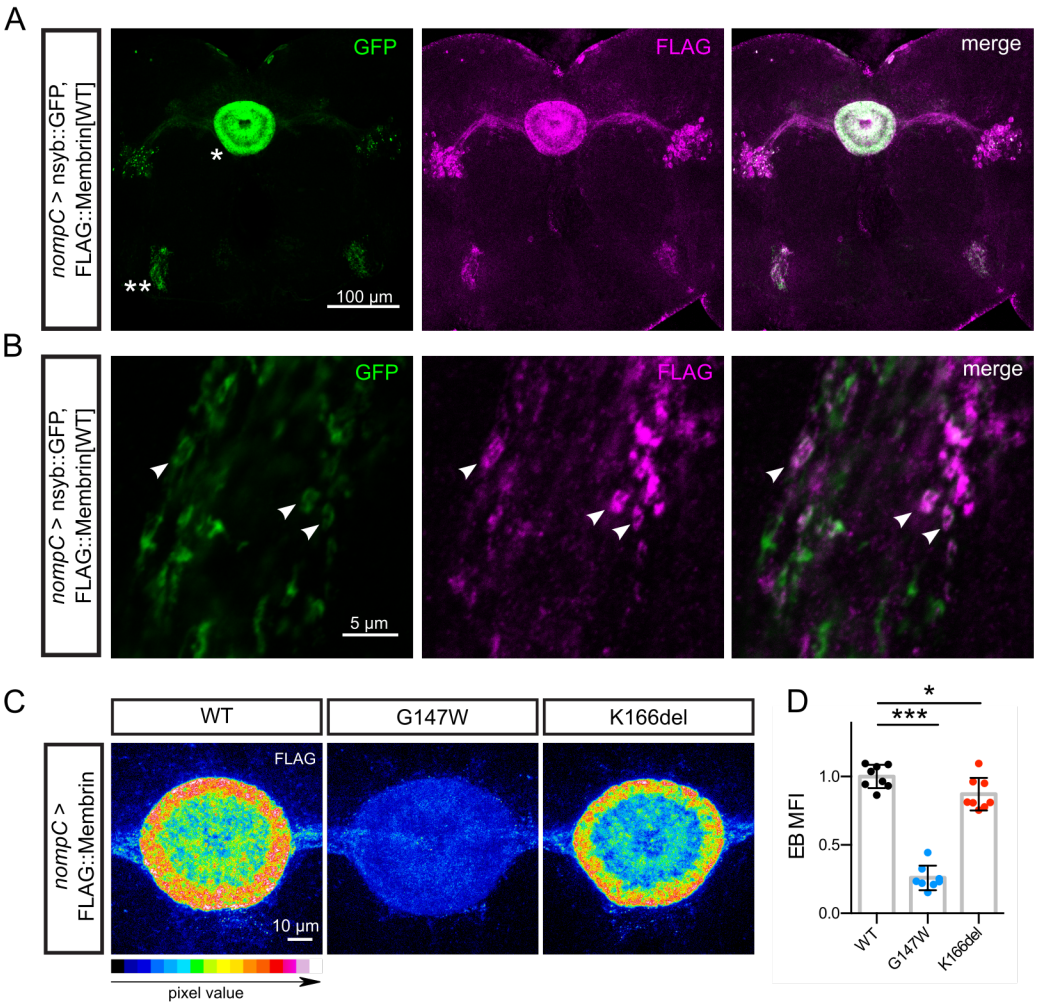

Figure 38. Axonal and synaptic localization of overexpressed Membrin
(A) Wild-type FLAG::Membrin was co-overexpressed with the synaptic marker nsyb::GFP utilizing the *nompC*-Gal4 driver. Maximum intensity projections indicating overlap between the FLAG and GFP signals in the ellipsoid body (EB, *) and antennal mechanosensory and motor center (AMMC, **) are shown.
(B) Single confocal slices in the AMMC of a *Drosophila* brain as described in (A) are depicted. In several instances colocalization between FLAG::Membrin and nsyb::GFP is apparent (arrowheads).
(C, D) Wild-type or mutant Membrin was overexpressed with the *nompC*-Gal4 driver and EB MFI quantified from maximum intensity projections. N = 8 *Drosophila* brains per genotype. Replicate values from individual brains, mean and SD are shown. *, *** represent $p < 0.05$, 0.001; one-way ANOVA with Dunnett's multiple comparison test.

At present it is unclear whether this represents spill-over from the somatic Golgi due to artificially high expression levels or reflects the localization of endogenous Membrin. If Membrin indeed localizes to this compartment we could imagine a local ERGIC or Golgi-like function, which is suggested by the observation that axons contain several key components of the secretory pathway (González et al., 2016). This could serve as an additional explanation for the observed synaptic abnormalities. Interestingly, G147W mutant Membrin localized to the synapse to greatly decreased amounts, while K166del mutant Membrin was only subtly reduced when compared to wild-type (Figure 38C, D). Thus, G147W/G144W might confer additional pathogenicity by this localization defect. In order to unambiguously study such a potential local axonal/synaptic role of Membrin, additional *Drosophila* models with lower expression levels would need to be created. Therefore knock-in fly lines would be the ideal tools, which should also be epitope tagged to allow for unambiguous immuno-staining.

4.5 Discussion

In this study, we developed the first multicellular in vivo model of *GOSR2*-PME, which was an important step towards uncovering disease *mechanisms* that are less intuitively inferable from the sequence alterations and more informative as to what the neuronal bottleneck might be. Previous investigations into the molecular consequences of the *GOSR2*-PME mutations carried out by Nancy Malintan revealed that these mutations cause a partial SNARE domain deficit in the yeast orthologue Bos1 and by inference the *Drosophila* and mammalian Membrin SNARE motifs.

4.5.1 The choice of *in vivo* model system

After careful consideration we chose *Drosophila* as our prime model. ER-to-Golgi trafficking is a highly conserved fundamental mechanism in all eukaryotic cells, which is illustrated by the fact that several of its key molecular players were first identified in yeast (Bonifacino and Glick, 2004; Novick et al., 1980). Importantly, *Drosophila*, as well as yeast, contains a single Membrin orthologue and no redundancy for this protein is present in the human genome. Thus, *Drosophila*, with its powerful genetics and rapid life cycle, appeared as the ideal 'minimal' model to gain critical insights into the neuronal consequences of the *GOSR2*-PME mutations. It facilitated expression of transgenic wild-type or mutant Membrin variants in flies where no endogenous wild-type Membrin was present, which could have otherwise potentially masked effects of the mutations. In this system, human Membrin was capable of partially functionally replacing its fruit fly orthologue, further supporting the validity of our approach. However, this was only an *incomplete* rescue, as human *GOSR2* expressing *membrin* null animals usually died within three days after eclosion from their pupal case. While this early lethality represents a profoundly reduced adult *Drosophila* life span, human *GOSR2* nevertheless was capable of extending the viability of *membrin* null animals approximately 10-fold, as they otherwise died as L1 larvae. Thus, this genetic evidence suggests that human Membrin might be functionally incorporated into the *Drosophila* cis-Golgi SNARE complex and thereby mediate ER-to-Golgi membrane fusion. While 12 of the 16 interacting

layer amino acids in the SNARE motifs of human and *Drosophila* Membrin are conserved, 4 are not (**Figure 5**). It is therefore conceivable that human Membrin in the *Drosophila* cis-Golgi SNARE complex might change the functional properties of this complex – such as force generation during SNARE zippering, overall SNARE complex stability and/or recycling of the SNARE complex after a completed round of fusion – and thus ultimately impair secretory trafficking. Therefore, in order to evaluate the human *GOSR2*-PME mutations in a more physiologic approach, we utilized wild-type or mutant *Drosophila* Membrin to rescue homozygous *membrin* null animals.Lessons from organismal *Drosophila* phenotypes

Remarkably, the Membrin mutations resulted in dramatic phenotypes also in *Drosophila*, with premature lethality, locomotor and seizure-like phenotypes, thereby recapitulating key aspects of the disorder in human patients. The early onset of symptoms in *GOSR2*-PME patients and early organismal abnormalities in the *Drosophila* models suggested developmental abnormalities as a source of the phenotypes. Because *GOSR2*-PME is a *neurological* syndrome, we hypothesized that aspects of *neuronal* development might be impaired. This idea was further reinforced by the finding that nervous system restricted over-expression of mutant Membrin was *sufficient* to recapitulate early adult lethality as observed in *GOSR2*-PME *Drosophila*. However, these experiments do not establish whether neuronal Membrin mutations are also *necessary* to cause the organismal phenotypes, which can readily be tested in *Drosophila* by overexpressing mutant Membrin in the entire animal *except* the nervous system. Therefore, the global *da*-Gal4 driver could be used and Gal4 selectively inhibited in the nervous system with *elav*-Gal80 (Suster et al., 2004). Should also these genetic modifications yield pharate adult stage lethality we know that also Membrin mutations in non-neuronal cell types can give rise to this phenotype, which could then be further dissected with tissue specific Gal4 driver lines.

Both Membrin mutations only partially rescued *membrin* null animals and global Membrin knockdown had similar phenotypic consequences. Therefore our *Drosophila* phenotypic data also provide genetic support for the notion

that the disease mutations confer *partial* (not complete) loss of function, which is consistent with Nancy Malintan's yeast liposome fusion studies.

4.5.2 Considerations about the *GOSR2*-PME *Drosophila* model

In our *Drosophila GOSR2*-PME models and their control – in shorthand termed Mem-G147W (orthologous to human G144W), Mem-K166del (orthologous to human K164del) and Mem-WT – the effects of the mutations are studied separately. We do not take into account the compound heterozygous state of G144W-K164del. It has to be noted however, that the Mem-K166del model does not reflect any known human patient. This mutation has a greater impact upon the Bos1/Membrin SNARE domain function and, judging from the profound reduction of steady state dendritic and axonal CD4::tdGFP, upon Golgi trafficking. Therefore I hypothesize that a K164del *GOSR2* homozygous patient might present with a different clinical syndrome, which might also include abnormalities in other highly Golgi-dependent organ systems. Paradoxically, the compound G144W-K164del *GOSR2*-PME patient did not have a more severe phenotype when compared to G144W homozygous patients, but a slightly milder presentation. This patient lived beyond 60 years of life as opposed to several homozygous G144W *GOSR2*-PME patients who died prematurely around 30 years of age (Boissé Lomax et al., 2013; Praschberger et al., 2015). However, it has to be noted that this observed difference might simply reflect an outlier within a very small patient cohort (less than 20 reported cases). Besides, the relative contribution of the K164del Membrin allele to the phenotype might be marginal, as a less disrupted G144W Membrin allele was also present in this patient.

Our *Drosophila* model also does not take into account reduced G144W Membrin levels as observed in patient fibroblasts, as expression levels are artificially high. Should decreased G144W Membrin levels indeed be functionally relevant – which thus far is unresolved – it would further aggravate the effects as seen in Mem-G147W. Therefore, if reduced G144W Membrin levels contribute to *GOSR2*-PME, our Mem-G147W model would underestimate the severity of G144W and does not bear the danger of

aggravating, or providing false positive results. Nevertheless, we detect a clear difference between Mem-G147W and Mem-WT, which is the ideal internal control, given that these flies are genetically identical except the absence of the pathogenic single codon alteration. Thus, all observed differences are directly attributable to the respective *GOSR2*-PME disease mutations in our *Drosophila* models. Because our Mem-G147W model shows clear organismal and cellular phenotypes while having high expression levels of the mutant protein, we can infer that the SNARE domain defect in itself is highly deleterious. Nevertheless, it would be an interesting avenue of future research to further investigate the potential pathogenicity of reduced amounts of Membrin due to the G144W mutation, as observed in patient-derived fibroblasts. Therefore, *Drosophila* phenotypes as a function of varying degrees of RNAi mediated Membrin knock-down could be evaluated. For this purpose, different RNAi targets within the Membrin mRNA could be utilized as well as varying ambient temperatures of the necessary crosses (*da*-Gal4 X UAS-Membrin RNAi), which changes the activity of Gal4 and therefore will impact the degree of knock-down (Duffy, 2002).

I also note that Mem-WT controls are not entirely wild-type but suffer presumably from mild secretory pathway impairment. This is likely due to artificially high Membrin levels in this control line, which has been shown in yeast liposome fusion studies to harbor the potential of inhibiting the trans-Golgi SNARE complex in a concentration-dependent manner (Varlamov et al., 2004). Consistently, we observed that Mem-WT animals sometimes exhibited downward turned wings, low penetrance dendrite growth and synaptic morphological abnormalities and also NMJ physiological alterations. Importantly however, phenotypic, cellular and physiological abnormalities were strikingly worse in either mutant and these effects can thus directly be attributed to the disease mutations.

4.5.3 Dendrite growth deficits

Utilizing our *GOSR2*-PME *Drosophila* models we were able to show that these mutations cause substantial dendritic growth deficits in genetically labeled model neurons. These results build upon the findings of Ye el al.,

who discovered in a *Drosophila* dendritogenesis screen that mutations in the ER-to-Golgi transport proteins Sec23, Sar1 and Rab1 severely interfered with dendritic outgrowth (Ye et al., 2007). Membrin is involved in the same trafficking step and thought to mediate its final task – membrane fusion of transport carriers with ERGIC and Golgi membranes and thereby the deposition of anterograde cargo into these compartments. Consistent with the previously established importance of ER-to-Golgi trafficking for dendritic growth, we also found significantly shorter dendrites in Membrin mutant *Drosophila*. Importantly, because our results are based on the study of a Mendelian human disorder, we thereby provide proof of principle that this key cellular pathway can be directly relevant for understanding the pathophysiology of a neurological disease.

Interestingly, other Mendelian human disorders due to ER-to-Golgi trafficking mutations in Sec23A, Sec23B, Sec24D and Sar1b present with largely non-neuronal clinical phenotypes of cranio-lenticulo-sutural dysplasia, congenital dyserythropoietic anemias, a syndromic form of osteogenesis imperfecta and lipid absorption disorders (Annesi et al., 2007; Bianchi et al., 2009; Boyadjiev et al., 2006; Garbes et al., 2015; Jones et al., 2003; Schwarz et al., 2009). This appears to be a consequence of tissue-specific differential utilization of the two available isoforms of Sec23 and Sar1 and special demands upon the COPII coat due to the large size of procollagen and chylomicrons (Canty and Kadler, 2005; Fromme et al., 2008; 2007; Jones et al., 2003).

A dendritic growth bottle-neck as observed in our *GOSR2*-PME model *Drosophila* directly links back to the human disease phenotype and provides a potential high-level *mechanism* for one of its hallmarks, i.e. ataxia. If Membrin mutations cause reduced dendritic growth due to limited lipid supplies during times of fast surface expansion, we would expect that neurons with the largest dendritic arbors would be affected most severely. One such neuron subtype with a particularly large dendritic arbor is the cerebellar Purkinje cell (Ramón y Cajal, 1906). These neurons and their cognate brain structure – the cerebellum – are critical for motor control and their dysfunction are tightly linked to many ataxias (Cerminara et al., 2015; Kasumu and Bezprozvanny, 2010). Interestingly, cerebellar defects have

also been implicated in the generation of cortical myoclonus, which is another clinical hallmark of *GOSR2*-PME (Ganos et al., 2014). In *Drosophila* the idea that neurons with larger dendritic arbors are more severely affected by Membrin mutations could be experimentally addressed. Therefore, highly elaborate class IV da neurons (as studied here) could be compared to less elaborate sensory body wall neurons, such as class I-III da neurons, in the presence of Membrin mutations (Grueber et al., 2002).

4.5.4 Partial ER-to-Golgi delays are sufficient to impair dendrite growth

Importantly, the impact of the Membrin PME mutations upon dendritic development also extends previous findings, because it clearly demonstrates that also *partial* delays – and not only a very large or complete block – in ER-to-Golgi transport can be sufficient to significantly impact neuronal integrity. Such subtle defects in this core cell biological process are more likely to be relevant for human disorders as opposed to a complete block, which would presumably cause zygotic or early developmental lethality. Intriguingly, while we could clearly detect a secretory pathway deficit in Membrin mutant neurons, ER-to-Golgi trafficking was almost indistinguishable in G144W mutant Membrin fibroblasts when compared to healthy controls. Neurons have extremely large secretory pathway demands, as their lipid surface is several orders of magnitude larger than in non-neuronal cells (Horton and Ehlers, 2004). Therefore, our finding lends experimental support to the postulated idea that because of special neuronal demands upon the secretory pathway, even subtle alterations could result in a selective neurological disorder while falling below a critical threshold in other organs (Pfenninger, 2009). This notion in turn provides an attractive solution for the seeming paradox of how mutations in this ubiquitously important protein could give rise to a selective neurological condition. The G144W Membrin SNARE motif mutation appears to only very subtly alter ER-to-Golgi trafficking rates – at the edge of detection thresholds of common assays used in this study – which therefore likely only affects cell types with high rates of secretion. Non-neuronal cell types with such characteristics might also display altered trafficking kinetics without leading to clinical symptoms

due to smaller temporal constraints than those imposed by a growing neuron. For example, plasma or exocrine pancreas cells have high secretory demands, but *GOSR2*-PME patients are not reported to have immuno-deficiency or exocrine pancreas insufficiency (Boissé Lomax et al., 2013; Farquhar and Palade, 1981; Palade, 1975). We can easily imagine a scenario where antibody and digestive enzyme secretion is subtly delayed in these patients, which however might not be physiologically relevant. An antibody that is available in the plasma or a digestive enzyme in the small intestine with a 30 min delay as compared to a healthy human might not significantly change the fate of combating a viral infection or significantly impact the digestion of a meal.

4.5.5 Privileged axonal growth

Our study also reinforces further findings of Ye et al., who proposed that axonal growth can be privileged in the face of secretory pathway defects (Ye et al., 2007). Consistent with this notion James Jepson found in Mem-G147W and Mem-K166del that class IV da neuron axon bundles (comprising of ddaC, v'ada, vdaB neuron axons) still managed to reach their distant ventral nerve cord targets. The mechanism of how axonal growth is preserved while dendritic growth is reduced during limitations in lipid supplies is currently unclear. It has been proposed that higher endocytosis rates in dendrites might account for this effect (Zhong, 2011). Nevertheless, the secretory pathway clearly is also required for axonal outgrowth because Brefeldin A treatment as well as early developmental Sar1b knock-down in mammalian neuronal cultures resulted in reduced axonal outgrowth (Aridor and Fish, 2009; Jareb and Banker, 1997). The notion that also axons have high trafficking demands is illustrated by James Jepson's finding that while class IV da neuron axons still reached their distant targets in *membrin* mutant *Drosophila*, they displayed significant steady-state reductions of secretory pathway dependent cargo in the larval ventral nerve cord. Such secretory pathway deficits in distal axons and/or synapses suggested that also synapses might be impaired as a consequence of delayed cargo delivery.

4.5.6 Synaptic abnormalities

We not only found that the partial loss of function Membrin mutations impair dendritic growth but that they also disrupt synaptic integrity. James Jepson performed a comprehensive structural investigation of the neuromuscular junction (NMJ) synapse, which revealed several salient abnormalities. Amongst them were malformed boutons, pre-synaptic retraction and cytoskeletal fragmentation. An interesting parallel of these NMJ abnormalities in our disease model has been reported in the human disorder. Some *GOSR2*-PME patients displayed signs of ongoing denervation in needle electromyography (EMG) studies (van Egmond et al., 2014). Importantly, Simon Lowe found at the NMJ of *GOSR2*-PME *Drosophila* also physiological defects. Spontaneous release was reduced and evoked synaptic transmission appeared hyperactive, which was particularly pronounced under repetitive stimulation. Given that Membrin is a ubiquitously important protein critical for the basic cell biology of every neuron we can infer that similar structural and physiological synaptic changes might also affect central synapses of *GOSR2*-PME model flies and human patients. Such synaptic abnormalities in turn would likely contribute to the severe neurological phenotype of *GOSR2*-PME patients. Given that the core neurological features of *GOSR2*-PME are of central origin, it would be important to address whether the morphological and physiological synaptic changes at the NMJ model synapse indeed also affect excitatory and inhibitory synapses of the *central* nervous system in our *Drosophila* models.

The *GOSR2*-PME models revealed that synaptic integrity depends upon tightly controlled ER-to-Golgi trafficking rates, which is a notion that has received little attention thus far and might have broad physiological relevance. It is not all too surprising, if we consider that synapses are highly specialized neuronal domains with many resident proteins that are secretory pathway dependent (Wilhelm et al., 2014). Given that Membrin is a cis-Golgi gatekeeper for all these proteins it is unlikely that individual proteins mediate these cellular phenotypes but rather the complex interaction of several of them. Presumably synaptic proteins with the highest turn-over and tightest temporal constrains will contribute to the synaptic abnormalities as observed

in *GOSR2*-PME model *Drosophila*. It is conceivable that changes in trans-synaptic anchoring proteins, ion channels, trophic factors and cytoskeleton regulating proteins could lead to synaptic retraction, changes in excitability and morphology of the *GOSR2*-PME model NMJ. Given the vast number of synaptic proteins that are secretory pathway – and thus Membrin – dependent, unbiased synaptic proteomics in these mutants might be able to point towards critical candidates. In addition, an EM based investigation of the ultrastructural changes at the NMJs and brains of our *GOSR2*-PME models might yield further mechanistic insights into the observed synaptic defects. To further dissect the relative contribution of the pre- vs. the postsynapse, Membrin mutations should selectively be introduced either into glutamatergic neurons or muscle and the resulting NMJ abnormalities evaluated. A very elegant way to establish the genetics of this experiment would be to replace endogenous *membrin* by a cassette containing FRT flanked wild-type *membrin* upstream of G147W or K166del mutant *membrin* (Baena-Lopez et al., 2013). Motoneuron or muscle specific expression of flippase would then yield animals that express mutant Membrin only in the pre- or postsynaptic cells of the NMJ in an otherwise wild-type Membrin animal.

In summary, the development of *Drosophila* models of *GOSR2*-PME allowed us extend our investigations at the protein and basic cellular levels and unravel the disease mechanisms which lie at the heart of neuronal dysfunction of this severe ataxia-epilepsy syndrome. We therefore are now left with a deeper understanding of this disorder at the molecular, cellular and neuronal levels, which will be summarized in Chapter 5. In addition, I will discuss lessons for neuronal cell biology learned from *GOSR2*-PME and how the disease mutations might serve as novel tools for future research.

Chapter 5. Concluding remarks

The main aim of this PhD project was to shed light upon the unresolved disease mechanism of *GOSR2*-PME. Prior to our functional investigations, I have expanded the genetics of this disorder by the novel K164del disease allele, and thereby facilitated our subsequent work by being able to compare the novel with the previously reported G144W mutation. The key scientific challenge we faced was how mutations in the ubiquitously important ER-to-Golgi SNARE protein Membrin could be reconciled with an almost exclusive neuronal phenotype. A priori, one can speculate that such selective vulnerability could either originate in particularly high demands of Membrin-mediated processes within the nervous system or alternatively in an additional, nervous system specific function of wild-type or mutant Membrin.

5.1 The *GOSR2*-PME disease *mechanisms*

By utilizing a multi-layered approach spanning from molecule to organism we have provided evidence for the prior notion. Nancy Malintan's work has revealed *partial* SNARE defects in liposome fusion studies conferred by the yeast orthologous *GOSR2*-PME mutations. These mutations were nevertheless substantial enough to severely disturb dendritic growth and synaptic integrity in *Drosophila*. Intriguingly, the G144W Membrin mutation did not cause significantly delayed ER-to-Golgi trafficking rates in a non-neuronal cell type, which therefore suggests that the selective nervous system vulnerability as observed in *GOSR2*-PME might have its origin in uniquely high Golgi trafficking demands of neurons (Horton and Ehlers, 2004; Pfenninger, 2009). Our work has thereby not only provided a possible explanation for the central paradox of this disease but also yielded insights into the pathophysiology *GOSR2*-PME at multiple levels, ranging from protein dysfunction to higher level neuronal circuit disturbances (for a summary illustration see Figure 39).

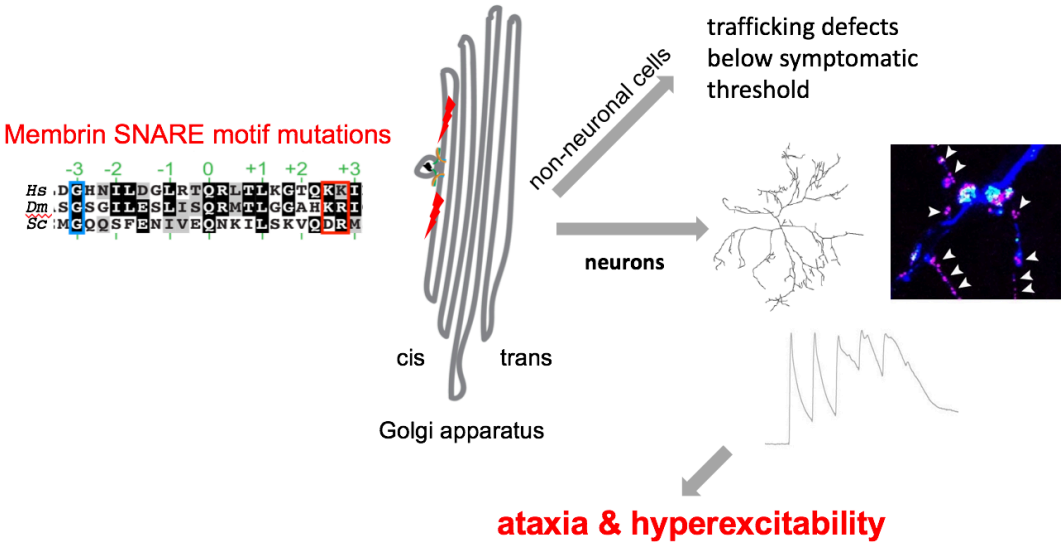

Figure 39. *GOSR2*-PME pathophysiology summary
The missense (blue) and deletion (red) mutations are shown in a portion of the Membrin/Bos1 SNARE domain of *Homo sapiens* (*Hs*), *Drosophila melanogaster* (*Dm*) and *Saccharomyces cerevisiae* (*Sc*). These changes are thought to result in reduced cis-Golgi membrane fusion. While the effects of the *GOSR2*-PME mutations appear to fall below a critical threshold in non-neuronal cells, they severely impair neurons. The core findings in *GOSR2*-PME *Drosophila* of reduced dendritic growth, synaptic retraction (by James Jepson) and hyperactive evoked neurotransmission (by Simon Lowe) are depicted. Such changes ultimately give rise to severe ataxia and profound nervous system hyperexcitability.

5.1.1 The molecular *mechanism*

The furthest 'upstream' mechanism of the *GOSR2*-PME phenotype is partially impaired Membrin due to the pathogenic SNARE motif mutations. This conclusion is most directly suggested by Nancy Malintan's yeast liposome fusion data. Indirectly, also the partial phenotypic rescue of *membrin* null *Drosophila* by mutant Membrin also supports this notion. Similarly, the observation that a key phenotype of *GOSR2*-PME *Drosophila* – pharate adult stage lethality – are recapitulated by *membrin* RNAi knock-down are in accord with reduced function conferred by mutant Membrin. A partial loss of function mechanism – as opposed to gain of function – is consistent with the autosomal-recessive transmission of the disorder and the observation that both pathogenic mutations disrupt the essential SNARE domain. Membrin with a reduced capability of forming a tight cis-Golgi SNARE complex (with its SNARE partners Bet1, Syntaxin-5 and Sec22b) will

cause reduced membrane fusion rates at the cis-Golgi. Increases in body temperature might further destabilize the mutant cis-Golgi SNARE complex, which could be an explanation why several *GOSR2*-PME patients were reported to have suffered from fever induced declines (Boissé Lomax et al., 2013; Praschberger et al., 2015).

5.1.2 Non-neuronal *mechanism*

Based on unimpaired ER-to-Golgi trafficking rates in a non-neuronal model cell type we now believe that these partial ERGIC/cis-Golgi fusion deficits are not sufficient to impair non-neuronal cells to a large enough degree to cause symptoms. This notion serves as a plausible explanation why tissues other than the nervous system do not largely contribute to the disease phenotype. It has to be noted however, that more detailed experimental and clinical analysis might reveal measurable abnormalities also in non-neuronal, asymptomatic organ systems. For instance, it is likely that other cell types with large ER-to-Golgi trafficking demands – such as plasma or exocrine pancreas cells – will display subtle delays when harboring a G144W or K164del Membrin mutation.

A non-neuronal cell type that appears to frequently cause measurable changes in *GOSR2*-PME is muscle, as several patients were reported to have increased creatine kinase levels. However, muscle histology was reported as normal throughout (Boissé Lomax et al., 2013; van Egmond et al., 2015). Nevertheless, this finding indicates that also muscle might be highly vulnerable to Membrin mutations.

5.1.3 Neuronal *mechanisms*

While partial ERGIC/cis-Golgi lipid fusion deficiencies due to the pathogenic Membrin mutations might fall below a symptomatic threshold in organs other than the nervous system, they seem nevertheless substantial enough to be highly deleterious in the context of the very large trafficking demands of neurons. Neurons appear like magnifying glasses for subtle early secretory pathway deficits induced by Membrin mutations. Our study thereby provides experimental support for the postulated idea that '*because of the extreme*

and specialized demands of neuronal membrane growth, relatively small losses of function in the pathway from synthesis to insertion might interfere with neuronal membrane expansion and nervous system function selectively, without critically affecting other organs' (Pfenninger, 2009). Also oligondendrocytes and Schwann cells have very large membrane demands, because they wrap around axons multiple times with thin membrane protrusions in order to provide efficient insulation (Nave and Werner, 2014; Sherman and Brophy, 2005). Therefore it is conceivable that also a partial hypomyelination might contribute to the neurological phenotype of *GOSR2*-PME. However, due to their expected partial nature they might frequently fall below the detection threshold of common clinical tests, which might be the explanation why nerve-conduction studies and MRI investigations do not typically indicate myelination defects in *GOSR2*-PME patients (Boissé Lomax et al., 2013).

Similar to the selective vulnerability of neurons amongst all the different cell types constituting a human being, we postulate that also amongst neurons certain neuronal subtypes are likely to be more severely disturbed than others by the pathogenic Membrin mutations. Such differential changes amongst various neuronal subpopulations might be the explanation of the neurological *GOSR2*-PME hallmarks, which are high level, complex network phenomena ultimately triggered by an innumerable number of individual neurons.

GOSR2-PME model *Drosophila* exhibited profoundly impaired dendritic growth in highly elaborate sensory body wall neurons – which served as model neurons to study dendritic plasma membrane expansion. This finding highlights the notion that the pathogenic Membrin mutations act as hindrances for dendritic growth by limiting the large amounts of required lipid supplies. Such a bottleneck might be particularly relevant for neurons with very large dendritic arbors, which require proportionally larger lipid supplies to enable their growth. One such neuron type is the cerebellar Purkinje cell. Thus we hypothesize that this neuron type is very likely to have underdeveloped dendritic arbors in *GOSR2*-PME patients. Its dysfunction is an attractive explanation why one of the syndrome's hallmarks is profound

ataxia, given the Purkinje cell's established role in motor coordination (Cerminara et al., 2015). In order to test our prediction, Golgi staining of *GOSR2*-PME cerebellar Purkinje cells would be an interesting future research avenue, should sufficient human brains of this very small cohort of patients become available.

Patients with *GOSR2*-PME do not typically present with mental retardation or a profound reduction in cognitive function, as opposed to several other forms of progressive myoclonus epilepsy, which are characterized by the development of dementia (Michelucci et al., 2012). While intelligence is usually largely normal in the early disease course of *GOSR2*-PME, some patients have been reported with mild cognitive impairment later in life (Boissé Lomax et al., 2013). We hypothesize that this remarkable preservation of cognitive function might also be explained by a differential effect of the Membrin mutations upon different neuronal subtypes. Possibly only neurons with very large dendritic arbors exhibit growth defects, while most neurons with smaller neuronal dendritic trees are spared from such defects. This hypothesis could readily be addressed in *Drosophila* by comparing dendritic growth defects in Membin mutant larval sensory neurons that are highly elaborate (class IV da neurons – see above) with those that have fewer and shorter dendrites (class I and II) (Grueber et al., 2002).

Consistent with the previous literature, we found that early secretory pathway defects conferred by Membrin mutations did not critically affect axonal outgrowth, while significantly impacting dendrite length (Ye et al., 2007). This privileged role of axons in *GOSR2*-PME *Drosophila* might provide an explanation why patients with this disorder suffer from ataxia, but not spastic paraplegia. After all, corticospinal neurons serving the lower limbs have the longest axons, which thus would be highly vulnerable targets should dendritic *and* axonal development be affected in equal measure (Synofzik and Schüle, 2017).

Also synaptic abnormalities found in *GOSR2*-PME *Drosophila* reveal valuable insights into the pathophysiology underlying the clinical presentation of this disorder. As a model synapse, James Jepson and Simon Lowe

studied the morphology and physiology of the larval neuromuscular junction (NMJ), because it is highly amenable for experiments (Harris and Littleton, 2015). There the most salient findings were a decrease in trans-synaptic stability and hyperactive evoked neurotransmission. Because the underlying partial secretory pathway disruption due to Membrin mutations are ubiquitous to all neurons we hypothesize that similar alterations are likely to also affect central synapses. Given that EPSP malformations were more pronounced under high-frequency stimulation we would expect central neurons with rapid firing patterns to be more severely affected, such as fast-firing GABAergic neurons (McCormick et al., 1985). It is conceivable that a systematic impairment of distinct neuronal subclasses based on their intrinsic electrophysiological properties would eventually tilt the balance between excitation and inhibition towards hyper-excitation. This thought thus provides – a necessarily oversimplified – explanatory framework of how cortical myoclonus and generalized epilepsy might arise from the *GOSR2* mutations.

Our NMJ findings of synaptic retraction and altered neurotransmission in *GOSR2*-PME *Drosophila* have interesting parallels in human patients. Several of them were found in electromyography studies to suffer from neuromuscular denervation (van Egmond et al., 2014). The *GOSR2*-PME clinical hallmark of absence of deep tendon reflexes might also be an indication of such changes, but could also point towards other deficiencies in the reflex arc, such as in afferent sensory neurons (Boissé Lomax et al., 2013).

Skeletal abnormalities have been reported in *GOSR2*-PME patients, most commonly scoliosis. As of now it is unclear whether this is a secondary consequence due to the severe neurological deficits in this disorder or a spine intrinsic developmental abnormality (Grauers et al., 2016; Trontelj et al., 1979). Possibly delayed cell surface/extracellular localisation of Notch, Wnt and/or fibroblast growth factor, which are critical for segmentation, could contribute to the development of scoliosis in *GOSR2*-PME (Boissé Lomax et al., 2013; Pourquié, 2011).

Why *GOSR2*-PME is a progressive disorder, characterized by rapid deterioration of movement disorder features and subsequent loss of ambulation, is presently unclear. Nevertheless, our *Drosophila* findings offer starting points to formulate hypotheses regarding the underlying pathophysiology. Several processes might act collectively at the heart of the disease progression observed in *GOSR2*-PME. The pathogenic Membrin mutations might continue to negatively impact neurodevelopment as the brains of children suffering from *GOSR2*-PME mature and grow into their fully connected adult versions (Giedd et al., 1999; Passemard et al., 2017; Supekar et al., 2009). In addition, our finding of trans-synaptic instability implies that functional active zones might gradually be removed with increasing age. It is also conceivable that changes in synaptic or dendritic proteomes as a result of secretory pathway deficits could contribute to the progressive nature of the disease. For instance, reduced levels of proteins critical for maintaining proteostasis could have age dependent synaptic/dendritic degeneration as a consequence. Interestingly, James Jepson found significantly reduced levels of the synaptic chaperone CSP at the NMJ of Membrin mutant *Drosophila*. The mammalian CSPα orthologue is a synaptic vesicle-associated chaperone that is critical for preventing neurodegeneration (Chandra et al., 2005; Fernández-Chacón et al., 2004). In turn, mutations in CSPα have been demonstrated to cause adult-onset neuronal ceroid-lipofuscinosis, which is a neurodegenerative form of PME (Benitez et al., 2011; Nosková et al., 2011). Thus, Membrin and more generally, efficient ER-to-Golgi trafficking, might not only be critical for dendritic and synaptic *development*, but also its *maintenance*. This is a readily testable hypothesis, with scientific relevance beyond the immediate problem of disentangling the causes of the progressive nature of *GOSR2*-PME. To this end, we could express the Membrin mutations – or induce even more severe secretory pathway disruption by expressing Rab1, Sar1 or Arf1 mutants – selectively at the adult stage and thereby bypass neurodevelopmental defects. Starting with a healthy neuron we could then assess the impact of the acutely induced disturbances upon dendritic elaboration and synaptic integrity as a function of time.

5.2 Lessons for neuronal cell biology

The mechanisms presented in this thesis are relevant for the pathophysiology of a very small patient cohort of thus far only 18 *GOSR2*-PME cases. However, this does not limit the relevance of our investigations, as we also yielded insights into the cell biology of neurons. We therefore provide results with wider applicability. While previous studies have established that a very large or complete block of ER-to-Golgi trafficking prevents efficient dendritic outgrowth, we have added experimental data, which support the postulated idea that even *minor* alterations along this route are sufficient to negatively impact neuronal plasma membrane expansion (Horton et al., 2005; Ye et al., 2011; Pfenninger, 2009). Partial alterations in this pathway are likely to be more relevant for human disorders as compared to a complete block, which is not compatible with cellular, let alone multicellular, life. Our study has also taught us that synaptic morphology and physiology depends upon tightly regulated ER-to-Golgi trafficking rates. One might think that such a result does not come as a complete surprise, given that functional synapses require timely delivery of a whole host of secretory pathway dependent proteins. Yet to our knowledge this connection of early secretory pathway trafficking rates and synaptic abnormalities has thus far not been a focus in the literature (Passemard et al., 2017). Taken together, because our findings are based on a very severe Mendelian human disorder we provide an instance that directly illustrates that partial ER-to-Golgi trafficking reductions can be highly relevant for human disease.

5.3 Future perspectives

Our study has provided a possible solution for the apparent paradox of how mutations in the ubiquitous Golgi SNARE protein Membrin can result in an almost exclusive neuronal phenotype. Yet some questions remain to be answered and several new questions have arisen from our results. It would be interesting to test whether neurons with very large dendritic arbors and neurons with high firing frequencies indeed are most vulnerable to the pathogenic Membrin mutations. The contribution of impaired dendritic and synaptic maintenance – as opposed to impaired development of these

compartments – to the pathogenesis of *GOSR2*-PME is another intriguing issue. Also, the mechanisms underlying the multifaceted synaptic abnormalities caused by Membrin mutations require further investigation. More generally, the relationship of tightly controlled trafficking rates and synaptic integrity could reveal insights that might also be valuable for the research of unrelated brain disorders. Which are the cargoes that are particularly relevant for the observed morphological and physiological abnormalities? Is it trans-synaptic adhesion molecules, ion channels, trophic factors, etc.? Many synaptic proteins will presumably be dysregulated due to a delay in transport vesicle fusion with the ERGIC/cis-Golgi. Therefore we are likely facing a complex phenomenon, which bears the danger of residing beyond the explicitly graspable. Unbiased synaptic proteomics in *Drosophila*, where key ER-to-Golgi trafficking proteins are either knocked-down or mutated, might nevertheless provide interesting candidates, that could then be validated in genetic interaction studies. However, given the very large amounts of *Drosophila* heads required for the preparation of synaptic fractions, mouse models might be experimentally more suitable for this question (Depner et al., 2014). Another interesting avenue of future research would be the investigation of potential shared molecular and/or cellular pathways of *GOSR2*-PME with other phenotypically similar forms of PMEs.

5.3.1 Knock-in strategy

Future studies into the mechanisms of *GOSR2*-PME would greatly be facilitated by the generation of additional *Drosophila* models. Our current models harbor two *membrin* null alleles, the global *da*-Gal4 driver and wild-type or mutant UAS-*membrin* transgenes. These components occupy both major autosomal *Drosophila* chromosomes, which makes genetic interaction studies more difficult. In addition, because the UAS-Gal4 system is already in use to globally express the transgenes, we cannot rely upon this most widely used binary system to access distinct neuronal circuits (Brand and Perrimon, 1993). Orthogonal binary systems, such as LexAop-LexA, would be required, where less tools are currently available as compared to the UAS-Gal4 system (Lai and Lee, 2006; Pfeiffer et al., 2010). The availability of fewer driver lines as well as high complexity of genetic crossing schemes would

make it rather cumbersome to express optogenetic actuators, neural activity sensors or knock-down genes of interest in our *GOSR2*-PME models. To circumvent these problems, *membrin* manipulations within its own genomic locus are required. Therefore, I have carefully designed and initiated two independent approaches, one based on ends-out homologous recombination, the other one based on CRISPR/Cas9 with subsequent homology directed repair from a single stranded oligonucleotide donor (Baena-Lopez et al., 2013; Gratz et al., 2013; 2014; Rong and Golic, 2000). Their common goal is the replacement of the *membrin* 5' UTR and most of the subsequent coding sequence with an attP landing site plus an adjacent loxP site. This make-up allows for efficient, site-specific retargeting of this *membrin* null locus with any sequence of choice and for the subsequent Cre-mediated removal of the plasmid backbone (Baena-Lopez et al., 2013; Bischof et al., 2007). In a first step, I would retarget wild-type and mutant N-terminal FLAG tagged *membrin* cDNA. These animals would represent single component *GOSR2*-PME *Drosophila* models, with expression levels close to physiological. Such models would also allow to test whether endogenous wild-type and mutant Membrin indeed localize to axons/synapses, as observed in overexpression studies. In a second step, I would retarget a FRT flanked wild-type *membrin* sequence, that is followed by mutant *membrin*. Such FRT-*membrin*[WT]-FRT-*membrin*[G147W]/[K166del] flies would allow for temporally and/or spatially controlled switching of the wild-type isoform for either of the mutants by restricted expression of the recombinase flippase (Baena-Lopez et al., 2013). This approach would facilitate the study of potential synaptic/dendritic maintenance defects in *membrin* mutant *Drosophila* as well as the investigation of the relative contributions of different neuronal subclasses to the pathophysiology of *GOSR2*-PME.

5.3.2 Shared *mechanisms* with other PMEs?

The progressive myoclonus epilepsies are phenotypically heterogeneous and several different causative genes are known to date (Michelucci et al., 2012). Therefore it is unlikely to find a common pathophysiological denominator for this whole diverse group. Nevertheless, some of the phenotypically more similar PMEs might share cellular pathways and/or neural circuits with

GOSR2-PME, which would be interesting avenues for future research. For instance, the PME gene *PRICKLE1* has been linked to neurite growth, which we found to also be abnormal in *Drosophila* harboring the pathogenic Membrin mutations (Liu et al., 2013). PME-linked mutations in the potassium channel gene *KCNC1* are thought to mainly impair fast-spiking neurons (Muona et al., 2015; Oliver et al., 2017). Such a preferential defect in high-frequency firing neurons is also conceivable in *GOSR2*-PME, where EPSP dysmorphologies are more pronounced under repetitive stimulation.

5.3.3 Membrin mutations as tools for cell biology and neuroscience

Finally, our study also suggests that the pathogenic *GOSR2*-PME mutations could serve as tools for cell biology and neuroscience. Because these mutations are not cell lethal they can be integrated into cell lines or whole organisms. Even more simple than that, they can be overexpressed in otherwise wild-type cells or animals, as we found that overexpression of mutant Membrin resulted in similar phenotypes as in our models where no endogenous wild-type Membrin was present. Similarly, dendritic growth was also inhibited when mutant Membrin was overexpressed in a wild-type *membrin Drosophila*, which therefore provides an indirect readout for impaired secretory trafficking. These findings imply that the more abundantly present mutant Membrin might outcompete the endogenous protein. If several-fold more mutant than wild-type Membrin proteins are present at the ERGIC/cis-Golgi, then it is conceivable that the majority of these SNARE complexes might contain mutant instead of wild-type Membrin. Thus overexpression of the reduction of function mutant Membrin alleles could mimic a gain of function mechanism and serve as valuable tools for basic cell biology studies. Other commonly overexpressed mutants in the ER-Golgi pathway are Sar1[H79G], Sar1[T39N], Arf1[Q71L], Arf1[T31N], Rab1[Q70L] and Rab1[S25N], which all disrupt different steps in this process (Allan et al., 2000; Dascher and Balch, 1994; Tisdale et al., 1992; Ward et al., 2001; Zhang et al., 2007). Overexpression of G144W/G147W, K164del/K166del mutant Membrin would inhibit another distinct step in this pathway.

Even overexpression of wild-type Membrin could be utilized as a milder allele to impair secretory trafficking. After all, we observed that overexpression of wild-type Membrin in flies where endogenous Membrin was present, resulted in organismal and dendritic phenotypes. However, these phenotypes were significantly weaker than those observed in either of the mutants. The seeming paradox of how similar phenotypes can arise from reduction of function Membrin alleles and increased wild-type Membrin levels might have an explanation in shared cellular, but distinct molecular mechanisms. Both interventions might partially block secretory trafficking, albeit at different steps. While the Membrin mutations are thought to impair the cis-Golgi SNARE complex, we hypothesize that increased wild-type Membrin levels partially inhibit the trans-Golgi SNARE complex by acting as an i-SNARE. Varlamov et al. demonstrated that increasing the concentrations of the Membrin ortholog Bos1 (or Bet1/Sec22) causes reduced fusion rates of liposomes reconstituted with the yeast trans-Golgi SNAREs (Varlamov et al., 2004). However, endogenous Membrin concentrations in the trans-Golgi are very low and therefore might only exert a comparably subtle inhibitory effect, that is thought to be relevant only for fine-tuning of fusion specificity (Varlamov et al., 2004; Volchuk et al., 2004; Hay et al., 1998). In contrast, if we artificially increase Membrin in this compartment by overexpression, the trans-Golgi SNARE complex might be significantly inhibited and thus secretory trafficking rates markedly reduced.

In neuroscience studies the mutant (and wild-type) Membrin transgenes could serve as tools to further investigate the consequences of partial secretory pathway defects in different neuron subclasses or simply to restrict dendritic outgrowth. Overexpressing the Membrin mutants in fully developed wild-type neurons would also allow to bypass neurodevelopmental defects conferred by the Membrin mutations and thus disentangle their impact upon neuronal maintenance.

5.4 Final conclusions

Taken together, our study investigating the pathophysiology of *GOSR2*-PME provided a potential multi-level explanation of this previously poorly

understood disorder. Partial SNARE defects are thought to subtly delay anterograde cargo trafficking via the Golgi apparatus. This kinetic change presumably falls below a critical threshold in non-neuronal cells but results in multifaceted effects upon neuronal development and function, because this cell type poses unique demands upon this basic cellular pathway. The pathogenic Membrin mutations significantly reduce dendritic outgrowth and cause morphologically abnormal, hyperactive synapses – neuronal abnormalities, which in turn are thought to give rise to the core features of ataxia and hyperexcitability as observed in *GOSR2*-PME patients. In addition to these pathophysiological insights, our study also highlights lessons for general neuronal cell biology. Our findings stress a very intimate connection of tightly controlled anterograde cargo trafficking rates and neuronal integrity. Finally, our approach of overexpressing mutant Membrin in an otherwise wild-type genetic background might facilitate future cell biological and neuroscience studies by readily enabling cis-Golgi SNARE complex inhibition in a temporally controlled and cell type specific manner.

Acknowledgements

I want to thank several individuals, who made this PhD research possible and contributed to a unique four years in the center of vibrant London.

First, I want to thank my supervisors. James Jepson was not only my primary supervisor but also scientific partner in the quest to unravel the disease mechanism of *GOSR2*-PME, which was truly an amazing ride. James introduced me to the exciting world of *Drosophila* genetics and neurobiology. He did so with outstanding enthusiasm and catching joy, which was critical for me to enjoy my PhD research and *Drosophila* as much as I did. I am also grateful to James for providing very helpful advice, mentorship and support *whenever* needed. My co-supervision by Jim Rothman was highly valuable for the *GOSR2*-PME project as well as for the growth of my scientific thinking. Given that my PhD work focused on a Golgi SNARE protein, it was extremely fortunate to have Jim – Golgi pioneer and the very person who gave SNARE proteins their name – open a lab next-door and join the project. Being able to learn from the example of a researcher who made several big scientific discoveries fuelled me with immense motivation and spurred me to scrutinize the potential impact of research questions. It was a great inspiration to be co-supervised by Dimitri Kullmann, who was always readily available to dissect my scientific problems with razor sharp logic. Especially in the light of the inherent difficulty of being a thorough basic scientist *and* practicing clinician, it was particularly valuable to learn from Dimitri's example. I am also grateful to Henry Houlden, who was a knowledgeable guide into the genetic causes of neurological disorders. This was particularly important to me given that neurology genetics is not only a cornerstone of 21st century neurology, but also a valuable window into the inner workings of the nervous system. I also want to thank my previous supervisor and mentor Heinz Zoller, who taught me with extraordinary dedication the necessary core science skills during my research as a student at the Medical University of Innsbruck.

I also want to thank Shyam Krishnakumar and Andreas Ernst from the Rothman lab. Shyam has contributed many ideas and shaped the path of the project. We had several conversations about the potential disease mechanisms of *GOSR2*-PME, which were very fruitful. Talking to Shyam also gave me the opportunity to learn how to think in a biochemical and biophysical way. Andreas provided critical technical advice for Golgi apparatus related cell biological studies. In addition, our conversations allowed me to understand key concepts related to Golgi trafficking.

Next, I want to thank Nancy Malintan, Simon Lowe, Carlo Giachello and Nian Patel for their important experimental contributions to this project during effortless and highly pleasant collaborations. Nancy performed liposome fusion assays and thus was critical for establishing SNARE defects due to the *GOSR2*-PME mutations; Simon detected electrophysiological defects at model synapses of *GOSR2*-PME *Drosophila*; Carlo found seizure-like phenotypes in these models; and Nian rigorously quantified effects of overexpressing mutant Membrin in wild-type Membrin flies and the consequences of Membrin RNAi knock-down.

I want to also thank my wider net of support during this PhD. A large portion of the *GOSR2*-PME work was carried out in the Institute of Neurology Fly lab, headed by James Jepson. With its current members Kofan Chen, Angelique Lamaze and Patrick Krätschmer this was a fun place to work, where ideas were constantly exchanged. Special thanks to Kofan for being a great advisor, in particular for molecular biology and *Drosophila* genetics. Also, the Department of Clinical and Experimental Epilepsy (DCEE) needs to be mentioned, whose members were always very generous with providing technical suggestions and fun to be around. Within the DCEE Juliet Solomon always looked out for me on an administrative and personal level and became an important source of feeling at ease at work, which I am truly grateful for. Amongst the wider net of support the *Drosophila* community at large needs to be mentioned. In my experience this community is remarkably warm and readily shares reagents and protocols. Thus, it is a real joy to be part of it. For financing and thereby enabling this PhD research I want to thank the Brain Research Trust.

For my human genetics work I want to thank Niccolo Mencacci and Bettina Balint. Niccolo introduced me to human genetics work, guided the project and introduced me to Queen Square. It was a real pleasure to work with Niccolo and to follow his positive attitude. Bettina provided very valuable first-hand clinical accounts to the genetics of the novel *GOSR2*-PME mutation.

Finally – and very importantly – I want to thank my family and friends, without whom this unique experience of my PhD research would not have been possible. My partner Alicia was an absolutely essential pillar during all this time in London. Her constant encouragement, support and love carried me through all the ups and downs of this PhD and I am so grateful for this. We enjoyed countless get-togethers with our good friends Oscar and Dani, which are precious memories of our unique London adventure. I also want to thank my parents and my brother, whose enduring backing was the foundation for me to fulfill my dream to pursue several years of full-time research.

References

Adolf, F., Rhiel, M., Reckmann, I., and Wieland, F.T. (2016). Sec24C/D-isoform specific sorting of the preassembled ER-Golgi Q-SNARE complex. Mol Biol Cell *27*, 2697-2707.

Adzhubei, I.A., Schmidt, S., Peshkin, L., Ramensky, V.E., Gerasimova, A., Bork, P., Kondrashov, A.S., and Sunyaev, S.R. (2010). A method and server for predicting damaging missense mutations. Nat Methods *7*, 248–249.

Alberts, B., Johnson, A., Lewis, J., Morgan, D., Raff, M., Roberts, K., Walter, P. (2015). Chapter 13: Intracellular Membrane Traffic. In Molecular Biology of the Cell - Sixth Edition. (New York: Garland Science), pp. 695-752.

Allan, B.B., Moyer, B.D., and Balch, W.E. (2000). Rab1 recruitment of p115 into a cis-SNARE complex: programming budding COPII vesicles for fusion. Science *289*, 444–448.

Allan, V.J., Thompson, H.M., and McNiven, M.A. (2002). Motoring around the Golgi. Nat Cell Biol *4*, E236–E242.

Annesi, G., Aguglia, U., Tarantino, P., Annesi, F., De Marco, E.V., Civitelli, D., Torroni, A., and Quattrone, A. (2007). *SIL1* and *SARA2* mutations in Marinesco-Sjögren and chylomicron retention diseases. Clin Genet *71*, 288–289.

Antonin, W., Fasshauer, D., Becker, S., Jahn, R., and Schneider, T.R. (2002). Crystal structure of the endosomal SNARE complex reveals common structural principles of all SNAREs. Nat Struct Biol *9*, 107–111.

Appenzeller-Herzog, C., and Hauri, H.-P. (2006). The ER-Golgi intermediate compartment (ERGIC): in search of its identity and function. J Cell Sci *119*, 2173–2183.

Aridor, M., and Fish, K.N. (2009). Selective Targeting of ER Exit Sites Supports Axon Development. Traffic *10*, 1669–1684.

Avanzini, G., Shibasaki, H., Rubboli, G., Canafoglia, L., Panzica, F., Franceschetti, S., and Hallett, M. (2016). Neurophysiology of myoclonus and progressive myoclonus epilepsies. Epileptic Disord *18*, 11–27.

Baena-Lopez, L.A., Alexandre, C., Mitchell, A., Pasakarnis, L., and Vincent, J.-P. (2013). Accelerated homologous recombination and subsequent genome modification in *Drosophila*. Development *140*, 4818–4825.

Balch, W.E., Dunphy, W.G., Braell, W.A., and Rothman, J.E. (1984). Reconstitution of the transport of protein between successive compartments of the Golgi measured by the coupled incorporation of N-acetylglucosamine. Cell *39*, 405–416.

Balreira, A., Gaspar, P., Caiola, D., Chaves, J., Beirão, I., Lima, J.L., Azevedo, J.E., and Miranda, M.C.S. (2008). A nonsense mutation in the *LIMP-2* gene associated with progressive myoclonic epilepsy and nephrotic syndrome. Hum Mol Genet *17*, 2238–2243.

Bannykh, S.I., Rowe, T., and Balch, W.E. (1996). The organization of endoplasmic reticulum export complexes. J Cell Biol *135*, 19–35.

Barlowe, C., Orci, L., Yeung, T., Hosobuchi, M., Hamamoto, S., Salama, N., Rexach, M.F., Ravazzola, M., Amherdt, M., and Schekman, R. (1994). COPII: a membrane coat formed by Sec proteins that drive vesicle budding from the endoplasmic reticulum. Cell *77*, 895–907.

Bassuk, A.G., Wallace, R.H., Buhr, A., Buller, A.R., Afawi, Z., Shimojo, M., Miyata, S., Chen, S., Gonzalez-Alegre, P., Griesbach, H.L., et al. (2008). A homozygous mutation in human PRICKLE1 causes an autosomal-recessive progressive myoclonus epilepsy-ataxia syndrome. Am J Hum Genet *83*, 572–581.

Bechtel, W. (2006). Discovering Cell Mechanisms: The Creation of Modern Cell Biology. (Cambridge studies in philosphy and biology), pp. 84-88 and pp. 244-249.

Ben-Tekaya, H., Miura, K., Pepperkok, R., and Hauri, H.-P. (2005). Live imaging of bidirectional traffic from the ERGIC. J Cell Sci *118*, 357–367.

Benitez, B.A., Alvarado, D., Cai, Y., Mayo, K., Chakraverty, S., Norton, J., Morris, J.C., Sands, M.S., Goate, A., and Cruchaga, C. (2011). Exome-sequencing confirms *DNAJC5* mutations as cause of adult neuronal ceroid-lipofuscinosis. PLoS ONE *6*, e26741.

Berkovic, S.F., Dibbens, L.M., Oshlack, A., Silver, J.D., Katerelos, M., Vears, D.F., Lüllmann-Rauch, R., Blanz, J., Zhang, K.W., Stankovich, J., et al. (2008). Array-Based Gene Discovery with Three Unrelated Subjects Shows SCARB2/LIMP-2 Deficiency Causes Myoclonus Epilepsy and Glomerulosclerosis. Am J Hum Genet *82*, 673–684.

Bethani, I., Werner, A., Kadian, C., Geumann, U., Jahn, R., and Rizzoli, S.O. (2009). Endosomal fusion upon SNARE knockdown is maintained by residual SNARE activity and enhanced docking. Traffic *10*, 1543–1559.

Bhatt, P.K., and Neckameyer, W.S. (2013). Functional analysis of the larval feeding circuit in *Drosophila*. J Vis Exp *81*, e51062.

Bi, X., Corpina, R.A., and Goldberg, J. (2002). Structure of the Sec23/24-Sar1 pre-budding complex of the COPII vesicle coat. Nature *419*, 271–277.

Bi, X., Mancias, J.D., and Goldberg, J. (2007). Insights into COPII coat nucleation from the structure of Sec23.Sar1 complexed with the active fragment of Sec31. Dev Cell *13*, 635–645.

Bianchi, P., Fermo, E., Vercellati, C., Boschetti, C., Barcellini, W., Iurlo, A., Marcello, A.P., Righetti, P.G., and Zanella, A. (2009). Congenital dyserythropoietic anemia type II (CDAII) is caused by mutations in the SEC23B gene. Hum Mutat *30*, 1292–1298.

Bischof, J., Maeda, R.K., Hediger, M., Karch, F., and Basler, K. (2007). An optimized transgenesis system for *Drosophila* using germ-line-specific phiC31 integrases. Proc Natl Acad Sci USA *104*, 3312–3317.

Bock, J.B., Matern, H.T., Peden, A.A., and Scheller, R.H. (2001). A genomic perspective on membrane compartment organization. Nature *409*, 839–841.

Boissé Lomax, L., Bayly, M.A., Hjalgrim, H., Møller, R.S., Vlaar, A.M., Aaberg, K.M., Marquardt, I., Gandolfo, L.C., Willemsen, M., Kamsteeg, E.-J., et al. (2013). “North Sea” progressive myoclonus epilepsy: phenotype of subjects with *GOSR2* mutation. Brain *136*, 1146–1154.

Bonfanti, L., Mironov, A.A., Martínez-Menárguez, J.A., Martella, O., Fusella, A., Baldassarre, M., Buccione, R., Geuze, H.J., Mironov, A.A., and Luini, A. (1998). Procollagen traverses the Golgi stack without leaving the lumen of cisternae: evidence for cisternal maturation. Cell *95*, 993–1003.

Bonifacino, J.S., and Glick, B.S. (2004). The mechanisms of vesicle budding and fusion. Cell *116*, 153–166.

Boyadjiev, S.A., Fromme, J.C., Ben, J., Chong, S.S., Nauta, C., Hur, D.J., Zhang, G., Hamamoto, S., Schekman, R., Ravazzola, M., et al. (2006). Cranio-lenticulo-sutural dysplasia is caused by a SEC23A mutation leading to abnormal endoplasmic-reticulum-to-Golgi trafficking. Nat Genet *38*, 1192–1197.

Braakman, I., and Hebert, D.N. (2013). Protein folding in the endoplasmic reticulum. Cold Spring Harb Perspect Biol *5*, a013201.

Brand, A.H., and Perrimon, N. (1993). Targeted gene expression as a means of altering cell fates and generating dominant phenotypes. Development *118*, 401–415.

Brandizzi, F., and Barlowe, C. (2013). Organization of the ER–Golgi interface for membrane traffic control. Nat Rev Mol Cell Biol *14*, 382–392.

Brennwald, P., Kearns, B., Champion, K., Keränen, S., Bankaitis, V., and Novick, P. (1994). Sec9 is a SNAP-25-like component of a yeast SNARE complex that may be the effector of Sec4 function in exocytosis. Cell *79*, 245–258.

Brown, M.S., and Goldstein, J.L. (1986). A receptor-mediated pathway for cholesterol homeostasis. Science *232*, 34–47.

Bulleid, N.J. (2012). Disulfide bond formation in the mammalian endoplasmic reticulum. Cold Spring Harb Perspect Biol *4*, a013219.

Cai, H., Reinisch, K., and Ferro-Novick, S. (2007a). Coats, tethers, Rabs, and SNAREs work together to mediate the intracellular destination of a transport vesicle. Dev Cell *12*, 671–682.

Cai, H., Yu, S., Menon, S., Cai, Y., Lazarova, D., Fu, C., Reinisch, K., Hay, J.C., and Ferro-Novick, S. (2007b). TRAPPI tethers COPII vesicles by binding the coat subunit Sec23. Nature *445*, 941–944.

Cai, Y., Chin, H.F., Lazarova, D., Menon, S., Fu, C., Cai, H., Sclafani, A., Rodgers, D.W., La Cruz, De, E.M., Ferro-Novick, S., et al. (2008). The structural basis for activation of the Rab Ypt1p by the TRAPP membrane-tethering complexes. Cell *133*, 1202–1213.

Cajigas, I.J., Tushev, G., Will, T.J., tom Dieck, S., Fuerst, N., and Schuman, E.M. (2012). The local transcriptome in the synaptic neuropil revealed by deep sequencing and high-resolution imaging. Neuron *74*, 453–466.

Canty, E.G., and Kadler, K.E. (2005). Procollagen trafficking, processing and fibrillogenesis. J Cell Sci *118*, 1341–1353.

Casso, D., Ramírez-Weber, F., and Kornberg, T.B. (2000). GFP-tagged balancer chromosomes for *Drosophila* melanogaster. Mech Dev *91*, 451–454.

Cerminara, N.L., Lang, E.J., Sillitoe, R.V., and Apps, R. (2015). Redefining the cerebellar cortex as an assembly of non-uniform Purkinje cell microcircuits. Nat Rev Neurosci *16*, 79–93.

Chandra, S., Gallardo, G., Fernández-Chacón, R., Schlüter, O.M., and Südhof, T.C. (2005). Alpha-synuclein cooperates with CSP alpha in preventing neurodegeneration. Cell *123*, 383–396.

Cole, N.B., Sciaky, N., Marotta, A., Song, J., and Lippincott-Schwartz, J. (1996). Golgi dispersal during microtubule disruption: regeneration of Golgi stacks at peripheral endoplasmic reticulum exit sites. Mol Biol Cell *7*, 631–650.

Cole, R.W., Jinadasa, T., and Brown, C.M. (2011). Measuring and interpreting point spread functions to determine confocal microscope resolution and ensure quality control. Nat Protoc *6*, 1929–1941.

Cong, L., Ran, F.A., Cox, D., Lin, S., Barretto, R., Habib, N., Hsu, P.D., Wu, X., Jiang, W., Marraffini, L.A., et al. (2013). Multiplex genome engineering using CRISPR/Cas systems. Science *339*, 819–823.

Corbett, M.A., Schwake, M., Bahlo, M., Dibbens, L.M., Lin, M., Gandolfo, L.C., Vears, D.F., O'Sullivan, J.D., Robertson, T., Bayly, M.A., et al. (2011). A mutation in the Golgi Qb-SNARE gene *GOSR2* causes progressive myoclonus epilepsy with early ataxia. Am J Hum Genet *88*, 657–663.

Cornejo, V.H., Luarte, A., and Couve, A. (2017). Global and local mechanisms sustain axonal proteostasis of transmembrane proteins. Traffic *18*, 255–266.

Crespel, A., Ferlazzo, E., Franceschetti, S., Genton, P., Gouider, R., Kälviäinen, R., Korja, M., Lehtinen, M.K., Mervaala, E., Simonato, M., et al. (2016). Unverricht-Lundborg disease. Epileptic Disord *18*, 28–37.

Cui-Wang, T., Hanus, C., Cui, T., Helton, T., Bourne, J., Watson, D., Harris, K.M., and Ehlers, M.D. (2012). Local zones of endoplasmic reticulum complexity confine cargo in neuronal dendrites. Cell *148*, 309–321.

Dancourt, J., Zheng, H., Bottanelli, F., Allgeyer, E.S., Bewersdorf, J., Graham, M., Liu, X., Rothman, J.E., and Lavieu, G. (2016). Small cargoes pass through synthetically glued Golgi stacks. FEBS Letters *590*, 1675–1686.

Dascher, C., and Balch, W.E. (1994). Dominant inhibitory mutants of ARF1 block endoplasmic reticulum to Golgi transport and trigger disassembly of the Golgi apparatus. J Biol Chem *269*, 1437–1448.

Dascher, C., and Balch, W.E. (1996). Mammalian Sly1 regulates syntaxin 5 function in endoplasmic reticulum to Golgi transport. J Biol Chem *271*, 15866–15869.

De Matteis, M.A., and Luini, A. (2011). Mendelian disorders of membrane trafficking. N Engl J Med *365*, 927–938.

Depner, H., Lützkendorf, J., Babkir, H.A., Sigrist, S.J., and Holt, M.G. (2014). Differential centrifugation-based biochemical fractionation of the *Drosophila* adult CNS. Nat Protoc *9*, 2796–2808.

Dibbens, L., Schwake, M., Saftig, P., and Rubboli, G. (2016). SCARB2/LIMP2 deficiency in action myoclonus-renal failure syndrome. Epileptic Disord *18*, 63–72.

Dibbens, L.M., Michelucci, R., Gambardella, A., Andermann, F., Rubboli, G., Bayly, M.A., Joensuu, T., Vears, D.F., Franceschetti, S., Canafoglia, L., et al. (2009). *SCARB2* mutations in progressive myoclonus epilepsy (PME) without renal failure. Ann Neurol *66*, 532–536.

Dietzl, G., Chen, D., Schnorrer, F., Su, K.-C., Barinova, Y., Fellner, M., Gasser, B., Kinsey, K., Oppel, S., Scheiblauer, S., et al. (2007). A genome-wide transgenic RNAi library for conditional gene inactivation in *Drosophila*. Nature *448*, 151–156.

Druker, B.J., Talpaz, M., Resta, D.J., Peng, B., Buchdunger, E., Ford, J.M., Lydon, N.B., Kantarjian, H., Capdeville, R., Ohno-Jones, S., et al. (2001). Efficacy and safety of a specific inhibitor of the BCR-ABL tyrosine kinase in chronic myeloid leukemia. N Engl J Med *344*, 1031–1037.

Druker, B.J., Tamura, S., Buchdunger, E., Ohno, S., Segal, G.M., Fanning, S., Zimmermann, J., and Lydon, N.B. (1996). Effects of a selective inhibitor of the Abl tyrosine kinase on the growth of Bcr-Abl positive cells. Nat Med *2*, 561–566.

Duffy, J.B. (2002). GAL4 system in *Drosophila*: A fly geneticist's swiss army knife. Genesis *34*, 1–15.

Dunn, K.W., Kamocka, M.M., and McDonald, J.H. (2011). A practical guide to evaluating colocalization in biological microscopy. Am J Physiol Cell Physiol *300*, C723–C742.

Ehlers, M.D. (2013). Dendritic trafficking for neuronal growth and plasticity. Biochem Soc Trans *41*, 1365–1382.

Emr, S., Glick, B.S., Linstedt, A.D., Lippincott-Schwartz, J., Luini, A., Malhotra, V., Marsh, B.J., Nakano, A., Pfeffer, S.R., Rabouille, C., et al. (2009). Journeys through the Golgi--taking stock in a new era. J Cell Biol *187*, 449-453.

Fabini, G., Freilinger, A., Altmann, F., and Wilson, I.B. (2001). Identification of core alpha 1,3-fucosylated glycans and cloning of the requisite fucosyltransferase cDNA from *Drosophila melanogaster*. Potential basis of the neural anti-horseadish peroxidase epitope. J Biol Chem *276*, 28058–28067.

Farquhar, M.G., and Palade, G.E. (1981). The Golgi apparatus (complex)-(1954-1981)-from artifact to center stage. J Cell Biol *91*, 77s–103s.

Farquhar, M.G., and Palade, G.E. (1998). The Golgi apparatus: 100 years of progress and controversy. Trends Cell Biol *8*, 2-10.

Fasshauer, D., Bruns, D., Shen, B., Jahn, R., and Brunger, A.T. (1997a). A structural change occurs upon binding of syntaxin to SNAP-25. J Biol Chem *272*, 4582–4590.

Fasshauer, D., Otto, H., Eliason, W.K., Jahn, R., and Brunger, A.T. (1997b). Structural changes are associated with soluble N-ethylmaleimide-sensitive fusion protein attachment protein receptor complex formation. J Biol Chem *272*, 28036–28041.

Fasshauer, D., Sutton, R.B., Brunger, A.T., and Jahn, R. (1998). Conserved structural features of the synaptic fusion complex: SNARE proteins reclassified as Q- and R-SNAREs. Proc Natl Acad Sci USA *95*, 15781–15786.

Fath, S., Mancias, J.D., Bi, X., and Goldberg, J. (2007). Structure and organization of coat proteins in the COPII cage. Cell *129*, 1325–1336.

Fernández-Chacón, R., Wölfel, M., Nishimune, H., Tabares, L., Schmitz, F., Castellano-Muñoz, M., Rosenmund, C., Montesinos, M.L., Sanes, J.R., Schneggenburger, R., et al. (2004). The synaptic vesicle protein CSP alpha prevents presynaptic degeneration. Neuron *42*, 237–251.

Ferreira, T.A., Blackman, A.V., Oyrer, J., Jayabal, S., Chung, A.J., Watt, A.J., Sjöström, P.J., and van Meyel, D.J. (2014). Neuronal morphometry directly from bitmap images. Nat Methods *11*, 982–984.

Fischer von Mollard, G., and Stevens, T.H. (1998). A human homolog can functionally replace the yeast vesicle-associated SNARE Vti1p in two vesicle transport pathways. J Biol Chem *273*, 2624–2630.

Franceschetti, S., and Canafoglia, L. (2016). Sialidoses. Epileptic Disord *18*, 89–93.

Franceschetti, S., Michelucci, R., Canafoglia, L., Striano, P., Gambardella, A., Magaudda, A., Tinuper, P., La Neve, A., Ferlazzo, E., Gobbi, G., et al. (2014). Progressive myoclonic epilepsies: definitive and still undetermined causes. Neurology *82*, 405–411.

Freeze, H.H., and Ng, B.G. (2011). Golgi glycosylation and human inherited diseases. Cold Spring Harb Perspect Biol *3*, a005371.

Fromme, J.C., Orci, L., and Schekman, R. (2008). Coordination of COPII vesicle trafficking by Sec23. Trends Cell Biol *18*, 330–336.

Fromme, J.C., Ravazzola, M., Hamamoto, S., Al-Balwi, M., Eyaid, W., Boyadjiev, S.A., Cosson, P., Schekman, R., and Orci, L. (2007). The genetic basis of a craniofacial disease provides insight into COPII coat assembly. Dev Cell *13*, 623–634.

Fukuda, R., McNew, J.A., Weber, T., Parlati, F., Engel, T., Nickel, W., Rothman, J.E., and Söllner, T.H. (2000). Functional architecture of an intracellular membrane t-SNARE. Nature *407*, 198–202.

Ganos, C., Kassavetis, P., Erro, R., Edwards, M.J., Rothwell, J., and Bhatia, K.P. (2014). The role of the cerebellum in the pathogenesis of cortical myoclonus. Mov Disord *29*, 437–443.

Gao, Y., Zorman, S., Gundersen, G., Xi, Z., Ma, L., Sirinakis, G., Rothman, J.E., and Zhang, Y. (2012). Single reconstituted neuronal SNARE complexes zipper in three distinct stages. Science *337*, 1340–1343.

Garbes, L., Kim, K., Rieß, A., Hoyer-Kuhn, H., Beleggia, F., Bevot, A., Kim, M.J., Huh, Y.H., Kweon, H.-S., Savarirayan, R., et al. (2015). Mutations in *SEC24D*, encoding a component of the COPII machinery, cause a syndromic form of osteogenesis imperfecta. Am J Hum Genet *96*, 432–439.

Gardiol, A., Racca, C., and Triller, A. (1999). Dendritic and postsynaptic protein synthetic machinery. J Neurosci *19*, 168–179.

Gasteiger, E., Gattiker, A., Hoogland, C., Ivanyi, I., Appel, R.D., and Bairoch, A. (2003). ExPASy: The proteomics server for in-depth protein knowledge and analysis. Nucleic Acids Res *31*, 3784–3788.

Genton, P., Striano, P., and Minassian, B.A. (2016). The history of progressive myoclonus epilepsies. Epileptic Disord *18*, 3–10.

Ghabrial, A.S., Levi, B.P., and Krasnow, M.A. (2011). A systematic screen for tube morphogenesis and branching genes in the *Drosophila* tracheal system. PLoS Genet *7*, e1002087.

Ghosh, P., Dahms, N.M., and Kornfeld, S. (2003). Mannose 6-phosphate receptors: new twists in the tale. Nat Rev Mol Cell Biol *4*, 202–212.

Giachello, C.N.G., and Baines, R.A. (2015). Inappropriate Neural Activity during a Sensitive Period in Embryogenesis Results in Persistent Seizure-like Behavior. Current Biology *25*, 2964–2968.

Giedd, J.N., Blumenthal, J., Jeffries, N.O., Castellanos, F.X., Liu, H., Zijdenbos, A., Paus, T., Evans, A.C., and Rapoport, J.L. (1999). Brain development during childhood and adolescence: a longitudinal MRI study. Nat Neurosci *2*, 861–863.

Girard, J.-M., Turnbull, J., Ramachandran, N., and Minassian, B.A. (2013). Progressive myoclonus epilepsy. Handb Clin Neurol *113*, 1731–1736.

Giraudo, C.G., Eng, W.S., Melia, T.J., and Rothman, J.E. (2006). A clamping mechanism involved in SNARE-dependent exocytosis. Science *313*, 676–680.

Glick, B.S., and Luini, A. (2011). Models for Golgi traffic: a critical assessment. Cold Spring Harb Perspect Biol *3*, a005215.

Goldstein, J.L., Anderson, R.G., and Brown, M.S. (1979). Coated pits, coated vesicles, and receptor-mediated endocytosis. Nature *279*, 679–685.

González, C., and Couve, A. (2014). The axonal endoplasmic reticulum and protein trafficking: Cellular bootlegging south of the soma. Semin Cell Dev Biol *27*, 23–31.

González, C., Cánovas, J., Fresno, J., Couve, E., Court, F.A., and Couve, A. (2016). Axons provide the secretory machinery for trafficking of voltage-gated sodium channels in peripheral nerve. Proc Natl Acad Sci USA *113*, 1823–1828.

Gratz, S.J., Cummings, A.M., Nguyen, J.N., Hamm, D.C., Donohue, L.K., Harrison, M.M., Wildonger, J., and O'Connor-Giles, K.M. (2013). Genome engineering of *Drosophila* with the CRISPR RNA-guided Cas9 nuclease. Genetics *194*, 1029–1035.

Gratz, S.J., Ukken, F.P., Rubinstein, C.D., Thiede, G., Donohue, L.K., Cummings, A.M., and O'Connor-Giles, K.M. (2014). Highly specific and efficient CRISPR/Cas9-catalyzed homology-directed repair in *Drosophila*. Genetics *196*, 961–971.

Grauers, A., Einarsdottir, E., and Gerdhem, P. (2016). Genetics and pathogenesis of idiopathic scoliosis. Scoliosis Spinal Disord *11*, 45.

Grueber, W.B., Jan, L.Y., and Jan, Y.N. (2002). Tiling of the *Drosophila* epidermis by multidendritic sensory neurons. Development *129*, 2867–2878.

Grueber, W.B., Ye, B., Moore, A.W., Jan, L.Y., and Jan, Y.N. (2003). Dendrites of Distinct Classes of *Drosophila* Sensory Neurons Show Different Capacities for Homotypic Repulsion. Current Biology *13*, 618–626.

Grueber, W.B., Ye, B., Yang, C.-H., Younger, S., Borden, K., Jan, L.Y., and Jan, Y.N. (2007). Projections of *Drosophila* multidendritic neurons in the central nervous system: links with peripheral dendrite morphology. Development *134*, 55–64.

Han, C., Jan, L.Y., and Jan, Y.N. (2011). Enhancer-driven membrane markers for analysis of nonautonomous mechanisms reveal neuron-glia interactions in *Drosophila*. Proc Natl Acad Sci USA *108*, 9673–9678.

Hantash, F.M., Goos, D.G., Tsao, D., Quan, F., Buller-Burckle, A., Peng, M., Jarvis, M., Sun, W., and Strom, C.M. (2010). Qualitative assessment of *FMR1* (CGG)n triplet repeat status in normal, intermediate, premutation, full mutation, and mosaic carriers in both sexes: implications for fragile X syndrome carrier and newborn screening. Genet Med *12*, 162–173.

Hanus, C., and Ehlers, M.D. (2008). Secretory outposts for the local processing of membrane cargo in neuronal dendrites. Traffic *9*, 1437–1445.

Hanus, C., and Ehlers, M.D. (2016). Specialization of biosynthetic membrane trafficking for neuronal form and function. Current Opinion in Neurobiology *39*, 8–16.

Hanus, C., Geptin, H., Tushev, G., Garg, S., Alvarez-Castelao, B., Sambandan, S., Kochen, L., Hafner, A.-S., Langer, J.D., and Schuman, E.M. (2016). Unconventional secretory processing diversifies neuronal ion channel properties. Elife *5*, e20609.

Hanus, C., Kochen, L., Dieck, S.T., Racine, V., Sibarita, J.-B., Schuman, E.M., and Ehlers, M.D. (2014). Synaptic Control of Secretory Trafficking in Dendrites. Cell Rep *7*, 1771–1778.

Harris, K.P., and Littleton, J.T. (2015). Transmission, Development, and Plasticity of Synapses. Genetics *201*, 345–375.

Hay, J.C., Chao, D.S., Kuo, C.S., and Scheller, R.H. (1997). Protein interactions regulating vesicle transport between the endoplasmic reticulum and Golgi apparatus in mammalian cells. Cell *89*, 149–158.

Hay, J.C., Klumperman, J., Oorschot, V., Steegmaier, M., Kuo, C.S., and Scheller, R.H. (1998). Localization, dynamics, and protein interactions reveal distinct roles for ER and Golgi SNAREs. J Cell Biol *141*, 1489–1502.

Helms, J.B., and Rothman, J.E. (1992). Inhibition by brefeldin A of a Golgi membrane enzyme that catalyses exchange of guanine nucleotide bound to ARF. Nature *360*, 352–354.

Honda, A., Al-Awar, O.S., Hay, J.C., and Donaldson, J.G. (2005). Targeting of Arf-1 to the early Golgi by membrin, an ER-Golgi SNARE. J Cell Biol *168*, 1039–1051.

Horton, A.C., and Ehlers, M.D. (2003). Dual modes of endoplasmic reticulum-to-Golgi transport in dendrites revealed by live-cell imaging. J Neurosci *23*, 6188–6199.

Horton, A.C., and Ehlers, M.D. (2004). Secretory trafficking in neuronal dendrites. Nat Cell Biol *6*, 585–591.

Horton, A.C., Rácz, B., Monson, E.E., Lin, A.L., Weinberg, R.J., and Ehlers, M.D. (2005). Polarized secretory trafficking directs cargo for asymmetric dendrite growth and morphogenesis. Neuron *48*, 757–771.

Huntwork, S., and Littleton, J.T. (2007). A complexin fusion clamp regulates spontaneous neurotransmitter release and synaptic growth. Nat Neurosci *10*, 1235–1237.

International Consortium for Blood Pressure Genome-Wide Association Studies, Ehret, G.B., Munroe, P.B., Rice, K.M., Bochud, M., Johnson, A.D., Chasman, D.I., Smith, A.V., Tobin, M.D., Verwoert, G.C., et al. (2011). Genetic variants in novel pathways influence blood pressure and cardiovascular disease risk. Nature *478*, 103–109.

Jahn, R., and Scheller, R.H. (2006). SNAREs--engines for membrane fusion. Nat. Rev. Mol. Cell Biol. *7*, 631–643.

Jareb, M., and Banker, G. (1997). Inhibition of axonal growth by brefeldin A in hippocampal neurons in culture. J Neurosci *17*, 8955–8963.

Jeans, A.F., Oliver, P.L., Johnson, R., Capogna, M., Vikman, J., Molnár, Z., Babbs, A., Partridge, C.J., Salehi, A., Bengtsson, M., et al. (2007). A dominant mutation in Snap25 causes impaired vesicle trafficking, sensorimotor gating, and ataxia in the blind-drunk mouse. Proc Natl Acad Sci USA *104*, 2431–2436.

Jones, B., Jones, E.L., Bonney, S.A., Patel, H.N., Mensenkamp, A.R., Eichenbaum-Voline, S., Rudling, M., Myrdal, U., Annesi, G., Naik, S., et al. (2003). Mutations in a Sar1 GTPase of COPII vesicles are associated with lipid absorption disorders. Nat Genet *34*, 29–31.

Käll, L., Krogh, A., and Sonnhammer, E.L.L. (2004). A combined transmembrane topology and signal peptide prediction method. J Mol Biol *338*, 1027–1036.

Kasumu, A., and Bezprozvanny, I. (2010). Deranged Calcium Signaling in Purkinje Cells and Pathogenesis in Spinocerebellar Ataxia 2 (SCA2) and Other Ataxias. Cerebellum *11*, 630–639.

Kienle, N., Kloepper, T.H., and Fasshauer, D. (2009a). Differences in the SNARE evolution of fungi and metazoa. Biochem Soc Trans *37*, 787–791.

Kienle, N., Kloepper, T.H., and Fasshauer, D. (2009b). Phylogeny of the SNARE vesicle fusion machinery yields insights into the conservation of the secretory pathway in fungi. BMC Evol Biol *9*, 19.

Kloepper, T.H., Kienle, C.N., and Fasshauer, D. (2007). An elaborate classification of SNARE proteins sheds light on the conservation of the eukaryotic endomembrane system. Mol Biol Cell *18*, 3463–3471.

Kloepper, T.H., Kienle, C.N., and Fasshauer, D. (2008). SNAREing the Basis of Multicellularity: Consequences of Protein Family Expansion during Evolution. Mol Biol Evol *25*, 2055–2068.

Klumperman, J. (2011). Architecture of the mammalian Golgi. Cold Spring Harb Perspect Biol *3*, a005181.

Kojovic, M., Cordivari, C., and Bhatia, K. (2011). Myoclonic disorders: a practical approach for diagnosis and treatment. Ther Adv Neurol Disord *4*, 47–62.

Kondylis, V., and Rabouille, C. (2009). The Golgi apparatus: Lessons from *Drosophila*. FEBS Letters *583*, 3827–3838.

Korbie, D.J., and Mattick, J.S. (2008). Touchdown PCR for increased specificity and sensitivity in PCR amplification. Nat Protoc *3*, 1452–1456.

Koressaar, T., and Remm, M. (2007). Enhancements and modifications of primer design program Primer3. Bioinformatics *23*, 1289–1291.

Kornfeld, S. (1987). Trafficking of lysosomal enzymes. FASEB J *1*, 462-468.

Krysa, W., Rajkiewicz, M., and Sułek, A. (2012). Rapid detection of large expansions in progressive myoclonus epilepsy type 1, myotonic dystrophy type 2 and spinocerebellar ataxia type 8. Neurol Neurochir Pol *46*, 113–120.

Kumar, P., Henikoff, S., and Ng, P.C. (2009). Predicting the effects of coding non-synonymous variants on protein function using the SIFT algorithm. Nat Protoc *4*, 1073–1081.

Lai, S.-L., and Lee, T. (2006). Genetic mosaic with dual binary transcriptional systems in *Drosophila*. Nat Neurosci *9*, 703–709.

Lalioti, M.D., Mirotsou, M., Buresi, C., Peitsch, M.C., Rossier, C., Ouazzani, R., Baldy-Moulinier, M., Bottani, A., Malafosse, A., and Antonarakis, S.E. (1997a). Identification of mutations in cystatin B, the gene responsible for the Unverricht-Lundborg type of progressive myoclonus epilepsy (EPM1). Am J Hum Genet *60*, 342–351.

Lalioti, M.D., Scott, H.S., Buresi, C., Rossier, C., Bottani, A., Morris, M.A., Malafosse, A., and Antonarakis, S.E. (1997b). Dodecamer repeat expansion in cystatin B gene in progressive myoclonus epilepsy. Nature *386*, 847–851.

Lamperti, C., and Zeviani, M. (2016). Myoclonus epilepsy in mitochondrial disorders. Epileptic Disord *18*, 94–102.

Lavieu, G., Zheng, H., and Rothman, J.E. (2013). Stapled Golgi cisternae remain in place as cargo passes through the stack. Elife *2*, e00558.

Lian, J.P., and Ferro-Novick, S. (1993). Bos1p, an integral membrane protein of the endoplasmic reticulum to Golgi transport vesicles, is required for their fusion competence. Cell *73*, 735–745.

Lippincott-Schwartz, J., Yuan, L.C., Bonifacino, J.S., and Klausner, R.D. (1989). Rapid redistribution of Golgi proteins into the ER in cells treated with brefeldin A: evidence for membrane cycling from Golgi to ER. Cell *56*, 801–813.

Liu, C., Lin, C., Whitaker, D.T., Bakeri, H., Bulgakov, O.V., Liu, P., Lei, J., Dong, L., Li, T., and Swaroop, A. (2013). Prickle1 is expressed in distinct cell populations of the central nervous system and contributes to neuronal morphogenesis. Hum Mol Genet *22*, 2234–2246.

Lorente-Rodríguez, A., and Barlowe, C. (2011). Entry and exit mechanisms at the cis-face of the Golgi complex. Cold Spring Harb Perspect Biol *3*, a005207.

Losev, E., Reinke, C.A., Jellen, J., Strongin, D.E., Bevis, B.J., and Glick, B.S. (2006). Golgi maturation visualized in living yeast. Nature *441*, 1002–1006.

Lowe, S.L., Peter, F., Subramaniam, V.N., Wong, S.H., and Hong, W. (1997). A SNARE involved in protein transport through the Golgi apparatus. Nature *389*, 881–884.

Lupas, A., Van Dyke, M., and Stock, J. (1991). Predicting coiled coils from protein sequences. Science *252*, 1162–1164.

Ma, L., Rebane, A.A., Yang, G., Xi, Z., Kang, Y., Gao, Y., and Zhang, Y. (2015). Munc18-1-regulated stage-wise SNARE assembly underlying synaptic exocytosis. Elife *4*, e09580.

Majoul, I., Straub, M., Hell, S.W., Duden, R., and Söling, H.D. (2001). KDEL-cargo regulates interactions between proteins involved in COPI vesicle traffic: measurements in living cells using FRET. Dev Cell *1*, 139–153.

Mali, P., Yang, L., Esvelt, K.M., Aach, J., Guell, M., DiCarlo, J.E., Norville, J.E., and Church, G.M. (2013). RNA-guided human genome engineering via Cas9. Science *339*, 823–826.

Malsam, J., and Söllner, T.H. (2011). Organization of SNAREs within the Golgi stack. Cold Spring Harb Perspect Biol *3*, a005249.

Malsam, J., Kreye, S., and Söllner, T.H. (2008). Membrane fusion: SNAREs and regulation. Cell Mol Life Sci *65*, 2814–2832.

Mancias, J.D., and Goldberg, J. (2008). Structural basis of cargo membrane protein discrimination by the human COPII coat machinery. EMBO J *27*, 2918–2928.

Margittai, M., Fasshauer, D., Pabst, S., Jahn, R., and Langen, R. (2001). Homo- and heterooligomeric SNARE complexes studied by site-directed spin labeling. J Biol Chem *276*, 13169–13177.

Marseille Consensus Group. (1990). Classification of progressive myoclonus epilepsies and related disorders. Ann Neurol *28*, 113–116.

Marsh, B.J., Volkmann, N., McIntosh, J.R., and Howell, K.E. (2004). Direct continuities between cisternae at different levels of the Golgi complex in glucose-stimulated mouse islet beta cells. Proc Natl Acad Sci USA *101*, 5565–5570.

Matsuura-Tokita, K., Takeuchi, M., Ichihara, A., Mikuriya, K., and Nakano, A. (2006). Live imaging of yeast Golgi cisternal maturation. Nature *441*, 1007–1010.

McCormick, D.A., Connors, B.W., Lighthall, J.W., and Prince, D.A. (1985). Comparative electrophysiology of pyramidal and sparsely spiny stellate neurons of the neocortex. J Neurophysiol *54*, 782–806.

McNew, J.A., Parlati, F., Fukuda, R., Johnston, R.J., Paz, K., Paumet, F., Söllner, T.H., and Rothman, J.E. (2000). Compartmental specificity of cellular membrane fusion encoded in SNARE proteins. Nature *407*, 153–159.

McNew, J.A., Sogaard, M., Lampen, N.M., Machida, S., Ye, R.R., Lacomis, L., Tempst, P., Rothman, J.E., and Söllner, T.H. (1997). Ykt6p, a prenylated SNARE essential for endoplasmic reticulum-Golgi transport. J Biol Chem *272*, 17776–17783.

McWilliam, H., Li, W., Uludag, M., Squizzato, S., Park, Y.M., Buso, N., Cowley, A.P., and Lopez, R. (2013). Analysis Tool Web Services from the EMBL-EBI. Nucleic Acids Res. *41*, W597–W600.

Meijering, E., Jacob, M., Sarria, J.-C.F., Steiner, P., Hirling, H., and Unser, M. (2004). Design and validation of a tool for neurite tracing and analysis in fluorescence microscopy images. Cytometry A *58*, 167–176.

Melia, T.J., Weber, T., McNew, J.A., Fisher, L.E., Johnston, R.J., Parlati, F., Mahal, L.K., Söllner, T.H., and Rothman, J.E. (2002). Regulation of membrane fusion by the membrane-proximal coil of the t-SNARE during zippering of SNAREpins. J Cell Biol *158*, 929–940.

Merianda, T., and Twiss, J. (2013). Peripheral nerve axons contain machinery for co-translational secretion of axonally-generated proteins. Neurosci Bull *29*, 493–500.

Merianda, T.T., Lin, A.C., Lam, J.S.Y., Vuppalanchi, D., Willis, D.E., Karin, N., Holt, C.E., and Twiss, J.L. (2009). A functional equivalent of endoplasmic reticulum and Golgi in axons for secretion of locally synthesized proteins. Mol Cell Neurosci *40*, 128–142.

Meyer, T.E., Shiffman, D., Morrison, A.C., Rowland, C.M., Louie, J.Z., Bare, L.A., Ross, D.A., Arellano, A.R., Chasman, D.I., Ridker, P.M., et al. (2009). *GOSR2* Lys67Arg is associated with hypertension in whites. Am J Hypertens *22*, 163–168.

Michelucci, R., Pasini, E., Riguzzi, P., Andermann, E., Kälviäinen, R., and Genton, P. (2016). Myoclonus and seizures in progressive myoclonus epilepsies: pharmacology and therapeutic trials. Epileptic Disord *18*, 145–153.

Michelucci, R., Pasini, E., Riguzzi, P., Volpi, L., Dazzo, E., and Nobile, C. (2012). Genetics of Epilepsy and Relevance to Current Practice. Curr Neurol Neurosci Rep *12*, 445–455.

Minassian, B.A. (2014). The progressive myoclonus epilepsies. Prog Brain Res *213*, 113–122.

Mironov, A.A., Mironov, A.A., Beznoussenko, G.V., Trucco, A., Lupetti, P., Smith, J.D., Geerts, W.J.C., Koster, A.J., Burger, K.N.J., Martone, M.E., et al. (2003). ER-to-Golgi carriers arise through direct en bloc protrusion and multistage maturation of specialized ER exit domains. Dev Cell *5*, 583–594.

Munro, S., and Pelham, H.R. (1987). A C-terminal signal prevents secretion of luminal ER proteins. Cell *48*, 899–907.

Muona, M., Berkovic, S.F., Dibbens, L.M., Oliver, K.L., Maljevic, S., Bayly, M.A., Joensuu, T., Canafoglia, L., Franceschetti, S., Michelucci, R., et al. (2015). A recurrent de novo mutation in *KCNC1* causes progressive myoclonus epilepsy. Nat Genet *47*, 39–46.

Nave, K.-A., and Werner, H.B. (2014). Myelination of the nervous system: mechanisms and functions. Annu. Rev. Cell Dev Biol *30*, 503–533.

Newman, A.P., and Ferro-Novick, S. (1987). Characterization of new mutants in the early part of the yeast secretory pathway isolated by a [3H]mannose suicide selection. J Cell Biol *105*, 1587–1594.

Newman, A.P., Shim, J., and Ferro-Novick, S. (1990). BET1, BOS1, and SEC22 are members of a group of interacting yeast genes required for transport from the endoplasmic reticulum to the Golgi complex. Mol Cell Biol *10*, 3405–3414.

Nita, D.A., Mole, S.E., and Minassian, B.A. (2016). Neuronal ceroid lipofuscinoses. Epileptic Disord *18*, 73–88.

Nixon-Abell, J., Obara, C.J., Weigel, A.V., Li, D., Legant, W.R., Xu, C.S., Pasolli, H.A., Harvey, K., Hess, H.F., Betzig, E., et al. (2016). Increased spatiotemporal resolution reveals highly dynamic dense tubular matrices in the peripheral ER. Science *354*, aaf3928.

North, S.J., Huang, H.-H., Sundaram, S., Jang-Lee, J., Etienne, A.T., Trollope, A., Chalabi, S., Dell, A., Stanley, P., and Haslam, S.M. (2010). Glycomics profiling of Chinese hamster ovary cell glycosylation mutants reveals N-glycans of a novel size and complexity. J Biol Chem *285*, 5759–5775.

Nosková, L., Stránecký, V., Hartmannová, H., Přistoupilová, A., Barešová, V., Ivánek, R., Hůlková, H., Jahnová, H., van der Zee, J., Staropoli, J.F., et al. (2011). Mutations in DNAJC5, encoding cysteine-string protein alpha, cause autosomal-dominant adult-onset neuronal ceroid lipofuscinosis. Am J Hum Genet *89*, 241–252.

Novick, P., Field, C., and Schekman, R. (1980). Identification of 23 complementation groups required for post-translational events in the yeast secretory pathway. Cell *21*, 205–215.

Oliver, K.L., Franceschetti, S., Milligan, C.J., Muona, M., Mandelstam, S.A., Canafoglia, L., Boguszewska-Chachulska, A.M., Korczyn, A.D., Bisulli, F., Di Bonaventura, C., et al. (2017). Myoclonus epilepsy and ataxia due to KCNC1 mutation: Analysis of 20 cases and K+ channel properties. Ann Neurol *81*, 677–689.

Orci, L., Ravazzola, M., Volchuk, A., Engel, T., Gmachl, M., Amherdt, M., Perrelet, A., Söllner, T.H., and Rothman, J.E. (2000). Anterograde flow of cargo across the golgi stack potentially mediated via bidirectional “percolating” COPI vesicles. Proc Natl Acad Sci USA *97*, 10400–10405.

Palade, G. (1975). Intracellular aspects of the process of protein synthesis. Science *189*, 347–358.

Park, J.K., Orvisky, E., Tayebi, N., Kaneski, C., Lamarca, M.E., Stubblefield, B.K., Martin, B.M., Schiffmann, R., and Sidransky, E. (2003). Myoclonic epilepsy in Gaucher disease: genotype-phenotype insights from a rare patient subgroup. Pediatr Res *53*, 387–395.

Parker, L., Padilla, M., Du, Y., Dong, K., and Tanouye, M.A. (2011). *Drosophila* as a model for epilepsy: bss is a gain-of-function mutation in the para sodium channel gene that leads to seizures. Genetics *187*, 523–534.

Parlati, F., McNew, J.A., Fukuda, R., Miller, R., Söllner, T.H., and Rothman, J.E. (2000). Topological restriction of SNARE-dependent membrane fusion. Nature *407*, 194–198.

Parlati, F., Varlamov, O., Paz, K., McNew, J.A., Hurtado, D., Söllner, T.H., and Rothman, J.E. (2002). Distinct SNARE complexes mediating membrane fusion in Golgi transport based on combinatorial specificity. Proc Natl Acad Sci USA *99*, 5424–5429.

Passemard, S., Perez, F., Colin-Lemesre, E., Rasika, S., Gressens, P., and Ghouzzi, El, V. (2017). Golgi trafficking defects in postnatal microcephaly: The evidence for "Golgipathies". Prog Neurobiol *153*, 46-63.

Pennacchio, L.A., Bouley, D.M., Higgins, K.M., Scott, M.P., Noebels, J.L., and Myers, R.M. (1998). Progressive ataxia, myoclonic epilepsy and cerebellar apoptosis in cystatin B-deficient mice. Nat Genet *20*, 251–258.

Pennacchio, L.A., Lehesjoki, A.E., Stone, N.E., Willour, V.L., Virtaneva, K., Miao, J., D'Amato, E., Ramirez, L., Faham, M., Koskiniemi, M., et al. (1996). Mutations in the gene encoding cystatin B in progressive myoclonus epilepsy (EPM1). Science *271*, 1731–1734.

Pfeiffer, B.D., Ngo, T.-T.B., Hibbard, K.L., Murphy, C., Jenett, A., Truman, J.W., and Rubin, G.M. (2010). Refinement of tools for targeted gene expression in *Drosophila*. Genetics *186*, 735–755.

Pfenninger, K.H. (2009). Plasma membrane expansion: a neuron's Herculean task. Nat Rev Neurosci *10*, 251–261.

Pierce, J.P., Mayer, T., and McCarthy, J.B. (2001). Evidence for a satellite secretory pathway in neuronal dendritic spines. Curr Biol *11*, 351–355.

Pierce, J.P., van Leyen, K., and McCarthy, J.B. (2000). Translocation machinery for synthesis of integral membrane and secretory proteins in dendritic spines. Nat Neurosci *3*, 311–313.

Popoff, V., Adolf, F., Brügger, B., and Wieland, F. (2011). COPI budding within the Golgi stack. Cold Spring Harb Perspect Biol *3*, a005231.

Pourquié, O. (2011). Vertebrate segmentation: from cyclic gene networks to scoliosis. Cell *145*, 650–663.

Praschberger, R., Balint, B., Mencacci, N.E., Hersheson, J., Rubio-Agusti, I., Kullmann, D.M., Bettencourt, C., Bhatia, K., and Houlden, H. (2015). Expanding the Phenotype and Genetic Defects Associated with the *GOSR2* Gene. Mov Disord Clin Pract *2*, 271–273.

Praschberger, R., Lowe, S.A., Malintan, N.T., Giachello, C.N.G., Patel, N., Houlden, H., Kullmann, D.M., Baines, R.A., Usowicz, M.M., Krishnakumar, S.S., et al. (2017). Mutations in Membrin/*GOSR2* Reveal Stringent Secretory Pathway Demands of Dendritic Growth and Synaptic Integrity. Cell Rep *21*, 97–109.

Presley, J.F., Cole, N.B., Schroer, T.A., Hirschberg, K., Zaal, K.J., and Lippincott-Schwartz, J. (1997). ER-to-Golgi transport visualized in living cells. Nature *389*, 81–85.

Preuss, D., Mulholland, J., Franzusoff, A., Segev, N., and Botstein, D. (1992). Characterization of the Saccharomyces Golgi complex through the cell cycle by immunoelectron microscopy. Mol Biol Cell *3*, 789–803.

Ramón y Cajal, S. (1906). Nobel Lecture: The structure and connexions of neurons. Nobelprize.org. Nobel Media AB 2014. Web. 25 May 2017. <http://www.nobelprize.org/nobel_prizes/medicine/laureates/1906/cajal-lecture.html>

Rao, S.S., Stewart, B.A., Rivlin, P.K., Vilinsky, I., Watson, B.O., Lang, C., Boulianne, G., Salpeter, M.M., and Deitcher, D.L. (2001). Two distinct effects on neurotransmission in a temperature-sensitive SNAP-25 mutant. EMBO J *20*, 6761–6771.

Rivera, V.M., Wang, X., Wardwell, S., Courage, N.L., Volchuk, A., Keenan, T., Holt, D.A., Gilman, M., Orci, L., Cerasoli, F., et al. (2000). Regulation of protein secretion through controlled aggregation in the endoplasmic reticulum. Science *287*, 826–830.

Rollins, C.T., Rivera, V.M., Woolfson, D.N., Keenan, T., Hatada, M., Adams, S.E., Andrade, L.J., Yaeger, D., van Schravendijk, M.R., Holt, D.A., et al. (2000). A ligand-reversible dimerization system for controlling protein-protein interactions. Proc Natl Acad Sci USA *97*, 7096–7101.

Rong, Y.S., and Golic, K.G. (2000). Gene targeting by homologous recombination in *Drosophila*. Science *288*, 2013–2018.

Roote, J., and Prokop, A. (2013). How to design a genetic mating scheme: a basic training package for *Drosophila* genetics. G3 (Bethesda) *3*, 353–358.

Rothman, J.E. (1994). Mechanisms of intracellular protein transport. Nature *372*, 55–63.

Rothman, J.E. (2010). The Future of Golgi Research. Mol Biol Cell *21*, 3776–3780.

Rothman, J.E. (2014). The Principle of Membrane Fusion in the Cell (Nobel Lecture). Angew Chem Int Ed Engl *53*, 12676-12694.

Rothman, J.E., and Wieland, F.T. (1996). Protein sorting by transport vesicles. Science *272*, 227–234.

Rowe, T., Dascher, C., Bannykh, S., Plutner, H., and Balch, W.E. (1998). Role of vesicle-associated syntaxin 5 in the assembly of pre-Golgi intermediates. Science *279*, 696–700.

Sáenz, J.B., Sun, W.J., Chang, J.W., Li, J., Bursulaya, B., Gray, N.S., and Haslam, D.B. (2009). Golgicide A reveals essential roles for GBF1 in Golgi assembly and function. Nat Chem Biol *5*, 157–165.

Saporta, A.S.D., Sottile, S.L., Miller, L.J., Feely, S.M.E., Siskind, C.E., and Shy, M.E. (2011). Charcot-Marie-Tooth disease subtypes and genetic testing strategies. Ann Neurol *69*, 22–33.

Schekman, R., and Novick, P. (2004). 23 genes, 23 years later. Cell *S116*, S13-S15.

Schiavo, G., Benfenati, F., Poulain, B., Rossetto, O., Polverino de Laureto, P., DasGupta, B.R., and Montecucco, C. (1992). Tetanus and botulinum-B neurotoxins block neurotransmitter release by proteolytic cleavage of synaptobrevin. Nature *359*, 832–835.

Schiavo, G., Matteoli, M., and Montecucco, C. (2000). Neurotoxins affecting neuroexocytosis. Physiol Rev *80*, 717–766.

Schubert, J., Siekierska, A., Langlois, M., May, P., Huneau, C., Becker, F., Muhle, H., Suls, A., Lemke, J.R., de Kovel, C.G.F., et al. (2014). Mutations in STX1B, encoding a presynaptic protein, cause fever-associated epilepsy syndromes. Nat Genet *46*, 1327–1332.

Schwarz, K., Iolascon, A., Verissimo, F., Trede, N.S., Horsley, W., Chen, W., Paw, B.H., Hopfner, K.-P., Holzmann, K., Russo, R., et al. (2009). Mutations affecting the secretory COPII coat component SEC23B cause congenital dyserythropoietic anemia type II. Nat Genet *41*, 936–940.

Schweizer, A., Fransen, J.A., Bächi, T., Ginsel, L., and Hauri, H.P. (1988). Identification, by a monoclonal antibody, of a 53-kD protein associated with a tubulo-vesicular compartment at the cis-side of the Golgi apparatus. J Cell Biol *107*, 1643–1653.

Schweizer, A., Fransen, J.A., Matter, K., Kreis, T.E., Ginsel, L., and Hauri, H.P. (1990). Identification of an intermediate compartment involved in protein transport from endoplasmic reticulum to Golgi apparatus. Eur J Cell Biol *53*, 185–196.

Schweizer, A., Matter, K., Ketcham, C.M., and Hauri, H.P. (1991). The isolated ER-Golgi intermediate compartment exhibits properties that are different from ER and cis-Golgi. J Cell Biol *113*, 45–54.

Sengupta, P., Satpute-Krishnan, P., Seo, A.Y., Burnette, D.T., Patterson, G.H., and Lippincott-Schwartz, J. (2015). ER trapping reveals Golgi enzymes continually revisit the ER through a recycling pathway that controls Golgi organization. Proc Natl Acad Sci USA *112*, E6752–E6761.

Shen, X.-M., Selcen, D., Brengman, J., and Engel, A.G. (2014). Mutant SNAP25B causes myasthenia, cortical hyperexcitability, ataxia, and intellectual disability. Neurology *83*, 2247-2255.

Sherman, D.L., and Brophy, P.J. (2005). Mechanisms of axon ensheathment and myelin growth. Nat Rev Neurosci *6*, 683–690.

Shim, J., Newman, A.P., and Ferro-Novick, S. (1991). The *BOS1* gene encodes an essential 27-kD putative membrane protein that is required for vesicular transport from the ER to the Golgi complex in yeast. J Cell Biol *113*, 55–64.

Silverstein, S.C., Steinman, R.M., and Cohn, Z.A. (1977). Endocytosis. Annu Rev Biochem *46*, 669–722.

Simino, J., Shi, G., Bis, J.C., Chasman, D.I., Ehret, G.B., Gu, X., Guo, X., Hwang, S.-J., Sijbrands, E., Smith, A.V., et al. (2014). Gene-Age Interactions in Blood Pressure Regulation: A Large-Scale Investigation with the CHARGE, Global BPgen, and ICBP Consortia. Am J Hum Genet *95*, 24-38.

Söllner, T., Bennett, M.K., Whiteheart, S.W., Scheller, R.H., and Rothman, J.E. (1993a). A protein assembly-disassembly pathway in vitro that may correspond to sequential steps of synaptic vesicle docking, activation, and fusion. Cell *75*, 409–418.

Söllner, T., Whiteheart, S.W., Brunner, M., Erdjument-Bromage, H., Geromanos, S., Tempst, P., and Rothman, J.E. (1993b). SNAP receptors implicated in vesicle targeting and fusion. Nature *362*, 318–324.

Stanley, P. (2011). Golgi glycosylation. Cold Spring Harb Perspect Biol *3*, a005199.

Stein, A., Weber, G., Wahl, M.C., and Jahn, R. (2009). Helical extension of the neuronal SNARE complex into the membrane. Nature *460*, 525–528.

Struck, D.K., Hoekstra, D., and Pagano, R.E. (1981). Use of resonance energy transfer to monitor membrane fusion. Biochemistry *20*, 4093–4099.

Su, A.I., Wiltshire, T., Batalov, S., Lapp, H., Ching, K.A., Block, D., Zhang, J., Soden, R., Hayakawa, M., Kreiman, G., et al. (2004). A gene atlas of the mouse and human protein-encoding transcriptomes. Proc Natl Acad Sci USA. *101*, 6062–6067.

Südhof, T.C. (2014). The molecular machinery of neurotransmitter release (Nobel lecture). Angew Chem Int Ed Engl *53*, 12696–12717.

Südhof, T.C., and Rothman, J.E. (2009). Membrane fusion: grappling with SNARE and SM proteins. Science *323*, 474–477.

Supekar, K., Musen, M., and Menon, V. (2009). Development of large-scale functional brain networks in children. PLoS Biol. *7*, e1000157.

Suster, M.L., Seugnet, L., Bate, M., Sokolowski, M.B. (2004). Refining GAL4-driven transgene expression in *Drosophila* with a GAL80 enhancer-trap. Genesis *39*,240-245.

Sutton, R.B., Fasshauer, D., Jahn, R., and Brunger, A.T. (1998). Crystal structure of a SNARE complex involved in synaptic exocytosis at 2.4 A resolution. Nature *395*, 347–353.

Synofzik, M., and Schüle, R. (2017). Overcoming the divide between ataxias and spastic paraplegias: Shared phenotypes, genes, and pathways. Mov Disord *32*, 332-345.

Thévenaz, P., Ruttimann, U.E., and Unser, M. (1998). A pyramid approach to subpixel registration based on intensity. IEEE Trans Image Process *7*, 27–41.

Tisdale, E.J., Bourne, J.R., Khosravi-Far, R., Der, C.J., and Balch, W.E. (1992). GTP-binding mutants of rab1 and rab2 are potent inhibitors of vesicular transport from the endoplasmic reticulum to the Golgi complex. J Cell Biol *119*, 749–761.

Trontelj, J.V., Pecak, F., and Dimitrijević, M.R. (1979). Segmental neurophysiological mechanisms in scoliosis. J Bone Joint Surg Br *61-B*, 310–313.

Trucco, A., Polishchuk, R.S., Martella, O., Di Pentima, A., Fusella, A., Di Giandomenico, D., San Pietro, E., Beznoussenko, G.V., Polishchuk, E.V., Baldassarre, M., et al. (2004). Secretory traffic triggers the formation of tubular continuities across Golgi sub-compartments. Nat Cell Biol *6*, 1071–1081.

Tsuji, S. (2012). Dentatorubral-pallidoluysian atrophy. Handb Clin Neurol *103*, 587–594.

Turnbull, J., Tiberia, E., Striano, P., Genton, P., Carpenter, S., Ackerley, C.A., and Minassian, B.A. (2016). Lafora disease. Epileptic Disord *18*, 38–62.

Untergasser, A., Cutcutache, I., Koressaar, T., Ye, J., Faircloth, B.C., Remm, M., and Rozen, S.G. (2012). Primer3--new capabilities and interfaces. Nucleic Acids Res *40*, e115.

Valenzuela, J.I., and Perez, F. (2015). Diversifying the secretory routes in neurons. Front Neurosci *9*, 358.

van Egmond, M.E., Kuiper, A., Elting, J.W.J., Brouwer, O.F., de Koning, T.J., and Tijssen, M.A.J. (2015). Cortical Myoclonus in a Young Boy with *GOSR2* Mutation Mimics Chorea. Mov Disord Clin Pract *2*, 61–63.

van Egmond, M.E., Verschuuren-Bemelmans, C.C., Nibbeling, E.A., Elting, J.W.J., Sival, D.A., Brouwer, O.F., de Vries, J.J., Kremer, H.P., Sinke, R.J., Tijssen, M.A., et al. (2014). Ramsay Hunt syndrome: clinical characterization of progressive myoclonus ataxia caused by *GOSR2* mutation. Mov Disord *29*, 139–143.

van Egmond, M.E., Weijenberg, A., van Rijn, M.E., Elting, J.W.J., Gelauff, J.M., Zutt, R., Sival, D.A., Lambrechts, R.A., Tijssen, M.A.J., Brouwer, O.F., et al. (2017). The efficacy of the modified Atkins diet in North Sea Progressive Myoclonus Epilepsy: an observational prospective open-label study. Orphanet J Rare Dis *12*, 45.

Varlamov, O., Volchuk, A., Rahimian, V., Doege, C.A., Paumet, F., Eng, W.S., Arango, N., Parlati, F., Ravazzola, M., Orci, L. et al. (2004). i-SNAREs: inhibitory SNAREs that fine-tune the specificity of membrane fusion. J Cell Biol *164*, 79–88.

Veit, M., Söllner, T.H., and Rothman, J.E. (1996). Multiple palmitoylation of synaptotagmin and the t-SNARE SNAP-25. FEBS Letters *385*, 119–123.

Velasco, A., Hendricks, L., Moremen, K.W., Tulsiani, D.R., Touster, O., and Farquhar, M.G. (1993). Cell type-dependent variations in the subcellular distribution of alpha-mannosidase I and II. J Cell Biol *122*, 39–51.

Venken, K.J.T., Schulze, K.L., Haelterman, N.A., Pan, H., He, Y., Evans-Holm, M., Carlson, J.W., Levis, R.W., Spradling, A.C., Hoskins, R.A., et al. (2011). MiMIC: a highly versatile transposon insertion resource for engineering *Drosophila* melanogaster genes. Nat. Methods *8*, 737–743.

Volchuk, A., Ravazzola, M., Perrelet, A., Eng, W.S., Di Liberto, M., Varlamov, O., Fukasawa, M., Engel, T., Söllner, T.H., Rothman, J.E., et al. (2004). Countercurrent distribution of two distinct SNARE complexes mediating transport within the Golgi stack. Mol Biol Cell *15*, 1506–1518.

Walter, P., Gilmore, R., and Blobel, G. (1984). Protein translocation across the endoplasmic reticulum. Cell *38*, 5–8.

Wang, T., Grabski, R., Sztul, E., and Hay, J.C. (2015). p115-SNARE interactions: a dynamic cycle of p115 binding monomeric SNARE motifs and releasing assembled bundles. Traffic *16*, 148–171.

Ward, T.H., Polishchuk, R.S., Caplan, S., Hirschberg, K., and Lippincott-Schwartz, J. (2001). Maintenance of Golgi structure and function depends on the integrity of ER export. J Cell Biol *155*, 557–570.

Warner, J.P., Barron, L.H., Goudie, D., Kelly, K., Dow, D., Fitzpatrick, D.R., and Brock, D.J. (1996). A general method for the detection of large CAG repeat expansions by fluorescent PCR. J Med Genet *33*, 1022–1026.

Weber, T., Zemelman, B.V., McNew, J.A., Westermann, B., Gmachl, M., Parlati, F., Söllner, T.H., and Rothman, J.E. (1998). SNAREpins: minimal machinery for membrane fusion. Cell *92*, 759–772.

Wilhelm, B.G., Mandad, S., Truckenbrodt, S., Kröhnert, K., Schäfer, C., Rammner, B., Koo, S.J., Claßen, G.A., Krauss, M., Haucke, V., et al. (2014). Composition of isolated synaptic boutons reveals the amounts of vesicle trafficking proteins. Science *344*, 1023–1028.

Willett, R., Kudlyk, T., Pokrovskaya, I., Schönherr, R., Ungar, D., Duden, R., and Lupashin, V. (2013). COG complexes form spatial landmarks for distinct SNARE complexes. Nat Commun *4*, 1553.

Wu, C., Jin, X., Tsueng, G., Afrasiabi, C., and Su, A.I. (2016). BioGPS: building your own mash-up of gene annotations and expression profiles. Nucleic Acids Res. *44*, D313–D316.

Wu, J.S., and Luo, L. (2006). A protocol for dissecting *Drosophila* melanogaster brains for live imaging or immunostaining. Nat Protoc *1*, 2110–2115.

Xu, D., and Hay, J.C. (2004). Reconstitution of COPII vesicle fusion to generate a pre-Golgi intermediate compartment. J Cell Biol *167*, 997–1003.

Xu, D., Joglekar, A.P., Williams, A.L., and Hay, J.C. (2000). Subunit structure of a mammalian ER/Golgi SNARE complex. J Biol Chem *275*, 39631–39639.

Yadav, S., and Linstedt, A.D. (2011). Golgi positioning. Cold Spring Harb Perspect Biol *3*, a005322.

Yamaguchi, T., Dulubova, I., Min, S.-W., Chen, X., Rizo, J., and Südhof, T.C. (2002). Sly1 binds to Golgi and ER syntaxins via a conserved N-terminal peptide motif. Dev Cell *2*, 295–305.

Ye, B., Kim, J.H., Yang, L., McLachlan, I., Younger, S., Jan, L.Y., and Jan, Y.N. (2011). Differential regulation of dendritic and axonal development by the novel Krüppel-like factor Dar1. J Neurosci *31*, 3309–3319.

Ye, B., Zhang, Y., Song, W., Younger, S.H., Jan, L.Y., and Jan, Y.N. (2007). Growing dendrites and axons differ in their reliance on the secretory pathway. Cell *130*, 717–729.

Zaal, K.J., Smith, C.L., Polishchuk, R.S., Altan, N., Cole, N.B., Ellenberg, J., Hirschberg, K., Presley, J.F., Roberts, T.H., Siggia, E., et al. (1999). Golgi membranes are absorbed into and reemerge from the ER during mitosis. Cell *99*, 589–601.

Zhang, J., Schulze, K.L., Hiesinger, P.R., Suyama, K., Wang, S., Fish, M., Acar, M., Hoskins, R.A., Bellen, H.J., and Scott, M.P. (2007). Thirty-one flavors of *Drosophila* rab proteins. Genetics *176*, 1307–1322.

Zhang, S., Masuyer, G., Zhang, J., Shen, Y., Lundin, D., Henriksson, L., Miyashita, S.-I., Martínez-Carranza, M., Dong, M., and Stenmark, P. (2017). Identification and characterization of a novel botulinum neurotoxin. Nat Commun *8*, 14130.

Zhang, Y. (2017). Energetics, kinetics, and pathway of SNARE folding and assembly revealed by optical tweezers. Protein Sci *26*, 1252-1265.

Zhong, W. (2011). Golgi during development. Cold Spring Harb Perspect Biol *3*, a005363.

Zhou, J., Tawk, M., Tiziano, F.D., Veillet, J., Bayes, M., Nolent, F., Garcia, V., Servidei, S., Bertini, E., Castro-Giner, F., et al. (2012). Spinal Muscular Atrophy Associated with Progressive Myoclonic Epilepsy Is Caused by Mutations in ASAH1. Am J Hum Genet *91*, 5–14.

Zorman, S., Rebane, A.A., Ma, L., Yang, G., Molski, M.A., Coleman, J., Pincet, F., Rothman, J.E., and Zhang, Y. (2014). Common intermediates and kinetics, but different energetics, in the assembly of SNARE proteins. Elife *3*, e03348.

Zwilling, D., Cypionka, A., Pohl, W.H., Fasshauer, D., Walla, P.J., Wahl, M.C., and Jahn, R. (2007). Early endosomal SNAREs form a structurally conserved SNARE complex and fuse liposomes with multiple topologies. EMBO J *26*, 9–18.

Appendix

Custom human *GOSR2* transgenes

WT

gcggccgccgacATGGACTACAAAGACGATGACGACAAGGATCCCCTGTTCCAGCAAACGCACAAGCA
GGTCCACGAGATCCAGTCTTGCATGGGACGCCTGGAGACGGCAGACAAGCAGTCTGTGCACATAGTAG
AAAACGAAATCCAAGCAAGCATAGACCAGATATTCAGCCGTCTAGAACGTCTGGAGATTTTGTCCAGC
AAGGAGCCCCCTAACAAAAGGCAAAATGCCAGACTTCGGGTTGACCAGTTAAAGTATGATGTCCAGCA
CCTGCAGACTGCGCTCAGAAACTTCCAGCATCGGCGCCATGCAAGGGAGCAGCAGGAGAGACAGCGAG
AAGAGCTTCTGTCTCGAACCTTCACCACTAACGACTCTGACACCACCATACCAATGGACGAATCACTG
CAGTTTAACTCCTCCCTCCAGAAAGTTCACAACGGCATGGATGACCTCATTTTAGATGGGCACAATAT
TTTAGATGGACTGAGGACCCAGAGACTGACCTTGAAGGGGACTCAGAAGAAGATCCTTGACATTGCCA
ACATGCTGGGCTTGTCCAACACAGTGATGCGGCTCATCGAGAAGCGGGCTTTCCAGGACAAGTACTTT
ATGATAGGTGGGATGCTGCTGACCTGTGTGGTCATGTTCCTCGTGGTGCAGTACCTGACATGAggtac
c

codons mutated in below transgenes

G144W

gcggccgccgacATGGACTACAAAGACGATGACGACAAGGATCCCCTGTTCCAGCAAACGCACAAGCA
GGTCCACGAGATCCAGTCTTGCATGGGACGCCTGGAGACGGCAGACAAGCAGTCTGTGCACATAGTAG
AAAACGAAATCCAAGCAAGCATAGACCAGATATTCAGCCGTCTAGAACGTCTGGAGATTTTGTCCAGC
AAGGAGCCCCCTAACAAAAGGCAAAATGCCAGACTTCGGGTTGACCAGTTAAAGTATGATGTCCAGCA
CCTGCAGACTGCGCTCAGAAACTTCCAGCATCGGCGCCATGCAAGGGAGCAGCAGGAGAGACAGCGAG
AAGAGCTTCTGTCTCGAACCTTCACCACTAACGACTCTGACACCACCATACCAATGGACGAATCACTG
CAGTTTAACTCCTCCCTCCAGAAAGTTCACAACGGCATGGATGACCTCATTTTAGATTGGCACAATAT
TTTAGATGGACTGAGGACCCAGAGACTGACCTTGAAGGGGACTCAGAAGAAGATCCTTGACATTGCCA
ACATGCTGGGCTTGTCCAACACAGTGATGCGGCTCATCGAGAAGCGGGCTTTCCAGGACAAGTACTTT
ATGATAGGTGGGATGCTGCTGACCTGTGTGGTCATGTTCCTCGTGGTGCAGTACCTGACATGAggtac
c

K164del

gcggccgccgacATGGACTACAAAGACGATGACGACAAGGATCCCCTGTTCCAGCAAACGCACAAGCA
GGTCCACGAGATCCAGTCTTGCATGGGACGCCTGGAGACGGCAGACAAGCAGTCTGTGCACATAGTAG
AAAACGAAATCCAAGCAAGCATAGACCAGATATTCAGCCGTCTAGAACGTCTGGAGATTTTGTCCAGC
AAGGAGCCCCCTAACAAAAGGCAAAATGCCAGACTTCGGGTTGACCAGTTAAAGTATGATGTCCAGCA
CCTGCAGACTGCGCTCAGAAACTTCCAGCATCGGCGCCATGCAAGGGAGCAGCAGGAGAGACAGCGAG
AAGAGCTTCTGTCTCGAACCTTCACCACTAACGACTCTGACACCACCATACCAATGGACGAATCACTG
CAGTTTAACTCCTCCCTCCAGAAAGTTCACAACGGCATGGATGACCTCATTTTAGATGGGCACAATAT
TTTAGATGGACTGAGGACCCAGAGACTGACCTTGAAGGGGACTCAGAAGA[]TCCTTGACATTGCCAA
CATGCTGGGCTTGTCCAACACAGTGATGCGGCTCATCGAGAAGCGGGCTTTCCAGGACAAGTACTTTA
TGATAGGTGGGATGCTGCTGACCTGTGTGGTCATGTTCCTCGTGGTGCAGTACCTGACATGAggtacc

GOSR2 CDS
FLAG
Kozac sequence
NotI
KpnI

Custom *Drosophila membrin* transgenes

WT

gcggccgccgacATGGACTACAAAGACGATGACGACAAGGAGAGCTTGTACCACCAAACCAACAATGT
GGTAAAGGACATCGAGCGCGATTTCCAGCGACTGAGTCAGCTCAGTGCCCAGGAATCGCTTGACGTGG
AAAACGGCATTCAATTGAAGATTACCCAGGCGAACGCAAACTGCGATCGGTTGGATGTGCTGTTGTAT
AAGGTGCCACCTTCGCAGCGACAAAGCTCCAAACTTCGTGTGGATCAGCTGAAATATGACCTGAGACA
CCTGCAGACATCACTGCAGACGGCGCGGGAACGAAGACAGCGACGGATGCAGGAGATCTCCGAGAGGG
AACAGCTGCTGAATCACAGATTCACGGCAAACAGCGCGCAGCCGGAGGAAACGCGCCTGCAATTGGAC
TACGAACTGCAGCATCATACGCAGCTGGGTAACGCCCATCGGGGTGTGGACGACATGATTGCCTCGGG
CAGCGGCATTCTCGAGAGCCTGATCTCGCAGAGAATGACGCTGGGCGGAGCGCACAAGAGAATCCAGG
CGATAGGCAGCACACTGGGTCTGTCCAATCACACGATGAAACTTATTGAACGCCGGCTGGTCGAGGAT
CGTCGGATATTCATCGGAGGAGTGGTGGTCACCTTGCTTATCATCGCCCTGATCATCTATTTCCTAGT
GCTCTAAggtacc

codons mutated in below transgenes

G147W

gcggccgccgacATGGACTACAAAGACGATGACGACAAGGAGAGCTTGTACCACCAAACCAACAATGT
GGTAAAGGACATCGAGCGCGATTTCCAGCGACTGAGTCAGCTCAGTGCCCAGGAATCGCTTGACGTGG
AAAACGGCATTCAATTGAAGATTACCCAGGCGAACGCAAACTGCGATCGGTTGGATGTGCTGTTGTAT
AAGGTGCCACCTTCGCAGCGACAAAGCTCCAAACTTCGTGTGGATCAGCTGAAATATGACCTGAGACA
CCTGCAGACATCACTGCAGACGGCGCGGGAACGAAGACAGCGACGGATGCAGGAGATCTCCGAGAGGG
AACAGCTGCTGAATCACAGATTCACGGCAAACAGCGCGCAGCCGGAGGAAACGCGCCTGCAATTGGAC
TACGAACTGCAGCATCATACGCAGCTGGGTAACGCCCATCGGGGTGTGGACGACATGATTGCCTCGTG
GAGCGGCATTCTCGAGAGCCTGATCTCGCAGAGAATGACGCTGGGCGGAGCGCACAAGAGAATCCAGG
CGATAGGCAGCACACTGGGTCTGTCCAATCACACGATGAAACTTATTGAACGCCGGCTGGTCGAGGAT
CGTCGGATATTCATCGGAGGAGTGGTGGTCACCTTGCTTATCATCGCCCTGATCATCTATTTCCTAGT
GCTCTAAggtacc

K166del

gcggccgccgacATGGACTACAAAGACGATGACGACAAGGAGAGCTTGTACCACCAAACCAACAATGT
GGTAAAGGACATCGAGCGCGATTTCCAGCGACTGAGTCAGCTCAGTGCCCAGGAATCGCTTGACGTGG
AAAACGGCATTCAATTGAAGATTACCCAGGCGAACGCAAACTGCGATCGGTTGGATGTGCTGTTGTAT
AAGGTGCCACCTTCGCAGCGACAAAGCTCCAAACTTCGTGTGGATCAGCTGAAATATGACCTGAGACA
CCTGCAGACATCACTGCAGACGGCGCGGGAACGAAGACAGCGACGGATGCAGGAGATCTCCGAGAGGG
AACAGCTGCTGAATCACAGATTCACGGCAAACAGCGCGCAGCCGGAGGAAACGCGCCTGCAATTGGAC
TACGAACTGCAGCATCATACGCAGCTGGGTAACGCCCATCGGGGTGTGGACGACATGATTGCCTCGGG
CAGCGGCATTCTCGAGAGCCTGATCTCGCAGAGAATGACGCTGGGCGGAGCGCACA[]GAATCCAGGC
GATAGGCAGCACACTGGGTCTGTCCAATCACACGATGAAACTTATTGAACGCCGGCTGGTCGAGGATC
GTCGGATATTCATCGGAGGAGTGGTGGTCACCTTGCTTATCATCGCCCTGATCATCTATTTCCTAGTG
CTCTAAggtacc

GOSR2 CDS
FLAG
Kozac sequence
NotI
KpnI